Planar microwave resonator sensor technology for real-time and contactless monitoring of microbial growth on solid media

by

Mandeep Chhajer Jain

B.Tech, The Jawaharlal Nehru Technological University, 2017

A THESIS SUBMITTED IN PARTIAL FULFILLMENT OF
THE REQUIREMENTS FOR THE DEGREE OF

MASTER OF APPLIED SCIENCE

in

THE COLLEGE OF GRADUATE STUDIES

(Electrical Engineering)

THE UNIVERSITY OF BRITISH COLUMBIA

(Okanagan)

August 2020

The following individuals certify that they have read, and recommend to the College of Graduate Studies for acceptance, a thesis/dissertation entitled:

PLANAR MICROWAVE RESONATOR SENSOR TECHNOLOGY FOR REAL-TIME AND CONTACTLESS MONITORING OF MICROBIAL GROWTH ON SOLID MEDIA

submitted by MANDEEP CHHAJER JAIN in partial fulfilment of the requirements of the degree of Master of Applied Science

Dr. Mohammad Hossein Zarifi, School of Engineering
Supervisor

Dr. Ian Foulds, School of Engineering
Supervisory Committee Member

Dr. Thomas Johnson, School of Engineering
Supervisory Committee Member

Dr. Abbas Milani, School of Engineering
University Examiner

Abstract

This thesis presents an innovative approach using microwave technology for contactless monitoring of microbial growth on solid growth matrices. Microwave sensors are widely employed in various biomedical applications owing to their portable, ease of fabrication, low cost, label-free, and contactless sensing capabilities. The unique ability of the microwave sensor to detect variations in the conductivity in the surrounding medium related to microbial growth makes it a promising candidate for microbial growth monitoring and related applications. This thesis presents an in-depth analysis of the design, fabrication, and testing of one-port planar microwave sensors. The designed sensors allow microbial growth monitoring capabilities in both temperature-controlled and uncontrolled environments.

Microbial growth largely depends on environmental factors that include growth temperature, nutrient availability, spatial position, and presence of growth-inhibiting compounds such as antibiotics. Through this research, the potential of designed microwave sensors to investigate the influence of these factors was explored. The first study utilized a microwave sensor to detect microbial growth on a solid matrix provided with different glucose concentrations (0- 10 % w/v). Experimental results demonstrated a positive correlation between microbial growth at different nutrient concentrations with the microwave sensor's response. In the second study, the microwave sensor successfully monitored the subsurface growth of microorganisms, confined between two layers of solid growth matrices. In the third study, the potential of the designed microwave sensor was investigated and was successfully demonstrated in monitoring the effect of antibiotics on microbial growth.

The data from all these experiments and supporting data from microbial growth imaging demonstrates the high efficiency of microwave sensors in fast and contactless monitoring of microbial growth and its effectiveness in biomedical applications. Through this work, the ability of microwave resonator sensor to rapidly detect bacterial growth before any visual indicators was demonstrated. These initial studies lay the foundation and prove the microwave sensor as a prospective tool to detect and monitor microbial growth in food and pharmaceutical industries. The sensor resolution and

sensitivity can be further improved by utilizing active resonators. Moreover, the sensor design can be modified and enhanced to operate wirelessly for long-range measurement systems.

Lay Summary

This thesis presents an innovative approach using microwave sensors for contactless monitoring of microbial growth on solid growth matrices. The designed sensors were employed in three independent studies to monitor microbial growth under different nutrient conditions, the position of microorganisms, and the presence of antibiotics. The first study utilized a microwave sensor to monitor the impact of the availability of nutrients on microbial growth. The second study demonstrated the microwave sensor's ability to successfully monitor the subsurface growth of microorganisms. Moreover, in the third application study, the potential of the designed microwave sensor in monitoring the effect of antibiotics on microbial growth was successfully demonstrated. These studies conclude that microwave sensors were able to detect microbial growth before any visual indicators demonstrating the rapid detection capabilities of the microwave sensor. These initial studies prove microwave sensors as a prospective tool to monitor microbial growth in the food and pharmaceutical industries.

Preface

This work was under the guidance and supervision of Prof. Mohammad Hossein Zarifi at the School of Engineering at The University of British Columbia. All copyrighted figures presented in chapters 1 and 2 were reprinted with permission, as indicated in the caption of the figures.
Portions of chapter 3 have been published in the following publication:

– M. C. Jain, A. V. Nadaraja, B. M. Vizcaino, D. J. Roberts, and M. H.Zarifi, "Differential Microwave Resonator Sensor Reveals Glucose-Dependent Growth Profile of *E. coli* on Solid Agar,"IEEE Microwave and Wireless Components Letters, pp. 1–4, 2020

Table of Contents

List of Tables

List of Figures

Acknowledgements

I would like to thank the Syilx Okanagan Nation for the use of their unceded territory, the land on which the research was conducted. I also acknowledge the support of the Natural Sciences and Engineering Research Council of Canada (NSERC) Discovery Grant Program, Canada Foundation for Innovation program for partial financial assistance, and CMC Microsystems for the use of their software and equipment.

I would like to express my gratitude towards my supervisor, Prof. Mohammad Hossein Zarifi, for his immense support and motivation throughout my research. Working under his guidance makes me competent to address challenging research questions and find solutions for them. I truly appreciate the support, help, and for all the advice that will always help me in my future endeavors. I would also like to thank the members of my committee, Prof. Thomas Johnson, Prof. Ian Foulds, and Prof. Abbas Milani for their wonderful guidance throughout the Master's program.

A special thanks to Dr. Anupama Pillai, for mentoring me with microbiology experiments and constant motivation. I would also like to thank the OMEGA lab team for the support and making my research days fun and memorable. I would like to extend my thanks to members of Prof. Johnson's lab members with whom we shared lab space. Special thanks to Aaron Clements. I like to thank Prof. Deborah Roberts for granting me access to her research laboratories to perform microbiology experiments.

Thanks to my friends in India for supporting and believing me in this journey. Last but not least, I sincerely thank my parents, Madhu Chhajer Jain and Lalit Kumar Chhajer Jain, my brother, Sandeep Chhajer Jain, my cousin Prerna Baid and, my grandparents for being on my side every single day and moment.

Dedication

To my father Lalit Kumar Chhajer Jain,
whose hardwork and sacrifices are the reason I am where I am.
To my Mother Madhu Chhajer Jain,
whose strength, kindness and support pushes me to my very best ever day.
To my brother Sandeep Chhajer Jain,
my strength and my partner in crime.
To my sister Prerna Baid, who supports me in my every endeavour

Chapter 1

Introduction

1.1 Motivation

Infections are an inevitable fact of life. They pose a serious challenge to public health and the global economy. This is evident from the current global pandemic caused by a novel coronavirus. As per the recent report published by the World Health Organization (WHO), the aforementioned virus spread rapidly across the globe affecting 188 countries with over 5 million cases and over 300 thousand deaths as of May 27, 2020 [1–6]. Statistics and future predictions have shown that deaths due to infection account for nearly 13-15 million deaths annually and is projected to remain constant or increase by 2050 [7]. Although mortality due to infections is projected to rise by the year 2050, early detection of infections and infection-causing bacteria can reduce the number of deaths per year significantly. Early detection of such disease-causing organisms can help in developing effective therapy and postulate various disease control measures against the pathogens [8]. Thus, biologists and other researchers are constantly in search of new technologies capable of detecting infections in earlier stages and to help develop vaccines against life-threatening infections.

The current technologies capable of detecting pathogens rely on either conventional techniques such as spread or pour plate techniques and molecular methods such as polymerase chain reaction (PCR) and enzyme-linked immunosorbent assays (ELISA) [9–11]. Although these techniques are reliable, conventional techniques are not real-time and difficult to automate while molecular methods require extensive sample preparation and expensive instruments [12–14]. To overcome the challenges presented by existing technologies, rapid and portable biosensors to detect bacterial growth have been developed [15–20]. Among all the available biosensors, optical and electrochemical biosensors were extensively used for biomedical applications due to their real-time, non-contact, and label-free detection capabilities [21–24]. However, optical biosensors suffer from high cost and quick degradation of reagents whereas electrochemical biosensors suffer from low selectivity, low limit of detection (LoD) and are single-use devices due to direct contact of

the sensor with the bacteria [20].

Recently, microwave sensors have emerged as a promising tool for material detection and characterization [25–29], liquids characterization [30–39], gas characterization [27, 40–43], ice detection [44], light and UV detection [45–47], and wearable RFID and biomedical technology [46, 48, 49], due to their low cost, real-time, label-free, and non-contact-based detection mechanisms. Interestingly, bacterial growth monitoring in liquid matrices using microwave technology has gained significant attention in recent years [50–53]. Liquid growth media is used extensively by microbiologists for bacterial growth monitoring. This is due to the availability of spectrophotometers or other sophisticated instruments capable of detecting bacterial growth in real-time [54, 55]. Also, the volume of the liquid bacteria culture can be significantly reduced by employing microfluidic channels [56].

Solid growth media, on the other hand, is primarily used to isolate bacteria to obtain pure bacterial cultures [54]. They are also extensively used to perform antibiotic susceptibility tests (AST) such as disk diffusion tests and epsilometer tests [9]. However, the complex nature of solid agar coupled with the limitations of conventional plating techniques holds back biologists and researchers to automate the bacterial detection process. Therefore, through this work, a proof of concept employing the microwave technology to monitor bacterial growth on solid agar media will be presented.

1.2 Outline

This chapter begins with an introduction to microwave technology, followed by the principles of operation of microwave sensors to sense and characterize materials. The discussion will then focus on the currently available methods for material sensing and characterization. Based on the merits and demerits of each sensing method, a sensing technology suitable for the current application will be chosen.

1.3 Introduction to microwave technology

The term microwave is associated with electromagnetic waves at frequencies in the range of 300 MHz to 300 GHz with a corresponding electric wavelength between 1m (for a frequency of 300 MHz) to 1 mm (for a frequency 300 GHz) respectively as shown in Figure 1.1.

The theoretical foundation of microwave technology was laid by Clark Maxwell in the early 1900s but it wasn't until the development of Radio

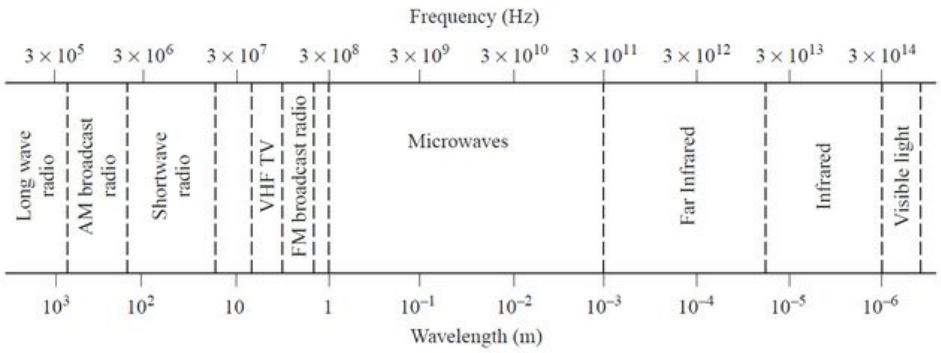

Figure 1.1: The electromagnetic spectrum. Copyright © 2005 John Wiley & Sons, Inc. All rights reserved [57].

Detection and Ranging, or RADAR in World War II that engineers and scientists began to show substantial interest. Since then, microwave technology has undergone significant development in terms of power consumption, size, and cost due to the development of solid-state devices, printed circuit board technology, and integrated circuits technology. Today, microwave technology finds applications in communication [58, 59], processing industry for sintering, drying and curing [60–64], healthcare [65–67] and food industry [16]. Microwave technology is also being extensively used in biomedical and pharmaceutical applications such as detecting and monitoring food spoilage, drug research, and manufacturing, human tissue characterization for cancer and tumor detection, fermentation and biomass system design, and bio-implant research [48, 68]. This is attributed to its low cost, robust, compact, non-contact, and label-free detection properties.

1.4 Principle of operation

A significant aspect of microwave technology is its ability to characterize and sense materials by measuring their complex dielectric properties such as permittivity and conductivity. Dielectric permittivity is a dimensionless quantity that gauges the degree of polarization in a material due to the presence of an external electric field [69]. In the presence of an electric field, charges in the atoms and molecules of a dielectric material undergo displacement. This results in the formation of dipoles along the direction of the applied electric field as shown in Figure 1.2 [69]. Dielectric permittivity

is thus, a measure of how effectively the dipoles are formed and aligned in the direction of electric field.

Relative permittivity or dielectric constant of the dielectric (ϵ_r) is represented as the ratio of the permittivity of the material to that of the free space (shown in equation 1.1)

$$\epsilon = \epsilon_r \epsilon_0 \tag{1.1}$$

Where ϵ is the permittivity of the material (F/m), ϵ_r is the relative permittivity and ϵ_0 is the permittivity of free space (8.85 x 10^{-12} F/m).

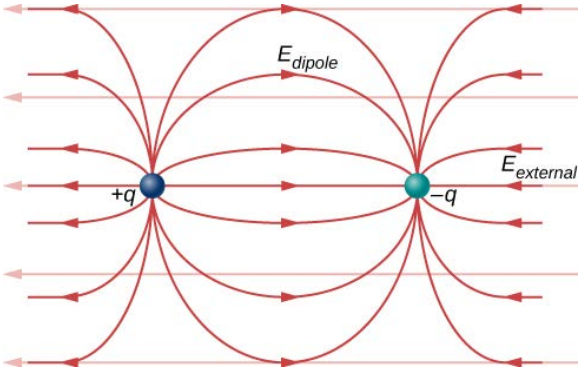

Figure 1.2: A dipole in the presence of an external electric field. All rights reserved [69].

The complex permittivity of the medium(ϵ) consists of real part known as the dielectric constant ($\epsilon^{'}$) and an imaginary part which accounts for the losses in material ($\epsilon^{''}$) as shown in equation 1.2 [70].

$$\epsilon = \epsilon^{'} - j.\epsilon^{''} \tag{1.2}$$

The dielectric constant ($\epsilon^{'}$) is a measure of the amount of energy from an external field stored in the material whereas loss factor($\epsilon^{''}$) is a associated to dielectric loss. Loss in dielectric materials are mainly caused by (i) dielectric damping, and (ii) conduction loss. Dielectric damping occurs due to the displacement of the centers of the charge carriers under the influence of the electric field whereas conductivity loss arises due to the movement of charge carriers in the dielectric material [71]. Thus, an important property of a dielectric material i.e. the loss tangent is defined as the ratio of imaginary part to real part of the complex permittivity and is presented in equation

1.3.

$$\tan \delta \ = \frac{\omega\epsilon^{''} + \sigma}{\omega\epsilon^{'}} \tag{1.3}$$

where, σ represents the conductive loss and $\omega\epsilon^{''}$ represents loss due to dielectric damping [70], [57].

Measuring the dielectric properties of materials plays an important role in food and pharmaceutical industries to detect tumours and monitor food decay by microorganisms [16, 30, 58–64, 72]. Various standard methods have been postulated and successfully applied to measure and determine the complex permittivity and loss factor of materials. These methods are thoroughly discussed in the next section.

1.5 Microwave technologies for complex permittivity extractions

Measurement of dielectric properties using microwave technology involves measuring the scattering parameters(S- parameters) using a vector network analyzer equipped with post-processing tools capable of extracting complex permittivity and loss tangent of the sample under test (SUT) [73]. Various methods have been developed to measure the dielectric properties of materials. In this section, four different permittivity characterization techniques will be discussed.

1.5.1 Free-space method

The Free-space method is widely used to determine the dielectric properties of a sample under test at high temperatures or in hostile environments. The measurements are carried out using two spot- focusing horn lens antennas facing each other as shown in Figure 1.3. The antenna is connected to a network analyzer loaded with a post-processing program capable of determining dielectric properties from the measured response. Prior to any measurements, the VNA is calibrated using a line- reflect- line calibration method. The response of the sensor in the presence of a sample holder with and without a sample is recorded. By using the de-embedding function provided in the VNA, the effect of the sample holder on the measured response is canceled [73].

For instance, Hakansson *et al.* [74], measured the dielectric properties of polymerized thin polypyrrole (PPy) films on synthetic textile substrates in the frequency range of $1 - 18$ GHz using the free-space method. Various

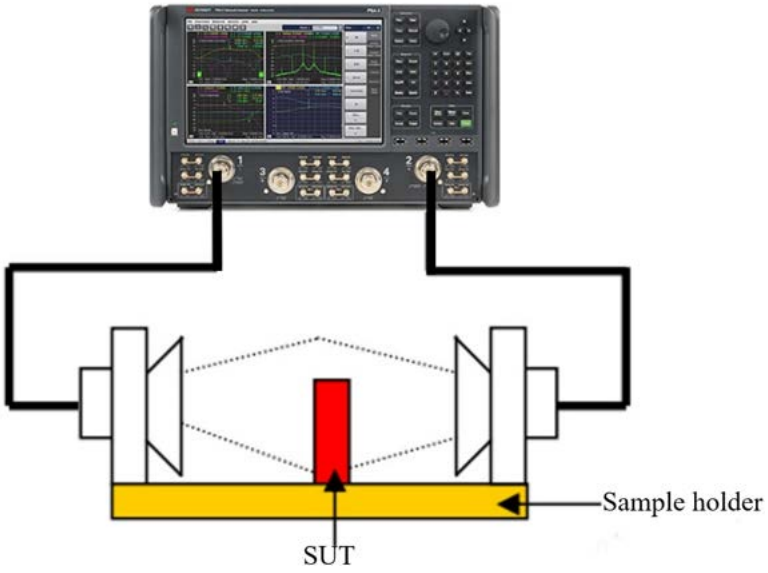

Figure 1.3: Measurement of complex permittivity of a sample using free space method. All rights reserved [73].

strategies such as mathematical diffraction removal program, time–gating tools, and high gain horns were used to improve the permittivity measurements. A stable real part of the permittivity was observed above a dopant concentration of 0.018 mol/1 p-toluene sulfonic acid (pTSA). Similarly, an increase in the imaginary part of the permittivity was observed as the dopant concentration was increased to 0.018 mol/1 pTSA. However, a further increase in the dopant concentration had a negligible effect on the imaginary part of permittivity.

The Free-space method is widely used to determine the dielectric properties of in-homogeneous material at high temperatures or in hostile environments [75–79]. This technique is fast and reliable but is not portable and requires a custom fabricated sample holder for each sample. Also, a large sample is needed for permittivity measurements to avoid multiple reflections within the sample and diffraction at the edge of the sample.

1.5.2 Open-ended coaxial probe method

The Open-ended coaxial probe method is a non- destructive testing method for complex permittivity characterization. In this method, the coax-

ial probe is placed against the specimen or immersed in the sample liquid as shown in Figure 1.4. The coaxial probe is connected to a vector network analyzer (VNA) and calibrated using a calibration standard (open, short, and a standard reference liquids such as water, saline, and methanol). The calibration program utilizes time gating function available in the VNA to decrease the reflections from the connector [80]. The calibration improves the ability of the network analyzer to accurately measure the dielectric properties of the sample under test. Complex permittivity of the sample under test (SUT) is assessed by analyzing the reflection coefficient of the coaxial probe using post-processing software embedded in the VNA [73]. Shim *et al.*

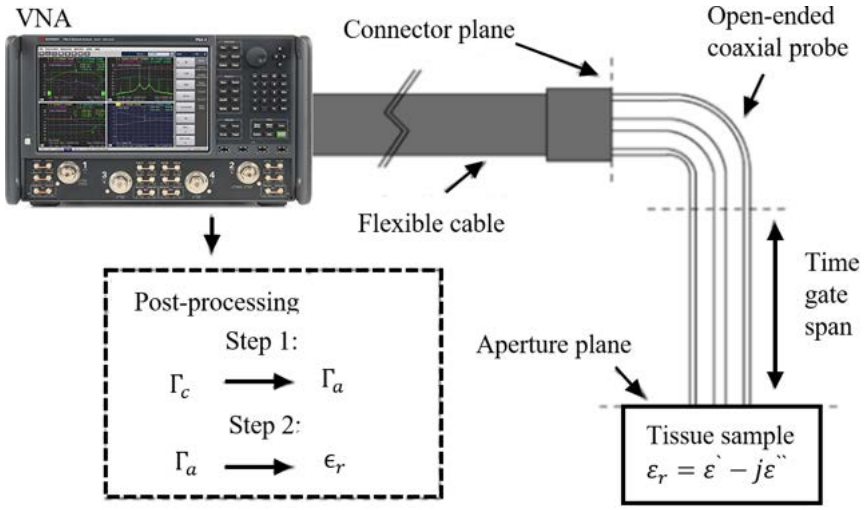

Figure 1.4: Measurement of tissue sample using open coaxial probe. All rights reserved [80].

[81], for instance, presented a complex permittivity measurement technique for artificial tissue emulating materials (ATEs). ATEs are used for in-vitro testing of implantable biomedical devices. The coaxial probe was calibrated between the frequency range 0.5- 6 GHz. The reported results were in good agreement with the results obtained by commercially available open-ended coaxial probe kits.

Open-ended coaxial probe method is extensively used for near field sensing applications and is portable and robust [82–86]. However, the device is expensive and requires a large and custom machined sample. The measurement is also sensitive to air gaps between the sample and the probe.

1.5.3 Transmission line method

In this method, a sample under test is used as a filling material of a waveguide or coaxial probe as shown in Figure 1.5. The sensor is connected to the vector network analyzer and calibrated to accurately measure the complex permittivity of the sample under test. The S- parameter response of the sensor is measured and processed using various conversion methods [73].

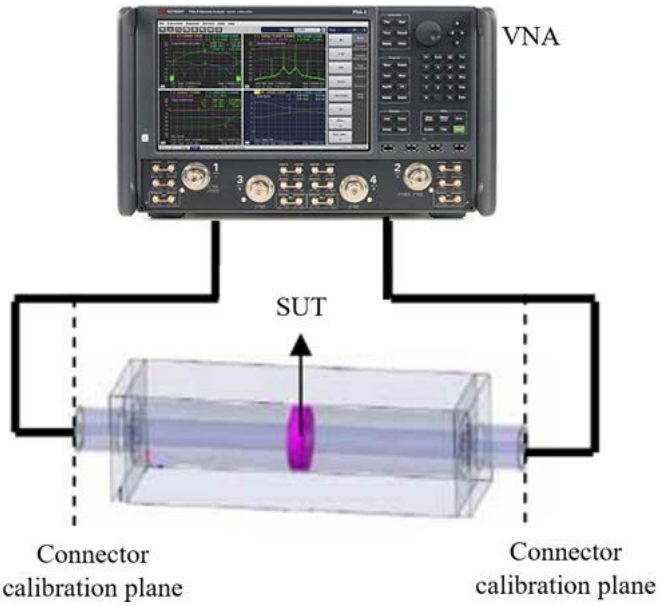

Figure 1.5: Measurement using TR method with a waveguide. All rights reserved [73].

For instance, Bogle *et al.* [87], presented a method for complex permittivity characterization of materials using a partially filled rectangular waveguide. The device was calibrated to operate between the frequency range 8- 12 GHz. Mode-matching technique was developed to accommodate the resulting waveguide discontinuity and a Newton root search method was utilized to subsequently extract the electromagnetic properties of the test sample.

Transmission line method is widely used for complex permittivity extraction for medium to high loss materials [73, 88, 89]. However, the measurement accuracy is limited by the air- gap effects and the samples may

need to be machined specifically.

1.5.4 Resonance based method

Resonant measurements are the widely used for obtaining complex dielectric properties such as permittivity of a given sample under test due to its non-contact, portable, and label-free sensing capabilities. There are two types of resonant measurements commonly used: perturbation and low loss method. Low loss measurement methods are suitable for measurement on low loss materials using larger samples. Perturbation methods are suitable for permittivity measurements of medium to high loss material [73, 90].

The experimental setup to measure complex permittivity of a thin film using a transverse magnetic (TM) cavity geometry employing perturbation method is shown in Figure 1.6. With resonance characteristics depending on

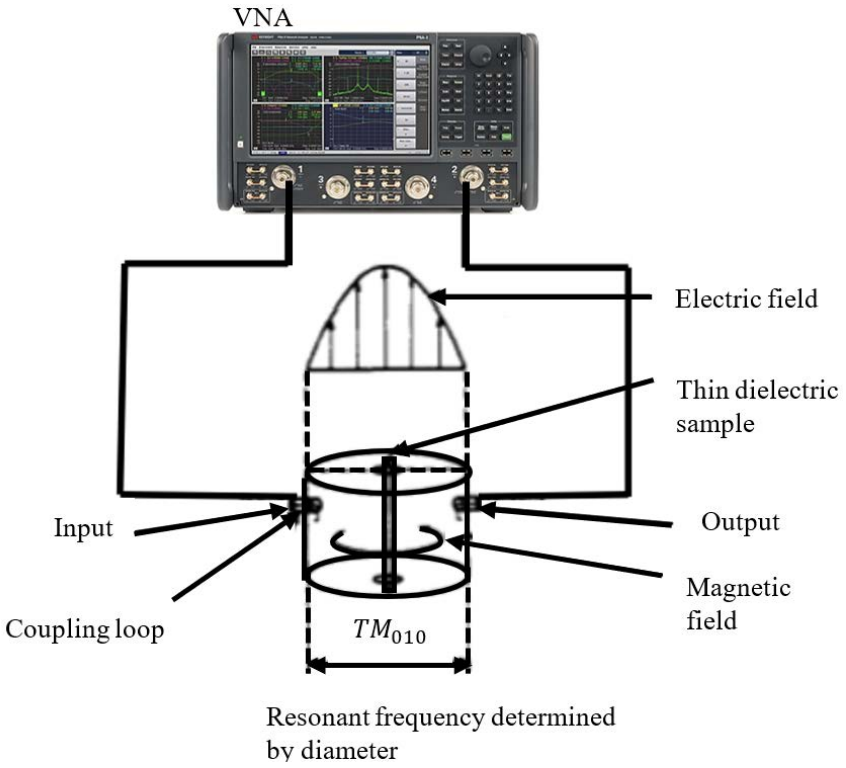

Figure 1.6: Measurement of thin film using cavity resonator. All rights reserved [73].

the material under test (MUT) in a cavity, its quality factor and resonant frequency can be monitored to determine the dielectric parameters. The resonant frequency and Q-factor of an empty cavity and a cavity with the material under test are measured and processed to determine the permittivity of the material.

Saeed *et al.* [91], presented a novel planar substrate integrated waveguide cavity resonator technique to determine and extract complex permittivity of the sample under test (SUT). The resonator was designed to resonate at 8 GHz and had a high Q- factor. The proposed design had low fabrication cost, is easy to fabricate, and provided contact-free detection capabilities.

Resonance-based method is used for measuring the complex dielectric properties of small sample under tests. However, there exist limitations on the frequencies and loss characteristics of the materials that can be measured with the method.

Table 1.1: Summary on the techniques to sense and measure dielectric properties using microwave technology

Method	Advantages	Disadvantages
Free-space method	Contactless, robust	Requires custom sample holders,large sample
Coaxial probe method	Portable, robust and contactless	large sample size, complex data analysis
Transmission line method	Portable, small sample size, non- contact,label- free	Requires custom samples for cavity resonators
Resonance-based method	Portable, non-contact based sensing and label- free	Sensor response depends on the loss characteristics of the MUT

Compared to free- space and open-ended transmission line methods, the resonance-based method uses inexpensive devices [92]. However, machining the sample to fit in the cavity of the waveguide can be challenging. To overcome this, a microstrip line sensors can be used. Microstrip line sensors offer

numerous advantages such as low-cost fabrication, small sample size, portability, robust, non-contact, and label-free detection and ease of integration with microfluidic chips [27, 37–39, 56, 91, 93, 94].

The summary of the above discussed microwave technologies for complex permittivity extractions is presented in Table 1.1.

Among the available techniques for material sensing and characterization using microwave sensors, microstrip line sensors offer numerous advantages such as low cost, contactless, ease of fabrication, and label-free detection and will be selected to monitor bacterial growth on solid media.

1.6 Thesis objective

This thesis aims to design a custom- designed microwave resonator sensor to monitor the influence of nutrients, subsurface position, and presence of inhibitory compounds on the growth of microorganisms on solid growth media. The designed sensor should be able to detect microbial growth before any visual indicators.
The following objectives have been set to achieve the aim:

1. Employing the designed microwave sensor resonator to detect and monitor the impact of variations in the glucose concentration in the solid media on the bacterial growth
   Hypothesis: The designed sensor will monitor the growth of bacteria in response to varying glucose concentration in the media.
   The tasks required to achieve this objective are:
   - Prepare LB agar medium with varying concentrations of glucose (0, 2, 5, and 10 %)
   - Monitoring variation in the bacterial growth at tested glucose concentrations using microwave sensor resonator
   - Analyze the data and plot the measured results. Compare the measured results with microscopic images taken at regular time intervals to validate the efficacy of the designed sensor to monitor bacterial growth.

2. Utilizing the designed microwave sensor to detect and monitor subsurface growth of bacteria confined between two layers of solid growth media
   Hypothesis: The designed sensor will monitor the transition of bacterial growth from 2-D surface growth to a 3-D subsurface growth.
   The tasks required to achieve this objective are:

- Prepare inoculated media plates with microorganisms confined between two layers of solid LB agar
- Measuring conductivity changes during the transition of surface to subsurface growth of bacteria using microwave sensor resonator
- Analyze, plot and compare the measured results with the captured microscopic images as mentioned earlier

3. Applying the designed microwave resonator sensor to monitor and differentiate the impact of various concentrations of antibiotic, erythromycin on the growth of Bacteria
   Hypothesis: The microwave sensor will monitor the dielectric properties of the (Mueller-Hinton) MH agar and differentiate the impact of various antibiotic concentrations on the bacterial growth.
   The tasks required to achieve the proposed objective are:

   - Prepare sample MH agar plates with varying concentrations of erythromycin (0, 7.5, 30, and 45 μg) using disk diffusion techniques
   - Measuring conductivity changes during bacterial growth inhibition at tested antibiotic concentrations using microwave sensor resonator
   - Analyze, distinguish, and compare the measured results with the captured microscopic images as mentioned earlier. Based on the measured results, determine the antibiotic concentrations capable of successfully inhibiting microbial growth

1.7 Thesis outline

This thesis is divided into four chapters. A brief summary of each chapter content is as follows:

- Chapter 2 focuses on the theory of operation of a microstrip resonator. An investigation of the existing planar microwave resonator sensors based on their geometry, robustness, and efficiency will be performed. This investigation will empower the choice of the appropriate sensor design for the proper environmental conditions. A critical review of various microwave resonators schemes available is presented, and the limitations associated with them will be discussed. Based on the drawbacks of the discussed resonator schemes and the nature of the study, a

thorough design procedure of the selected microwave resonator scheme will be presented. The design procedure will encompass the Finite Element Method (FEM) analysis of complex planar resonator structures aimed at determining the sensitive regions, impact on the sample under test, and the electrical characteristics of the resonator.

– Chapter 3 is devoted to the fabrication and functional verification of the sensor designed in Chapter 2. This chapter begins with the step by step in- house fabrication procedure followed to precisely and accurately fabricate the sensor. The fabricated sensor will then be subjected to various functional verification using standard samples to verify the sensor's operation as per the designed parameters.

– Chapter 4 presents the capability of the designed and fabricated sensor discussed in chapter 3 to detect and monitor the impact on bacterial growth on solid media subject to three mutually exclusive conditions: varying nutrient concentration, spatial position, and the presence of inhibitory compounds such as antibiotics.

– Finally, Chapter 5 concludes and summarizes the work presented in the thesis, and discusses ideas for future work

Chapter 2

Principle of operation, design, and optimization of planar microstrip resonator

This chapter aims to introduce a planar microwave resonator and explore various factors that dictate the operation of the resonator such as resonant frequency, resonant amplitude, and quality factor. It is followed by a thorough discussion of different types of planar microstrip resonator technologies. An in-depth analysis of frequency variation resonator and differential model resonator will be undertaken. In addition to this, the steps followed to design and study the resonator will be discussed. Various studies such as EM field analysis, sensitive region analysis, and the impact of permittivity and loss tangent of a sample under test on the response of the modelled sensors will be performed in this chapter. The sensor design modelled in this chapter is the result of weeks and months of numerous changes in the sensor design and optimizations to improve the sensitivity of the resonator.

2.1 Introduction to planar microwave resonator

A resonator is a device that stores energy at the resonant frequency [57]. Consider a series RLC resonance circuit as shown in the Figure 2.1.

where V is the voltage of the input electromagnetic signal(Volt), R is the resistance (Ω), L is the inductance(Henry), C is the capacitance (Farad), I is the net current (Ampere) flowing through these elements, and Z_{in} is the input impedance. The input impedance Z_{in} can be calculated using equation 2.1 [57].

$$Z_{in} = \frac{2 * P_{in}}{|I|^2} = \frac{P_{loss} + 2j\omega(W_m - W_e)}{0.5 * |I|^2} \tag{2.1}$$

where P_{in} is the power delivered to the series RLC resonator at the input, P_{loss} is the power dissipated by the resistor R, ω is the angular frequency

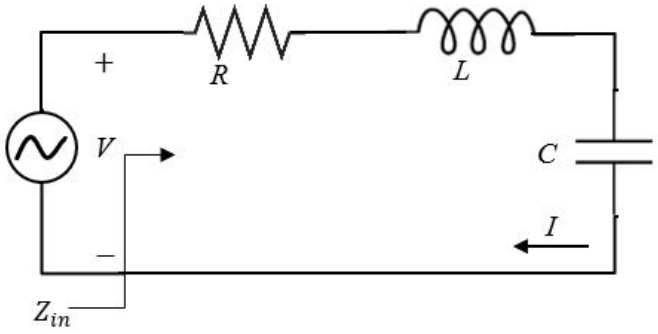

Figure 2.1: Lumped element model of a series RLC resonator. All rights reserved [57].

(Radian), W_m is the average magnetic energy stored in the inductor and W_e is the average electrical energy stored in the capacitor. The series RLC circuit is said to be at resonance when the average stored magnetic energy in the circuit is equal to the average stored electrical energy. At, $W_m = W_e$, the input impedance is purely real as shown in equation 2.2.

$$Z_{in} = \frac{P_{loss}}{0.5 * |I|^2} = R\Omega \tag{2.2}$$

The frequency at which the input impedance is purely real is known as the resonant frequency. The resonant frequency can be calculated using the equation 2.3.

$$f = \frac{1}{2\pi\sqrt{LC}} = \frac{c}{\lambda\sqrt{\epsilon_{eff}}}\text{Hz} \tag{2.3}$$

Where f is the resonant frequency in Hz, c is the speed of light in millimeter per second and λ is the wavelength in millimeter of the EM wave, ϵ_{eff} is the effective permittivity.

An important parameter associated with a resonator is the quality factor. It is used to represent the EM loss in the resonator. A lower loss implies a higher Q-factor. The relation between Q and loss tangent tan δ, a dimensionless quantity to determine the amount of electromagnetic energy absorbed within the material and dissipated as heat, is given by the equation 2.4.

$$Q = \frac{1}{tan\delta} = \frac{\omega\epsilon}{\sigma} = -\frac{\epsilon^{'}}{\epsilon^{''}} \tag{2.4}$$

Where σ is conductivity in siemens/m, ω is the angular frequency in

rad, $\epsilon^{'}$ of the real part of the permittivity, $\epsilon^{''}$ is the imaginary part of the permittivity.

2.2 Investigation on the various types of planar microwave sensors

Among the available techniques for dielectric characterization using microwave sensors, microstrip line sensors offer numerous advantages such as low cost, contactless, ease of fabrication, and label-free detection capabilities. There are two versions of microstrip planar sensors, resonant based and non- resonant based. Resonant based planar sensors offer better sensitivity and are compact as compared to non- resonant based planar sensors and therefore were selected for this study. Based on the principle of operation, planar stripline resonators can be broadly grouped into four categories:

- Frequency variation sensors
- Coupling modulation sensors
- Frequency splitting sensors
- Differential- mode sensor

2.2.1 Frequency variation sensor

A frequency variation sensor consists of a transmission line loaded with a resonant element as shown in Figure 2.2. Material characteristics are determined by measuring the variation in the resonant frequency, quality factor, or resonant amplitude in the presence of a sample under test on the resonant element. These sensors can be used to characterize and determine the dielectric properties of liquids and solids in environments where ambient factor changes such as temperature and humidity have a negligible effect on the electrical properties of the sample under test. Mohammadi *et al.* [31] presented a low- cost and hazard free 3D printed microfluidic microwave-based method for water quality monitoring. They employed a 2- port double-ring resonator operating at 4.5 to 4.6 GHz with a quality factor of 120. The study was able to achieve real-time monitoring of water contaminants comparing to standard chemical-based methods. In another study, Wiltshire *et al.* [44] demonstrated the capabilities of a 2- port microwave resonator to detect ice and frost. The designed sensor operated between 3.5 GHz to 5

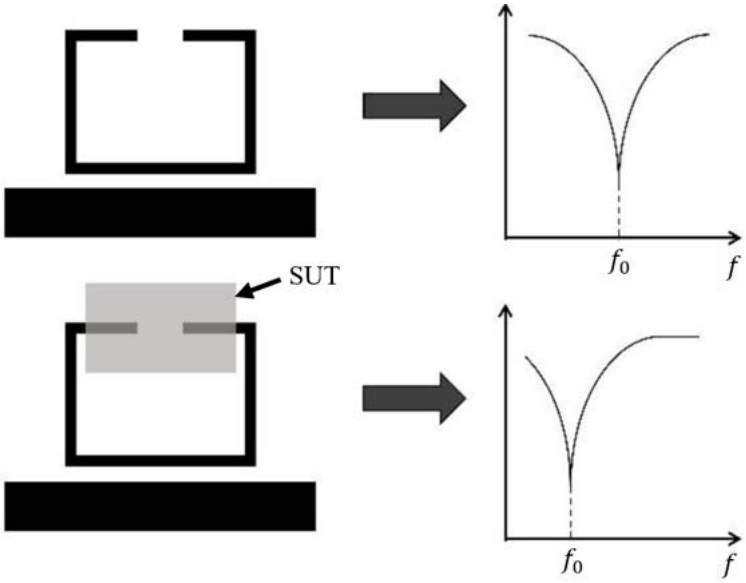

Figure 2.2: Principle of operation of frequency variation sensor. All rights reserved [95].

GHz with a quality factor of 250. The sensor was successfully able to detect the phase transition between ice to water and vice- versa.

Frequency variation resonator sensors suffer significant degradation of the response due to cross-sensitivity caused by variations in ambient factors such as temperature and humidity.

2.2.2 Coupling modulation sensors

The impact of the cross-sensitivity of a microstrip sensor to ambient changes can be eliminated using symmetry-based sensors such as coupling modulation sensors. In such sensors, the transmission line is arbitrarily loaded using a symmetrical resonator. (Figure 2.3). In the case of perfect symmetric loading of the transmission line by the sensor, no resonance occurs, and the frequency response does not exhibit a notch. However, as symmetry of the resonator is disturbed due to the dielectric loading or displacement of the resonator, the transmission line couples to the resonator, and the resonant profile appear. The magnitude of the resonant profile (typically a notch) is determined by the degree of coupling which is closely related to the level of the asymmetry [96–99].

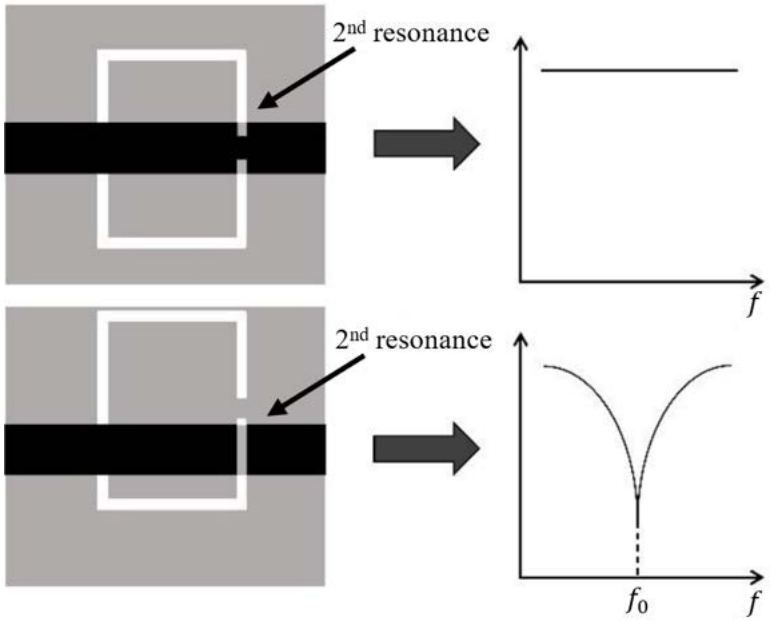

Figure 2.3: Principle of operation of coupling modulation sensor. All rights reserved [95].

The sensor is easy to design and fabricate. However, the sensitivity of the sensor's notch amplitude to displacement due to external factors limits the operation of the sensor in external environments.

2.2.3 Frequency splitting sensors

The next scheme of microstrip resonator is the frequency splitting sensors. In these sensors, transmission line-based structures are symmetrically loaded with a pair of (not necessarily symmetric) resonators (Figure 2.4) leveraging the advantages of both frequency variation and coupling modulation sensor. In the absence of any sample on the sensor, the sensor response is unchanged and a single resonant notch is observed. However, in the presence of test material, the symmetry of the sensor is disturbed and the resonant profile splits into two notches, one for each resonator. Thus, differences in the frequency and amplitude between the two notches can be associated with the level of asymmetry caused by a dielectric sample through which dielectric properties can be inferred [100–103]. The sensor

configuration is robust and easy to fabricate and operate but suffers from limited sensitivity and resolution as the frequency overlap of two resonators can affect the quality factor of the notch.

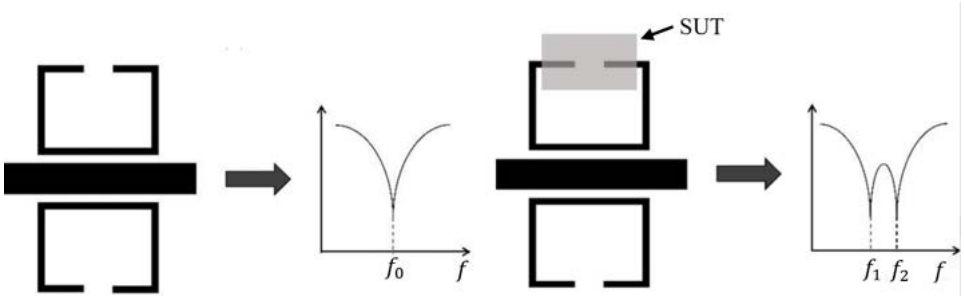

Figure 2.4: Principle of operation of frequency splitting sensor. All rights reserved [95].

2.2.4 Differential-mode sensor

Differential-mode sensors comprise two sensors, one sensitive to the sample whose dielectric properties need to be determined and the other sensitive to reference material. The output of these sensors is the difference between the output of the two sensors as shown in Figure 2.5. Thus, the cross-sensitivity of the sensor to ambient factors is eliminated making the sensor robust to external factor variations. Various works using differential sensors to detect and characterize liquid samples have been reported [30, 33, 101, 103, 104]. These devices can be used as a four-port device or be coupled with additional microwave circuitry to reduce the ports to two or one.

Therefore, based on the investigation of different schemes of microwave resonators, frequency variation and differential-mode resonator schemes are chosen for microbial growth monitoring due to ease of design, and fabrication. The selected designs also aid in performing complex dielectric measurements in both temperature-controlled and uncontrolled environments.

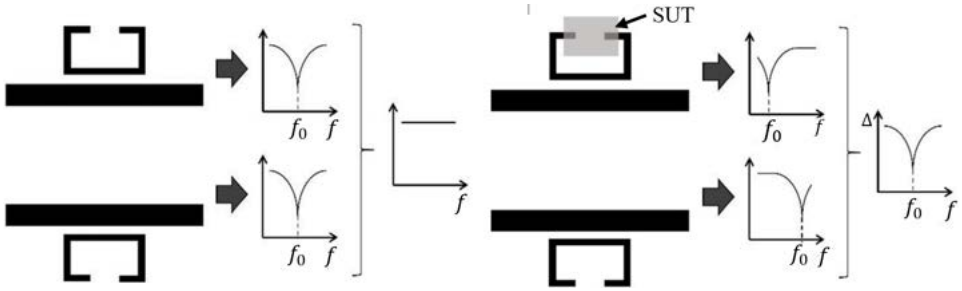

Figure 2.5: Principle of operation of differential mode sensor. All rights reserved [95].

2.3 FEM analysis of a planar microstrip resonator

From the discussion presented in the previous sections, the frequency variation sensor and a differential- mode resonator design were selected for further analysis owing to their ease of design, operation, simplicity, and robustness. In this section, the selected microstrip resonator models will be analyzed using sophisticated Computer-Aided Design (CAD) tools capable of performing complex electromagnetic simulations on the designed resonator structures. To achieve accurate simulation results, the dimension of the mesh selected for the simulation must be less than or equal to the minimum feature size of the designed sensor. The dimension of the mesh depends upon the available Random Access Memory, or RAM on the system hosting the CAD software.Therefore, based on the available systems hosting the CAD tool and the minimum feature size of the sensor, 0.8 mm and 0.4 mm mesh sizes were selected. With a 0.8 mm mesh size, a bare sensor modelled in High Frequency Structure Simulator, or HFSS took approximately 20 minutes to complete simulation as opposed to 40 minutes using 0.4 mm mesh size. In addition to this, the difference between the resonant amplitude of the simulated sensor at 0.8 mm and 0.4 mm mesh size was -0.3 dB and 0.7 MHz respectively. Therefore, as the output results of the simulation with 0.8 mm and 0.4 mm mesh sizes were similar, mesh size of 0.8 mm was chosen to achieve faster and accurate simulation results of the designed sensors. Section 2.1 presented the lumped element model of a simple series resonance circuit. They are extensively used to describe a network at low frequencies. However, at microwave frequencies, the wave-

length of the signal is comparable to the dimension of lumped elements such as resistors, capacitors, and inductors leading to variation in the current and voltage across the device. Thus, at such frequencies, distributed elements consisting of lengths of transmission lines are widely used. A distributed element design of a microstrip resonator is shown in Figure 2.6.

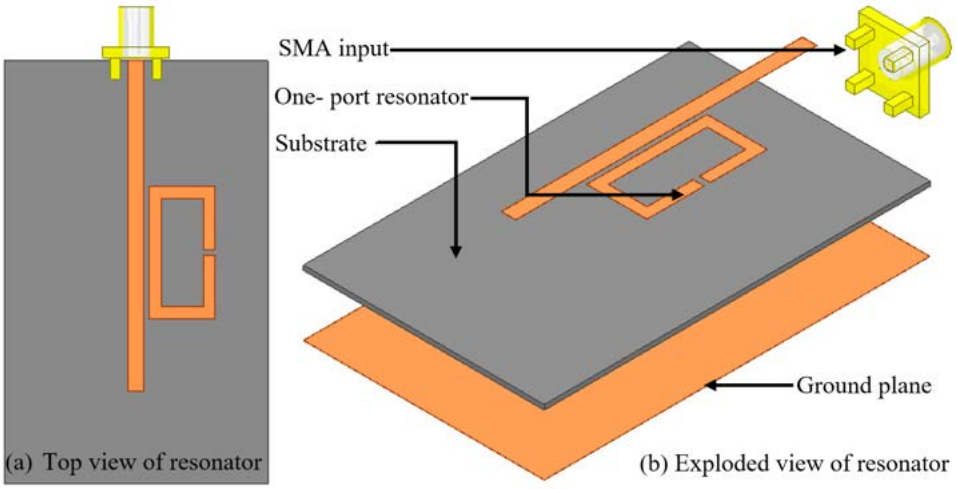

Figure 2.6: Planar microstrip resonator. Top view (a) and exploded view (b).

The main components of a resonator are feed-line, split ring resonator, substrate, and ground plane as shown in Figure 2.6. The feed-line couples the input electromagnetic waves to the split-ring resonator. The substrate on which the resonator is fabricated should be selected carefully as the electrical and physical characteristics of the substrate can affect the resonant frequency of the device. The split ring resonator is the key component and needs to be carefully designed based on the required application. The length of the split ring, the width of the coupling gap between the resonator and the feed-line, and the width of the ring gap play an important role in determining the resonant frequency, resonant amplitude and quality factor. In this section, the impact of substrate properties such as permittivity and loss tangent on the dimensions of the microstrip resonator will be discussed. This will be followed by the design of the microstrip feed line and the split ring resonator.

2.3.1 Impact of substrate on the microstrip resonator design

A substrate can be defined as a structural material to develop RF or Microwave Printed circuit boards. Soft substrates such as FR- 4, Duroids, and polytetrafluoroethylene (PTFE) are used to design microwave PCBs as they are easy to handle and readily available. Microwave substrates are often referred to as "laminates" due to the presence of copper cladding attached to either one or both sides of the dielectric material. Copper cladding can be of various thicknesses and aid in improving the thermal characteristics of the laminate in addition to providing weight to the board. A substrate is defined by several electrical and mechanical properties such as dielectric constant, dissipation factor, coefficient of thermal expansion (CTE), thermal conductivity, and dielectric constant. These parameters can influence the working of the device and must be carefully selected while designing.

- Dielectric permittivity: The dielectric permittivity of the substrate can impact the dimension of the microstrip conductors fabricated on it. For high-frequency applications, a low dielectric constant substrate is preferred as it minimizes the parasitic capacitance developed between traces and conductive structures.

- Dissipation factor : Substrates with low loss tangents are desirable for high performance and high-power applications, as it would minimize the amount of loss within a transmission line or along the structure.

- Surface roughness : The surface roughness is a measure of the smoothness of the surface of the copper cladding. Conductor surface roughness can substantially affect the loss of the conductor. Therefore, based on the reported surface roughness by Rogers Corp, laminates with small surface roughness was selected [105].

- Dielectric strength : This parameter is a measure of the intensity of the electric field strength required to strip electronics from the dielectric material [106]. This parameter has a negligible impact on the material at low voltage and power but for application involving high voltage and high-power, this could be a limiting factor in a device's operation.

Therefore, based on the above factors/parameters that could influence the operation of the sensing device, a substrate with low dielectric permittivity, low loss tangent, and low surface roughness was considered by referring

the data sheets of the available substrates to design and fabricate the resonator [105]. The surface roughness of the copper was not measured as it was out of scope of the current work. However, through normalization and other data analysis techniques performed on the response of the resonator during contactless bacterial growth monitoring, the effect of any microscopic imperfections and ambient factors was minimized.

Therefore, among the laminates available at our disposal, Rogers 5880 was selected to fabricate our resonators. The electrical and mechanical properties of the available laminates from Rogers is given in Table 2.1.

Table 2.1: Electrical and mechanical properties of Rogers 5880, 6006 and 6010 substrates

Laminate name	Permittivity	Loss tangent
Rogers 5880	2.2	0.0009
Rogers 6006	6.15	0.0027
Rogers 6010	10.2	0.0023

2.3.2 Microstrip transmission line design and matching

A microstrip transmission line consists of a conductor attached to a dielectric substrate with a grounded plane as shown in Figure 2.7.

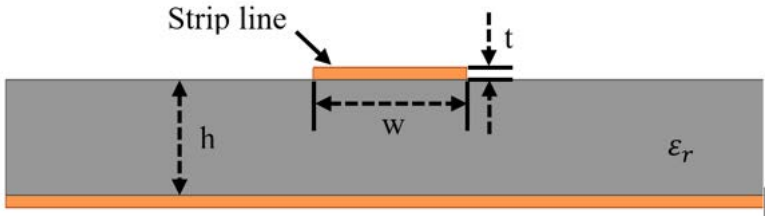

Figure 2.7: Cross-section of a microstrip transmission line.

They are planar, easy to fabricate, portable, and support other device integration such as microfluidic or passive microwave devices such as power splitter, couplers, and mixers.

Various parameters influence the signal transmission through a microstrip line such as physical dimensions of the transmission line, substrate thickness, permittivity, and loss tangent. The physical dimensions of the transmission

line and substrate such as width (w) of the stripline and the height (h) of the substrate define the ratio of the voltage and current signals traveling through the microstrip structure. This ratio is the characteristic impedance (Z_0) of the line and is kept constant for reliable signal transmission.

Theoretical analysis of a microstrip feed line

A time-varying electromagnetic signal traveling through a transmission line generates electric and magnetic fields around it. The electric field is uniformly distributed across the transmission line structure. However, in the presence of a dielectric (commonly thin with d << λ), the electric field lines are concentrated in the region between the conductor and the ground plane, with some fraction being in the air region above the conductor as shown in the Figure 2.8.The non-uniformity in the electric field is due to (small) longitudinal electric and magnetic field components generated at the air-substrate interface. These components arise due to the change in the dielectric properties at the air-substrate interface [107].

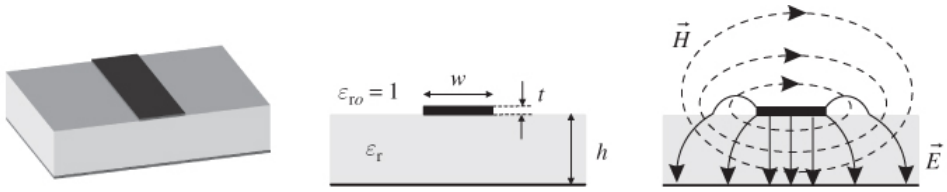

Figure 2.8: Electric field (E- field) and magnetic field (H-field) distribution across a microstrip transmission line. All rights reserved [107].

As electric field propagates in more than one medium, the effective permittivity is calculated using equation 2.5 to 2.8.

when $(\frac{\mathrm{w}}{\mathrm{h}} \geq 1)$

$$\epsilon_{eff} = \frac{\epsilon_r + 1}{2} + \frac{\epsilon_r - 1}{2}\left[\left(1 + 12\left(\frac{h}{w}\right)\right)^{-0.5}\right] \tag{2.5}$$

$$Z_0 = \frac{120\pi}{\sqrt{\epsilon_{eff} * \left[\frac{w}{h} + 1.393 + \frac{2}{3}ln\left(\frac{w}{h} + 1.444\right)\right]}}\Omega \tag{2.6}$$

when $(\frac{\mathrm{w}}{\mathrm{h}} < 1)$

$$\epsilon_{eff} = \frac{\epsilon_r + 1}{2} + \frac{\epsilon_r - 1}{2}\left[\left(1 + 12\left(\frac{h}{w}\right)\right)^{-0.5} + 0.04\left(1 - \left(\frac{w}{h}\right)\right)^2\right] \tag{2.7}$$

$$Z_0 = \frac{60}{\sqrt{\epsilon_{eff}}} ln\left(8\frac{h}{w} + 0.25\frac{w}{h}\right)\Omega \tag{2.8}$$

Where ϵ_{eff} is effective relative dielectric constant, w is width of the microstrip line, h is the height of the microstrip line, Z_0 is the characteristic impedance of the line, ϵ_r is the relative permittivity of the substrate. Therefore, to achieve an input impedance of 50 Ω, the width of the microstrip line was calculated to be 2.48 mm as shown in the Figure 2.9.

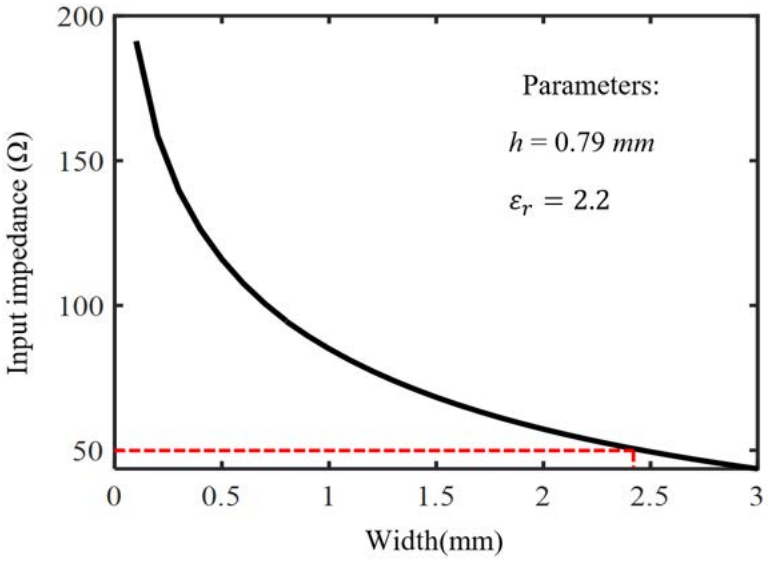

Figure 2.9: Width of the transmission line (mm) versus input impedance (Ω) for a constant dielectric height of 0.79 mm and permittivity of 2.2.

Note that the thickness of the copper cladding and the effect of frequency was omitted while calculating the width of the transmission line. A more accurate value for the width can be extracted using the Keysight's LineCalc tool.

Microstrip feedline design and simulation

Upon determining the optimum microstrip width to height ratio to achieve a characteristic impedance of 50 Ω, a simple two-port model of a microstrip line was simulated in High-Frequency Structure Simulator (HFSS). One port was connected to a source and the other was connected to a 50 Ω load as

shown in Figure 2.10. The reflection coefficient S_{11} was measured and plotted as shown in Figure 2.10.

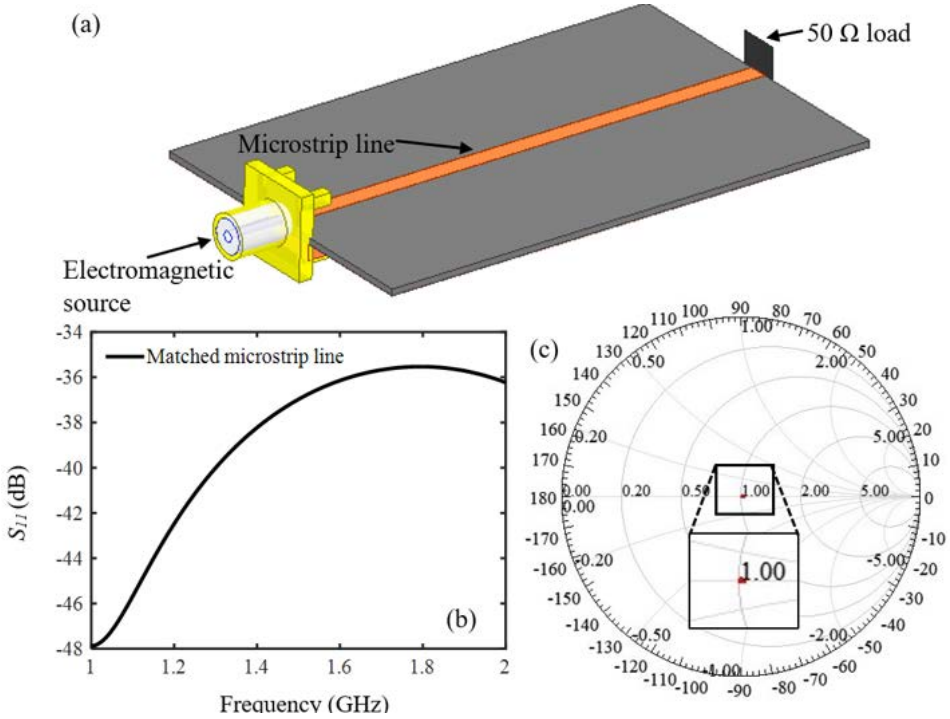

Figure 2.10: HFSS model of a matched transmission line connected to a 50 Ω load (a). Measured transmission coefficient (b), and transmission coefficient plotted on a smith chart (c).

The feedline was matched to the characteristic impedance i.e. 50 Ω. Therefore, the EM signal was transferred from the input to output through characteristic impedance i.e. 50 Ω load with little to no reflection. This is reflected in the low magnitude of the reflection coefficient from 1 GHz to 2 GHz. Also, to confirm the matching, the reflection coefficient was plotted on a smith chart. As the load was matched to the feed line, the measured result was close to the center of the smith chart.

2.3.3 Split ring resonator design

A ring resonator is a transmission line formed in a closed loop. For a resonator to operate at a certain resonant frequency, the circumference of

the resonator must be equal to a multiple of half of the wavelength calculated at that frequency. Equation 2.9 calculates the length of the ring resonator required to achieve resonance at the desired frequency (f GHz).

$$l = \frac{c}{2f\sqrt{\epsilon_{eff}}}\text{cm} \tag{2.9}$$

Where f is the resonant frequency in GHz, c is the speed of light in millimeter per second and l is the length of the resonator in millimeter, ϵ_{eff} is the effective permittivity of the medium surrounding the resonator. A resonator in its simple form consists of a split ring coupled to a feed line as shown in Figure 2.11.

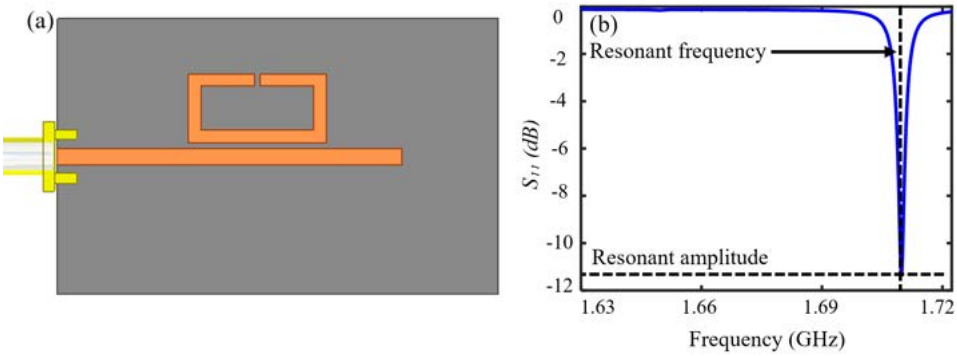

Figure 2.11: A Model of a split ring resonator (a) and the $S_{11}(dB)$ response of the model resonator (b).

The circumference of the resonator calculated to resonate at 1.76 GHz was found to be 57.4 mm. The resonant frequency was selected to accommodate the loss characteristics of the solid agar. A major portion of solid agar constitutes water trapped between agar matrix. Based on the measured effective loss characteristics of solid agar at lower frequencies using N1501A dielectric probe from keysight (Appendix A.1), the resonant frequency was considered from the lower spectrum of microwave frequencies. However, at lower frequencies, the size of resonator increases. Therefore, to design a compact and portable resonator while considering the low loss characteristics of solid agar at low frequencies, the resonant frequency was chosen to be in the L- band (1 GHz– 2 GHz) of the microwave spectrum.

Based on the application, it can be designed as a one-port device or two-port devices. Several sophisticated and complex resonator designs can

be formed by cascading two resonators together or integrating active and passive devices such as power splitters and transistors. In this section, we design a single-port device as it requires less electronic circuitry to measure the response and occupies less substrate space.

Study on the impact of coupling gap width on the resonator

Two transmission lines are said to be coupled when power is transferred due to electromagnetic field interaction between the lines [57]. There are two main modes of propagation of the signal through a coupled transmission line pair: even mode and odd mode. Even mode occurs when the currents in the transmission lines are in equal in amplitude and in the same direction. Odd mode on the other hand occurs when the current in the coupled lines are equal in amplitude but in opposite directions. In a coupled transmission line, the amplitude of the signal can be treated as a superposition of appropriate amplitudes of even and odd modes [57, 108].

The coupling gap (CG) length between the feed line and the split ring resonator impacts the resonant frequency and quality factor of the resonator. Coupling between the feed-line and resonator can be either loose or tight coupling. The coupling between the resonator and the feed-line is considered as loose coupling if the distance between the resonator and the feed line is large. Loose coupling is an indication of the presence of a small capacitance between the coupling gaps. Tight coupling on the other hand arises when the feed line and resonator are closer to each other leading to a large capacitance between the transmission line. Therefore, to determine the optimal coupling distance between the feed line and the split ring such that the capacitance between the feed line and split-ring resonator is minimum, a simulation study was performed where the response of the sensor at different coupling gap distance was performed. The split ring was positioned at an initial distance of 0.4 mm and gradually increased to 1.4 mm in steps of 0.2 mm. The response of the study is shown in Figure 2.12 (b). To understand the impact of coupling gap variation on the electric and magnetic field distribution across the split ring resonator, an EM field simulation was performed. The results of the EM field simulation is presented in Figure 2.12 (c) and (d).

As per the simulated results shown in Figure 2.12 (b), the response of the sensor improved progressively with each increment in the width coupling gap up to 1.2 mm. Further increase in the width of coupling gap from 1.2 mm to 1.4 mm resulted in a decrease in the quality factor of the resonant profile. However, observing the electric and magnetic field distribution across the split ring resonator at various coupling gap widths, the electric field strength

across the coupling gap decreases as the coupling gap width increases.

From Figure 2.12 (d), feed line and split ring resonator is magnetically coupled with each other. The magnetic coupling between the two transmission line is observed to be strongest at a coupling gap width of = 0.8 mm and 1 mm. Further, the coupling capacitance between the feed line and split

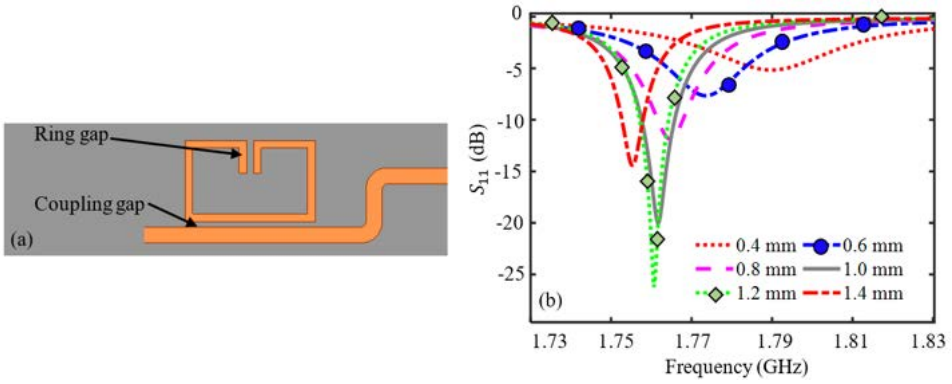

(c) Electric field distribution

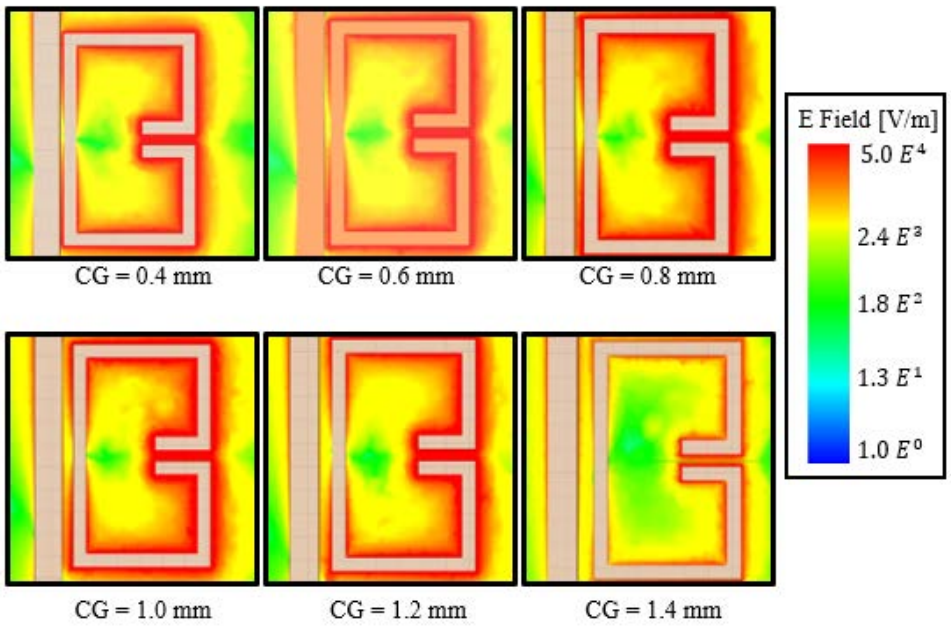

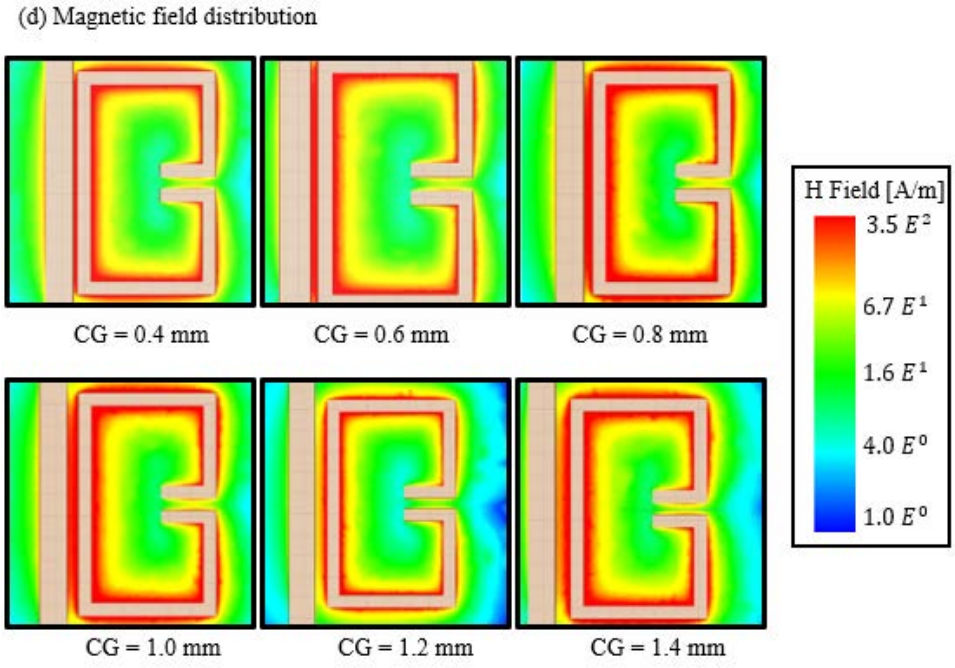

Figure 2.12: A simple split ring resonator with ring gap (RG) and coupling gap (CG) (a). The coupling gap was varied from 0.4 mm to 1.4 mm in steps of 0.2 mm. The S_{11} (dB) vs Frequency (GHz) response of the sensor for different coupling gap widths (b). Electric field distribution (c) and magnetic field distribution (d) across the split ring resonator for various coupling gap widths.

ring resonator at various gap distances was calculated using the equations 2.10 to 2.12 for parallel plate capacitors [109].

$$\Delta t = d + \frac{0.0885 * 10 * d * ln(Lw + 1)}{\pi} \tag{2.10}$$

$$C = \frac{0.0885 * \epsilon_r * 10 * (L + \Delta t) * (w + \Delta t)}{d} \tag{2.11}$$

$$C_{norm} = \frac{0.0885 * \epsilon_r * L * w}{d} \tag{2.12}$$

Where L is the length of the capacitor plates in mm, W is the width of the capacitor plates in mm, d is the distance between the feed line and

split ring resonator in mm, ϵ_r is the relative permittivity of the substrate, C is the total capacitance including fringing capacitance in pF, Δt is the increase in the length and width of the capacitor due to fringing effect.

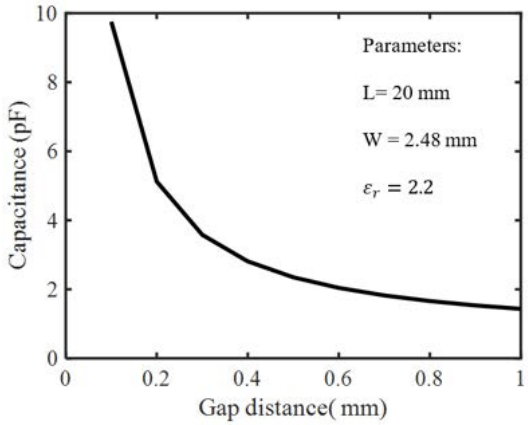

Figure 2.13: Gap distance (mm) versus capacitance (pF) for a parallel plate capacitance.

The effect of the gap distance on the coupling capacitance is presented in Figure 2.13. From the results, it can be observed that as the coupling gap width increases, the coupling capacitance decreases and remains constant after a gap distance of 0.8 mm. Therefore, considering the electric field, magnetic field distribution, and coupling capacitance variation with respect to gap distance, 0.8 mm was selected as the optimum coupling gap width between the feed line and split-ring resonator.

Previous studies on bacterial growth on solid agar such as the one conducted by Mohammadi *et al.* [30] using microwave resonators highlighted the importance of the sensing area to detect bacterial growth. The experiments performed by the team utilized a resonator whose sensitive region covered an area of 2 mm^2(L=2 mm and W= 1 mm). The area covered was able to monitor 1.5 μL of *E. coli*. Thus, to measure a significant area of bacteria using our designed sensor, the ring gap was elongated. The proposed design is shown in Figure 2.14. An alignment marker was added to the design to align the petri dish between the resonator and the test sample.

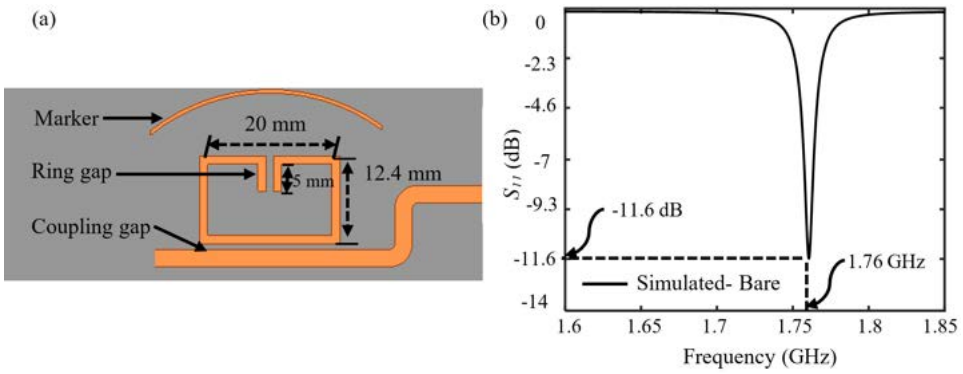

Figure 2.14: Planar split ring resonator modelled in HFSS (a) and the simulated response of the microstrip resonator (b).

Sensitive region determination

A resonator detects changes in the dielectric properties in the vicinity of the sensor by measuring the interaction between the material and the electric field around the resonator. These interactions alter the electrical characteristics of the resonator such as resonant amplitude, resonant frequency, and quality factor through which dielectric properties of the test sample can be interpreted. Thus, it is important to determine the regions across the resonator where electric field intensity is maximized. To determine the electric field distribution across the resonator, the sensor is simulated in High-Frequency Structure Simulator (HFSS) and the magnitude of electric field (E-field) and magnetic field (H-field) across the sensor at the resonant frequency is plotted. The field distributions are shown in Figure 2.15. According to Figure 2.15 (a), a strong magnetic field intensity across the coupling gap of the resonator was observed. The presence of a strong magnetic field indicates strong inductive coupling between the feed line and split ring resonator.

According to the distribution of electric field intensity shown in Figure 2.15 (b), the maximum E-field intensity was observed at the resonant gap indicating high sensitivity to variations of the dielectric properties in its near medium. The presence of a strong electric field intensity indicates a strong capacitance between the ring gap. The electric field intensity is weaker near the coupling gap indicating the presence of a weak capacitance between the feed line and the resonator.

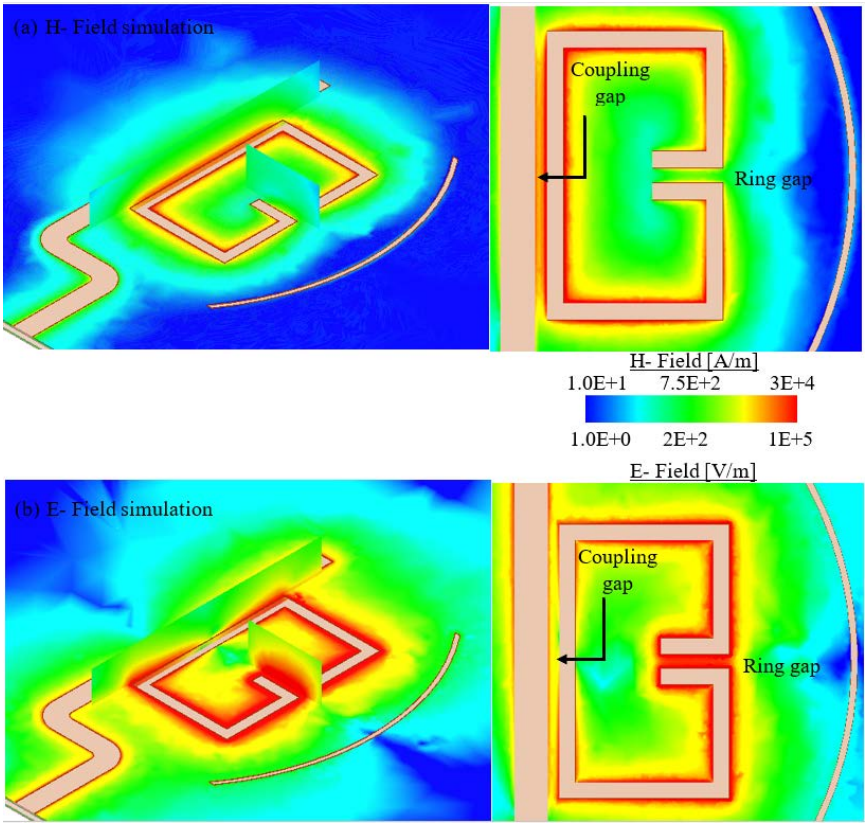

Figure 2.15: H- Field (a) and E- Field (b) analysis of a microstrip resonator.

To further study the impact of the coupling gap and ring gap on the resonator, a test sample is placed on the ring gap and the coupling gap as shown in Figure 2.16 (a)- (c). The test material is a standard sample with permittivity 2.2, loss tangent 0.0009, and dimension 6 x 6 x 1.57 mm. The sample is placed at a height of 0.1 mm above the surface of the sensor. The material characteristics and distance from the substrate were held constant for all the simulations. The simulation results are shown in the Figure 2.16 (b) .

The resonant frequency of the simulated bare sensor was 1.76 GHz. In the presence of a test material covering the entire ring gap, a shift in the resonant frequency was observed from 1.76 GHz to 1.722 GHz with a drop in resonant amplitude from -11.57 dB to -14.36 dB. On the other hand, when the test material was placed on the coupling gap as shown in Figure 2.16

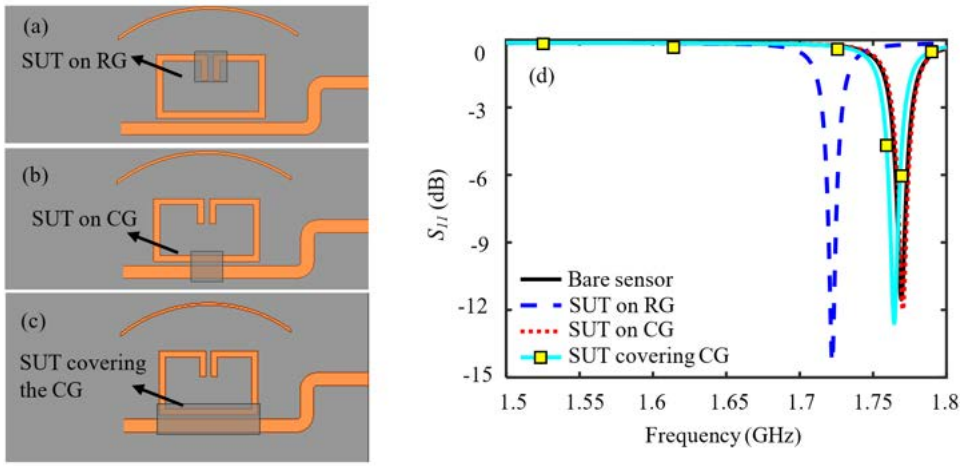

Figure 2.16: Simulation results (d) of a planar microwave resonator with test sample on the ring gap (RG) (a), coupling gap (CG) (b), and on the entire CG (c).

(b), a negligible change in the resonant amplitude and resonant frequency was observed. Therefore, based on the response of the sensor to a test sample placed on the ring and coupling gap, the ring gap was selected as the sensitive region to detect bacterial growth.

Study on the response of the sensor to changes in permittivity and loss tangent at the ring gap

In the previous section, the sensitive region of the sensor was determined by studying the electric field distribution and the impact of test material on the resonant frequency and amplitude of the resonator. In this section, the response of the sensor to changes in the permittivity and loss tangent of a test material on the ring gap will be analyzed and interpreted.

A test sample is placed on the ring gap of the split ring resonator as shown in Figure 2.17 (a). The dimension of the sample was 6 x 6 x 1.57mm and was placed at a height of 0.1 mm from the surface of the substrate. The attributes of the test sample such as orientation, dimension, and the gap between the substrate and the sample were held constant throughout the study. According to the simulation results shown in Figure 2.17 (b) and (c), the resonant frequency and resonant amplitude decreased as the permittivity of the sample increased from 2 to 4 in steps of 0.5 with a

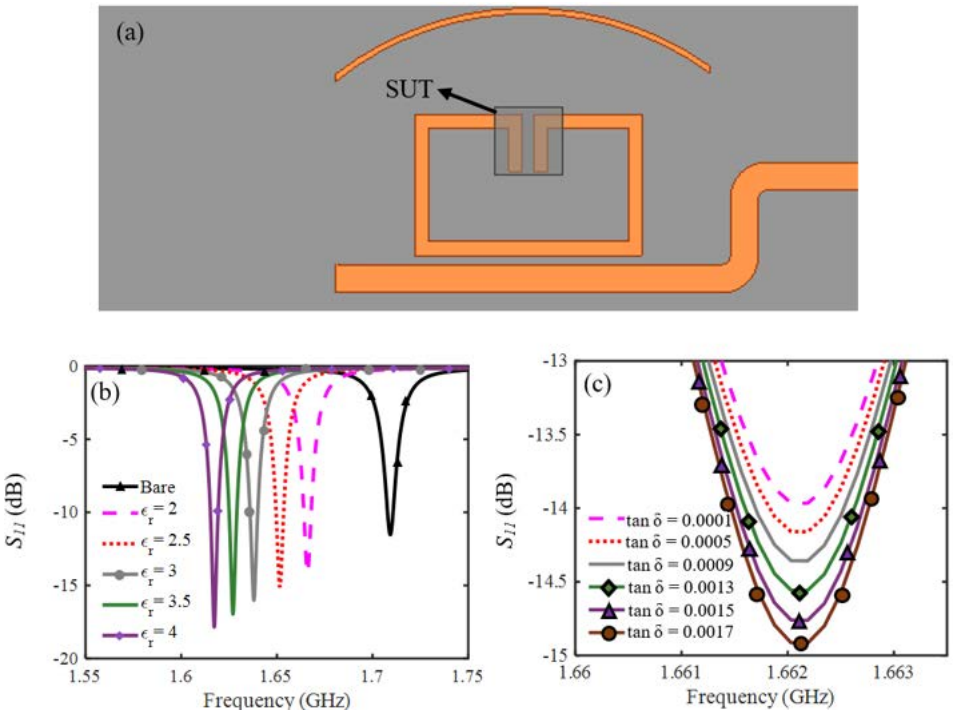

Figure 2.17: A HFSS simulated model of the microstrip resonator with a SUT on the ring gap (a). Effect on the resonant profile (resonant amplitude and frequency) due to variation of permittivity (b) and loss tangent (c) of a sample under test on the ring gap.

constant loss tangent of 0.0009. However, as the loss tangent of the sample was increased from 0.0001 to 0.0017 in steps of 0.0004 while maintaining a constant permittivity, the resonant amplitude decreased with no change in the resonant frequency. Thus, the resonant amplitude was found to be responsive to changes in loss tangent or conductivity of the SUT whereas resonant frequency was found to be responsive to changes in permittivity of the SUT.

Lumped parameter model

Previous sections on the microstrip resonator aimed to understand the distributed model of the resonator utilizing the transmission line. The distributed model enabled us to use complex CAD tools such as HFSS to

understand the interaction between the electric field and the dielectric material under test. However, to understand the behavior of the resonator, a lumped parameter model is used. Figure 2.18 (a) shows the lumped parameter model of the designed resonator. The behavior of the structure is modeled using lumped elements such as resistors (Ohm), inductors (Henry), and capacitors (Farad). In this work, the lumped-element model of the res-

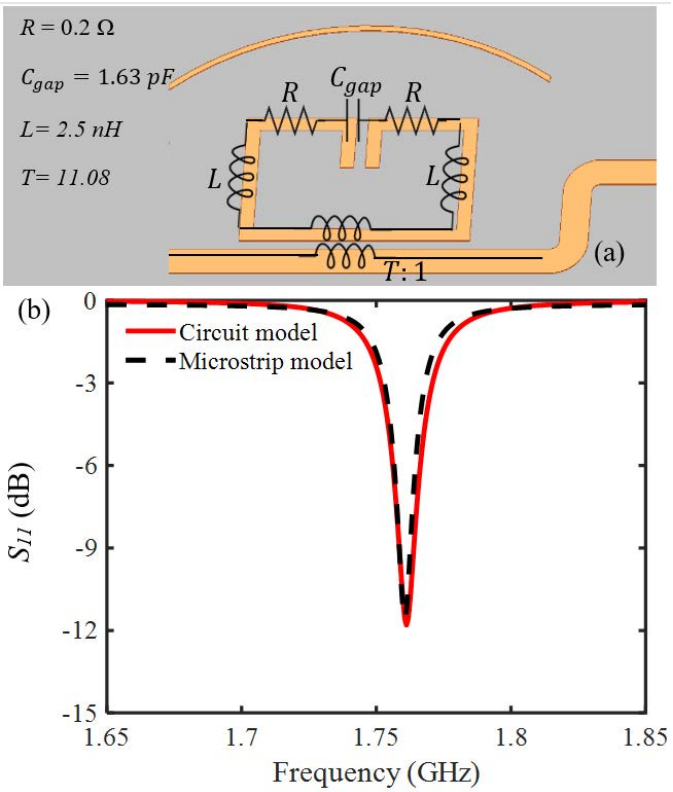

Figure 2.18: Lumped-element model of a frequency variation resonator (a) and the recorded $S_{11}(dB)$ response (b).

onator was designed and simulated in Advanced Design Systems (ADS) 2020 by Keysight Technologies. Based on the resonant frequency, the inductance (L) and capacitance (C_{gap}) of the network were calculated using equation 2.13.

$$L * C_{gap} = (2\pi f_{res})^{-2} \tag{2.13}$$

The series resistance (R Ω) of the network was kept to a minimum to

avoid power loss and the turn's ratio (T = 11.08:1) of the transformer coupling the magnetic field from the feed line to the resonator was adjusted to improve the quality factor of the S_{11} notch. The inductance (L nH) and capacitance ($C_{gap}pF$) was calculated and found to be 5 nH and 1.63 pF, respectively. The coupling capacitance ($C_c = 0.0001pF$) was negligible and had no impact on the result. On further analysis, it was observed that by maintaining a low coupling capacitance (C_cpF) and low series resistance (R Ω), a desired S_{11} response at the desired resonant frequency and quality factor was obtained by modeling the sensor structure. The result of the simulated lumped-element model is presented in Figure 2.18 (b). According to the simulated results, the S_{11} response of the Lumped- element model is in good agreement with the simulated bare result of HFSS.

Challenges to frequency variation sensor

A frequency mode sensor is effective in determining the characteristics of a material such as permittivity and conductivity in environments where ambient fluctuations have a negligible effect on the output of the sensor. However, they lose their advantage to cross-sensitivity caused by variations in ambient factors such as temperature and humidity. Therefore, to overcome this limitation, a differential mode resonator is used. The next section is thus dedicated to the design and analysis of differential mode resonators.

2.3.4 Differential mode resonator design

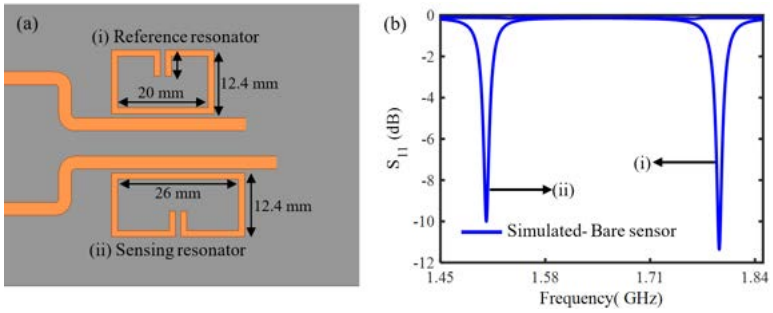

Figure 2.19: Proposed sensor design and its simulated S_{11} (dB) in HFSS.

A differential mode resonator consists of two resonators, sensing, and a reference resonator. The sensing resonator is sensitive to changes in the

dielectric properties of the material and the surrounding environment. The reference resonator, on the other hand, is only sensitive to changes in the surrounding environment and so acts as a control. Therefore, a difference between the sensing and reference resonator outputs eliminates the cross-sensitivity of the ambiance on the measured result.

The proposed differential resonator is shown in Figure 2.19. The two resonators: sensing resonator operating at 1.514 GHz and a reference resonator operating at 1.797 GHz were designed. The sensor was designed on rogers 5880 with permittivity 2.2, loss tangent 0.0009, and thickness 0.79 mm. Based on the resonant frequencies and permittivity of the substrate, the length of the sensing and reference resonators was calculated as 67 mm and 56.3 mm respectively. However, as a capacitive arm of 5 mm was required to detect and monitor bacteria growth, the lengths of the resonator was adjusted to achieve the selected resonant frequencies. The width of the microstrip transmission line was calculated to be 2.48 mm. The ring gap and coupling gap for both the sensing and reference resonator was selected as 1 mm and 0.8 mm respectively. The dimensions of the resonator are shown in Figure 2.19.

Sensitive region determination

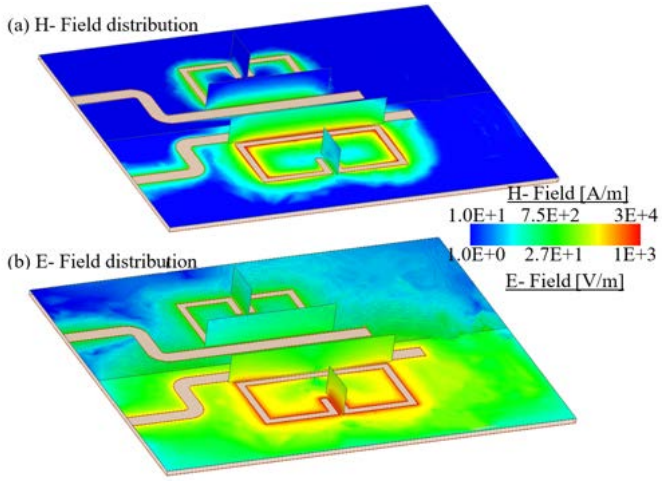

Figure 2.20: H- Field distribution (a) and E field distribution (b) of the designed differential resonator at 1.502 GHz.

To determine the sensitive region of the resonator, an electric field and magnetic field simulation was performed in HFSS. Figure 2.20 presents the EM field distribution at 1.509 GHZ. According to the simulated results, a region of strong magnetic field was observed at the coupling gap as compared to the ring gap indicating a strong electromagnetic coupling between feed line and the resonator. However, figure 2.20 (b) shows strong electric field intensity concentrated at the ring gap of the sensing resonator indicating high sensitivity to variations in the dielectric properties in its vicinity.

However, to validate the sensing region of the resonator, an analysis in HFSS has been performed by placing a test material at two different locations as shown in 2.21.

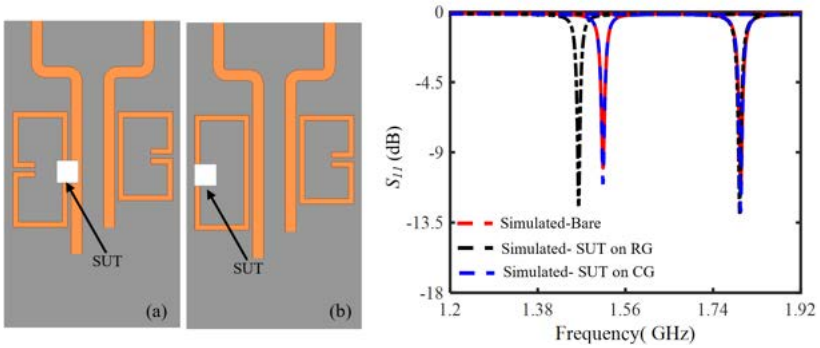

Figure 2.21: Simulation results of a differential microwave resonator with test sample on the coupling gap (CG) (a) and ring gap (RG) (b) of the sensing resonator.

The test material simulated was a standard sample with a permittivity of 2.2, loss tangent of 0.0009, and the dimension of 6 x 6 x 1.79 mm. The parameters of the test sample such as orientation, dimension, and the distance between the substrate and the test material were kept constant. According to the simulated results shown in Figure 2.21, a frequency shift of 50 MHz was observed when the material was placed at the ring gap while the reference output was unaffected. However, as the material was placed on the coupling gap, a negligible change in the resonant amplitude and resonant frequency of both the sensing and the reference resonator was observed. Therefore, the ring gap was found to be more responsive to the presence of a dielectric material as opposed to the coupling gap and was chosen for measurements.

2.4 Chapter conclusion

In this chapter, two different schemes of microstrip resonators: frequency variation resonators and differential mode resonators have been discussed. The proposed resonator designs were thoroughly analyzed and studies to determine the sensitive regions of the resonator. Based on the study, frequency variation resonators found applications where temperature and other environmental factors were constant and had minimal impact on the resonator outputs. However, in the case of significant variation in the ambient factors, differential mode resonators were used. The next chapter will discuss the steps followed to fabricate the resonator and also discuss the various functional tests performed to validate the operation of the sensor.

Chapter 3

Fabrication and evaluation of the designed sensor

This chapter focuses on the fabrication and functional verification of the sensor. This chapter begins with the step by step in- house fabrication procedure followed to precisely and accurately fabricate the sensor. The operation of the fabricated sensor will then be investigated using a standard dielectric test material. This chapter presents the best outcomes of the several tested sensors. The final sensor design of the microwave sensors was achieved after weeks and months of numerous sensor design optimizations, and an in-depth analysis of the measured results.

3.1 Sensor fabrication

To test the viability of the simulated designs, the sensors need to be fabricated. Fabrication is a crucial step and involves various chemicals and strong etchants. If performed incorrectly, errors in this step can damage the fabricated sensor. The steps followed to fabricate the resonator using in-house fabrication equipment is described below. The finalized layout of the resonator was first transferred to laminated paper. To preserve the intricate features of the resonator, a high-resolution laser printer was used to transfer the design to a photocopy paper. The printed design was then patterned on the selected substrate using a swingline thermal laminator. Under the application of heat, the pattern from the photo paper was transferred to the selected laminate i.e. Rogers 5880 with permittivity of 2.2 and dielectric thickness of 0.79 mm. The patterned substrate was then subjected to an etching process using a bath containing 750 gm ammonium persulphate in 5 liters of water. Ammonium persulphate is an excellent copper etchant and is widely used for PCB fabrication. The ammonium persulphate reacts with the exposed unwanted copper forming copper sulfate that dissolves in the bath. The bath was constantly aerated and warmed to increase the etching rate. The etching was thoroughly monitored as over-etching could result in

an irreversible damage to the designed sensor.Once, the unwanted copper was etched from the substrate, the etched substrate was washed using 95% acetone. This substrate was rinsed until the ink from the patterned design was completely removed revealing the copper traces. The sensor was then washed in RO water to remove traces of acetone from the substrate. A SubMiniature version A or SMA connector was soldered to the sensor. The fabricated sensor is shown in Figure 3.1 and was functionally verified before using it for its intended application.

To verify the working of the developed sensor, the fabricated sensor was connected to a vector network analyzer (VNA) ZNB20 from Rhode and Schwarz. The fabricated sensor was mechanically stabilized on the table to avoid measurement errors due to mechanical vibrations from the environment. The VNA was calibrated from 1 GHz to 2 GHz with an intermediate frequency bandwidth of 300 Hz and an input power of 0 dBm. The resolution or number of points was set to 6401 before measurements. An automated program was coded in LabVIEW to extract the resonant profile details such as resonant amplitude and the resonant frequency at a rate of every 2 minutes.

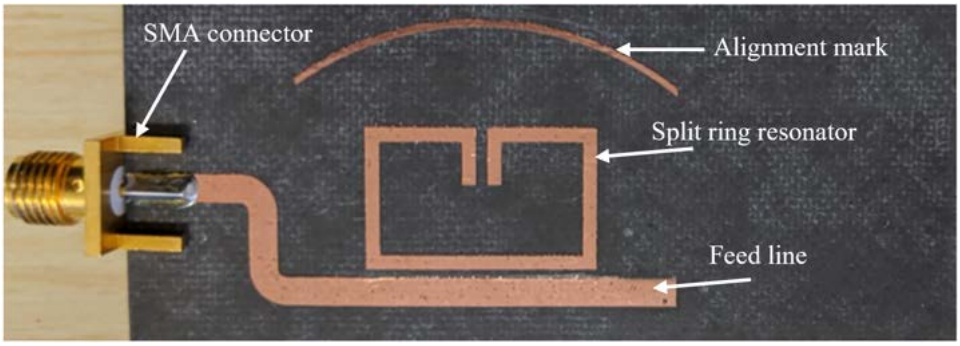

Figure 3.1: Fabricated planar microstrip resonator.

While performing a time-based measurement of the fabricated sensor, it was observed that the response of the sensor was degrading over time. Upon investigation, this phenomenon was linked to the accumulation of static charge on the surface of the resonator. Therefore, to discharge the static, the resonator had to be connected to ground without impacting the operation of the designed sensor. Thus, the resonator was redesigned to incorporate a quarter wavelength microstrip short stub connected to a ground plane. The microstrip stub acts as open circuit to the electromagnetic signals at

the resonant frequency and short circuit to the static charges. The modified resonator design is shown in Figure 3.2.

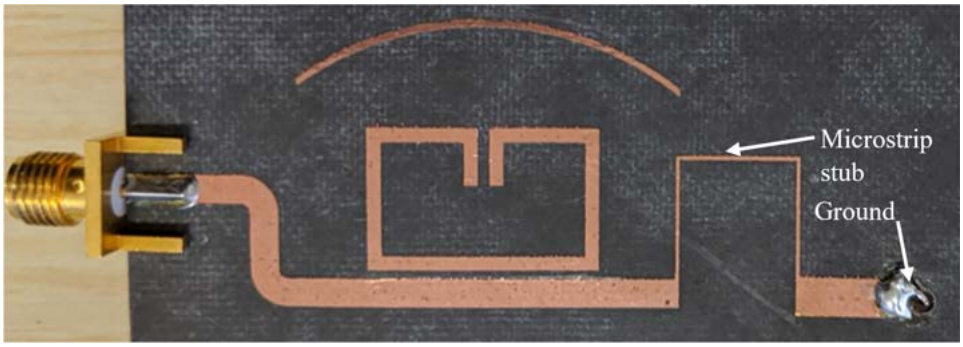

Figure 3.2: Fabricated planar microstrip resonator with ground.

3.2 Evaluation of Frequency variation sensor

3.2.1 Impact of SUT on the sensitive region of the sensor on the electrical characteristic of the sensors

To study the impact on the response of the resonator in the presence of a sample under test, the reflection coefficient or S_{11} response of the fabricated sensor was measured. The response of the sensor in the absence of any test material is shown in Figure 3.3. The resonant frequency and resonant amplitude of the fabricated sensor in the absence of any test material were measured to be 1.76 GHz and -13.52 dB respectively.

To determine the sensitive region of the resonator, a test sample whose permittivity was close to the effective permittivity of solid agar in a petri dish was chosen. The steps followed to measure the effective dielectric properties of solid agar is presented in Appendix A.1. Among the available test substrates, a 6 x 9 mm test sample machined from a standard Rogers 5880 substrate with permittivity of 2.2, loss tangent of 0.0009 and thickness 1.79 mm was chosen to study the effect of test material on the response of the sensor. The sample was placed on the ring gap and the coupling gap and the response of the sensor was measured as shown in Figure 3.3.

As evident from the measured results, a resonant frequency shift of 50 MHz is observed when the test sample is placed on the ring gap whereas a negligible resonant frequency shift of 1 MHz was observed when the mate-

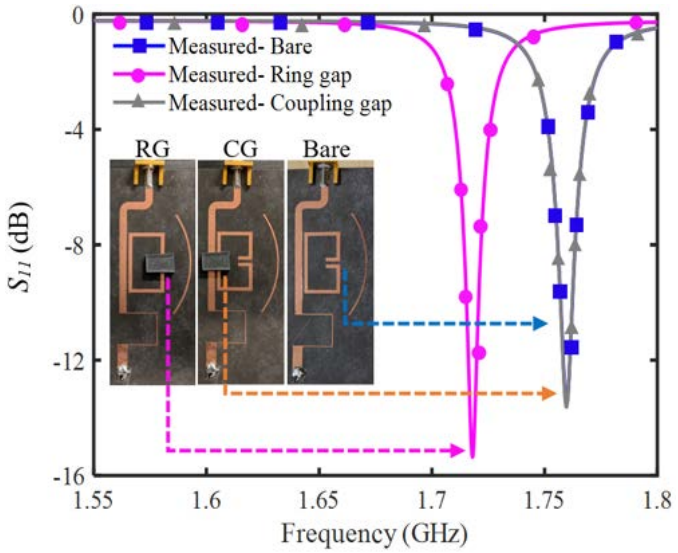

Figure 3.3: Measured response of the sensor in the presence of test sample on the ring gap and coupling gap.

rial was placed on the coupling gap. Thus, the ring gap was found to be responsive to the presence of a test material as opposed to the coupling gap and is in good agreement with the simulated results.

3.3 Evaluation of differential mode resonator

3.3.1 Impact of SUT on the sensitive region of the sensor on the electrical characteristic of the sensors

The fabricated differential-mode resonator is shown in Figure 3.4 (a). The sensor consists of two simple resonators: one acts as a sensing resonator and the other as a reference resonator. The resonators are grounded using microstrip stubs as shown in Figure 3.4 (a). The response of the bare resonator in the absence of a sample under test is shown in Figure 3.4 (b). To study the impact on the response of the resonator in the presence of a sample under test, the reflection coefficient, or S_{11} response of the fabricated sensor was measured. The resonant amplitude and resonant frequency of the sensing resonator and the reference resonator in the absence of any test material were measured to be -10.38 dB at 1.508 GHz and -11.56 at 1.7946

GHz respectively. To determine the sensitive region of the resonator, a 6 x 6 mm test sample machined from a standard Rogers 5880 substrate with permittivity of 2.2, loss tangent of 0.0009 and thickness 1.79 mm was obtained. The response of the sensing and reference resonator due to the presence of test material on the ring and coupling gap of the sensing resonator is shown in Figure 3.4 (b).

A shift in the resonant profile of the sensing resonator was observed from -10.38 dB at 1.508 GHz to -11.51 dB at 1.465 GHz due to the presence of the test sample with minimum to no impact on the output of the reference resonator. However, the presence of the test sample at the coupling gap (CG) had no impact on the output of the sensing and reference resonator as seen in Figure 3.4. Thus, the ring gap was found to be responsive to the material as opposed to the coupling gap and is in good agreement with the simulated results.

3.3.2 Conversion of two- port to one- port microstrip device using a power splitter

The differential resonator fabricated in the previous section was a two-port device operating at 1.509 GHz and 1.798 GHz respectively. However, to reduce the electronics required to perform measurements, the device was transformed into a one-port device using microwave power splitters or power dividers. Among the available power splitters such as Wilkinson, T- Junction, and Rat- race junction power dividers, the Wilkinson power divider was widely used due to its ability to efficiently split the input power between its outputs while maintaining a matched condition on all ports. However, conventional Wilkinson power splitters operate in a narrow range of frequencies and fail to efficiently divide input power at frequencies outside their operational bandwidth. Thus, to overcome this limitation, an off the shelf wideband power splitter was used.

The advantage of using a wideband power splitter lies in its ability to provide stable power output at its output ports for a wide range of frequencies. The power splitter also provides a high degree of isolation between its output ports. Therefore, a wide band power splitter ZAPD-21-S+ from Mini circuits capable of providing a stable power output between 0.5 and 2 GHz was used with the sensor as shown in the Figure 3.5 (a).

To study the effect of the power divider on the response of the resonator, the transmission coefficient of the sensing and reference resonator was measured individually and compared with the transmission coefficient of the sensor combined with the power divider (shown in Figure 3.5 (b)).

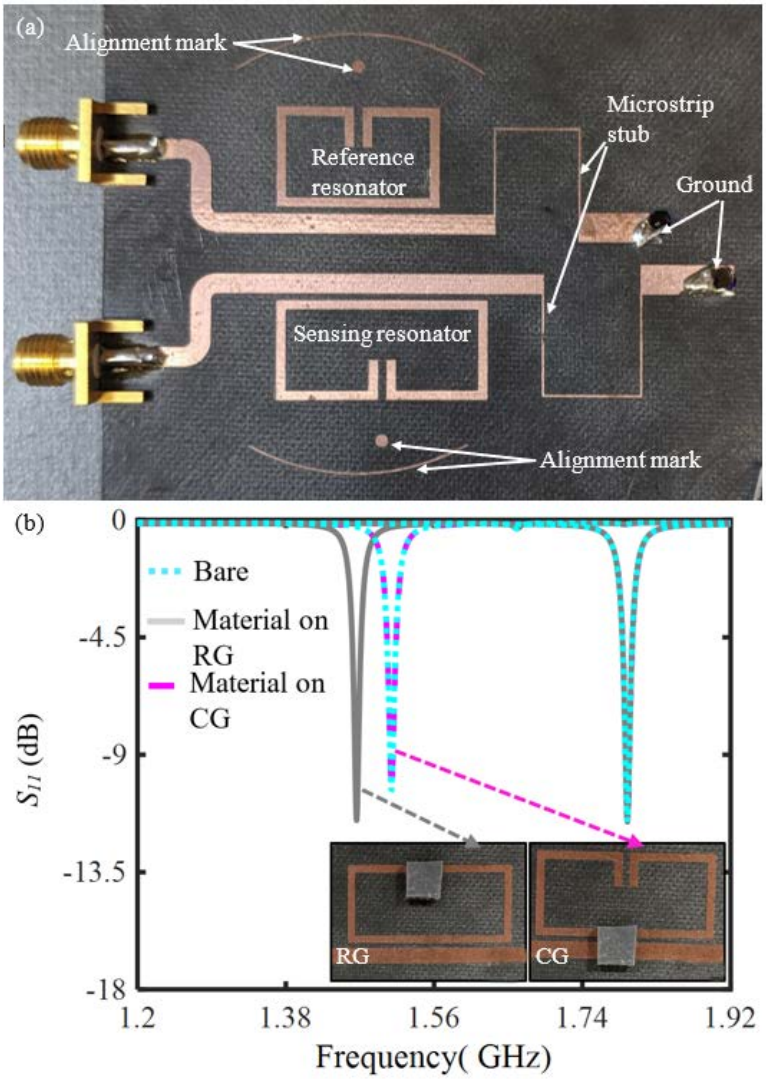

Figure 3.4: Fabricated resonator on Rogers 5880 (a) and measured results with test sample on the ring gap (RG) and coupling gap (CG) of the sensing resonator (b).

According to the measured results, due to the integration of a power divider with the fabricated resonator, a -3 dB drop in the resonant amplitude is observed with minimum impact on the resonant frequency. The drop in

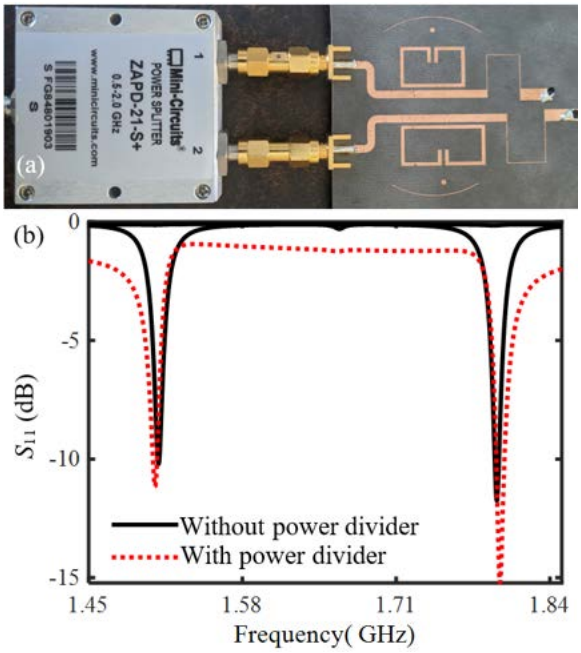

Figure 3.5: Fabricated differential resonator with a wide band power splitter (a) and measured $S_{11}(dB)$ response of the fabricated sensor with and without the power splitter (b).

the amplitude can be attributed to the insertion loss of the power splitter. Thus, integration of power divider had a minimum impact on the electrical characteristic of the resonator and thus was used to convert the two-port differential sensor to a one-port device.

3.4 Chapter conclusion

In this chapter, the steps followed to fabricate two different designs of microstrip resonators such as frequency variation resonators and differential mode resonators have been discussed. The fabricated sensor was then subjected to a test to determine the sensitive region of the sensor. Determining the sensitive region of the sensor enables us to proceed further and investigate and monitor bacterial growth on solid media subjected to various external factors such as nutrient availability, subsurface position, and presence of antibiotics.

Chapter 4

Application of custom-designed microstrip resonators for real-time and contactless monitoring of bacterial growth on solid media

This chapter includes the experiments conducted to assess the ability of the designed planar microwave resonators for real-time and contactless bacterial growth monitoring on solid agar medium. The growth of bacteria is influenced by several factors including temperature, growth media composition, nutrients availability, and presence/absence of inhibitory compounds. Precisely, through this chapter, we demonstrate the ability of microwave device to detect and characterize the impact of external factors on the growth profile of bacteria (*E. coli*).

The first study presented in this chapter is a proof of concept and examines the potential of a microwave sensor to detect and monitor the influence of various amounts of glucose (0, 2, 5, and 10 %) in Luria-Bertani (LB) agar on the growth profile of *E. coli*. Glucose supplements at varying concentrations to growth media can accelerate or inhibit the growth of bacteria. Therefore, through this study, the ability of the microwave resonator to accurately and swiftly differentiate the impact of glucose concentration on the growth of bacteria is also presented. The measured results were compared with the microscope images captured at constant intervals of time to verify the sensor's competency as a bacterial growth monitoring tool. The second study investigates the capability of the sensor resonator to monitor subsurface growth of *E. coli* confined between two layers of LB agar. The growth of bacteria confined between two layers of solid growth media progresses by

transitioning from a 2-Dimensional growth to 3-Dimensional growth. The variations in the dielectric properties of the growth medium due to lateral and subsurface growth of *E. coli* were monitored by the sensor and presented here. A third novel study demonstrates the potential of the designed microwave sensor to monitor the effect of antibiotics, erythromycin (0, 7.5, 30, and 45 μg) on the growth of *E. coli*. It is well known that various concentrations of antibiotics have a different impact on bacterial growth. Therefore, early detection and monitoring of the growth of bacteria in the presence of antibiotics using sensor technology can contribute to antibiotic treatment.

The studies presented in this chapter demanded a year of continuous measurements and sample preparations which includes the failed attempts to prepare an agar plate for bacterial growth monitoring growth. Moreover, throughout the course of this work, a considerable amount of time was spent on researching and optimizing the sample preparation technique, analyzing the measured results, and upgrading the experimental setup to avoid any interference of external factor (e.g. temperature) on sensor measurements.

4.1 Microwave resonator reveals glucose dependent growth profile of *E. coli* on solid agar

4.1.1 Background

Bacteria require nutrients during metabolism to sustain growth. The availability of crucial nutrients such as carbon can modify the morphology and impact the growth rate of microorganisms such as *E. coli*[110, 111]. Traditional plating methods such as spread and pour plate techniques have been widely employed to monitor and characterize the impact of nutrient availability on bacterial growth [112]. However, these methods were not real-time, require a longer incubation period to detect noticeable bacterial growth, and were more prone to contamination. Recently, non-contact microwave sensors have proved to be a viable tool to measure bacterial growth in liquid matrices [50, 113, 114]. A recent study by Mohammadi *et al.* [30] demonstrated the capability of planar microwave sensors to monitor bacterial growth on solid media. This research further investigates the capability of a microwave sensor to study the impact of nutritional parameters on the growth profile of *E. coli*. Their work was able to successfully demonstrate the capability of a microstrip resonator to monitor bacteria growth on the surface of solid agar. The bacterial growth was monitored by gauging the

change in the resonant amplitude due to variation of the conductivity of growth medium due to bacteria metabolism.

4.1.2 Material and method

Sample preparation

To prepare solid LB agar media with 2%, 5%, and 10% glucose concentration, 1 gm of LB broth and 0.75 gm of LB agar was mixed with 50 ml RO water in a flask. The resultant solution was then mixed with 1 gm, 2.5 gm, and 5 gm of powdered glucose to achieve 2%, 5%, and 10% of glucose concentration in the media respectively. The media was placed in an autoclave for 15 minutes at 121 $^{\circ}C$ to completely sterilize and kill any bacteria spores present in the growth media. The sterile media was cooled down to 50 $^{\circ}C$. To achieve a uniform thickness of 1 mm across the petri dish, 3 ml of the sterilized media was poured in the petri dish. The cross-section of the agar plate is shown in Figure 4.1.

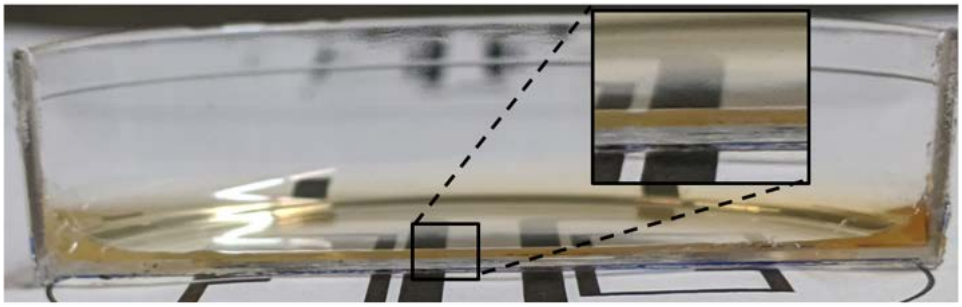

Figure 4.1: Cross-section of a solid agar plate.

The media preparation was performed in a fume hood or in the presence of a bunsen burner to avoid contamination of the sample with unwanted and airborne fungi. Fungi contamination leads to degradation of the plate and results in false positives. The fungi-contaminated agar plate is shown in Figure 4.2 (a). The plate was carefully sealed using a parafilm after the solid media reached room temperature. Sealing the media plate while the agar is still under the process of solidification leads to precipitation which alters the water content in the petri dish and thereby render the plate unusable for future experiments as shown in Figure 4.2 (b).

The above steps outline the general steps followed to prepare a control plate i.e. with no bacteria inoculated on the surface of the agar. To prepare

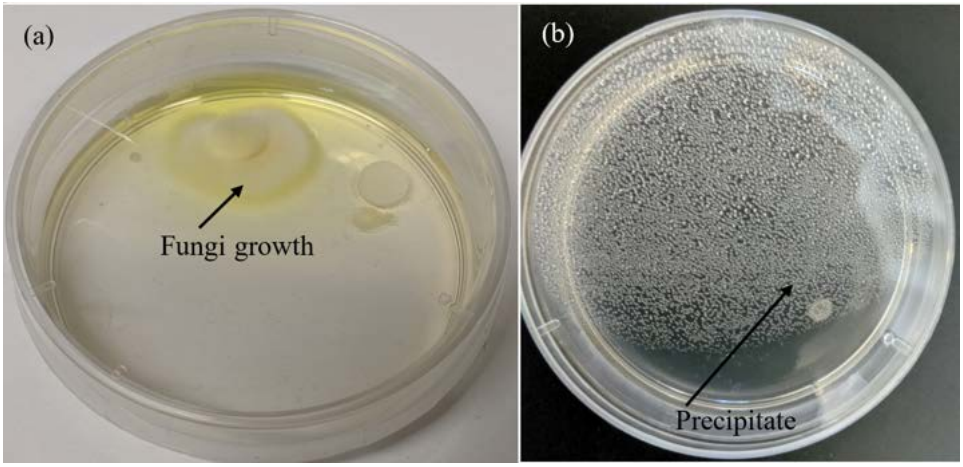

Figure 4.2: solid agar plate contaminated with airborne fungi (a) and solid agar plate with precipitation (b).

inoculated agar plates, 3 μL of *E. coli* sample is spotted onto the agar plate using a sterilized loop or pipette at the desired location and dried. In this study, the HB101 strain of *E. coli* was used. The *E. coli* strain is non-pathogenic and has a rapid growth rate at optimal growth conditions. The optical density at wavelength of 600 nm (OD_{600nm}) measured using a spectrophotometer was found to be 1.5. The plate is then sealed using parafilm to avoid cross-contamination and preserve the nature of the contents of the petri dish.

Experimental setup and procedure

To monitor the influence of 0 % (no glucose), 2 %, 5 % and 10 % glucose on the growth profile of *E. coli*, a differential microstrip resonator was used. The inoculated solid agar plate was placed on the sensor covering the sensing resonator and the reference resonator. The inoculated bacterial spot was aligned directly above the sensitive region of the sensing resonator as shown in Figure 4.3.

To measure the response of the fabricated resonator, the sensor was connected to a vector network analyzer, ZNB20 from Rhode and Schwarz. The VNA was calibrated from 1 GHz to 2 GHz with an Intermediate frequency bandwidths of 300 Hz and an input power of 0 dBm. The resolution or number of points was set to 6401 before measurements. An automated program

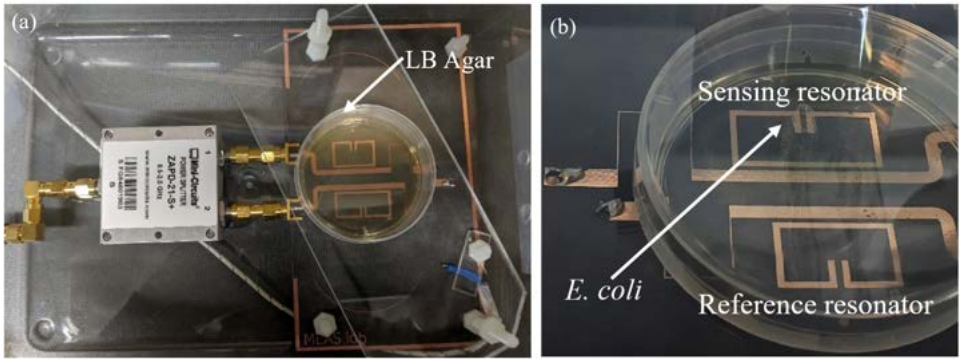

Figure 4.3: Placement of agar plate on the differential resonator (a). Inoculated bacteria aligned with the sensing region of the sensing resonator (b).

was coded in LabVIEW to extract the resonant profile details such as the resonant amplitude and the resonant frequency at a rate of every 2 minutes. The experimental setup is shown in Figure 4.4.

4.1.3 Measurement result and discussion

To monitor the growth of *E. coli* in solid media, an experiment was conducted using an inoculated agar plate with no added glucose (control plate). The aim of this experiment was to test the working of the microwave resonator as a device capable of monitoring bacteria growth. The sensing resonator was employed to monitor the media surrounding the *E. coli*. The reference resonator was used to monitor variations in the media due to temperature fluctuations. The measured resonant amplitude of sensing and reference resonator was normalized by subtracting with the initial value of their respective resonant amplitudes to diminish the impact of external factors. Further, the difference between the normalized sensing and reference resonators' amplitudes (Δ Resonant Amplitude (dB)) was calculated to nullify the impact of ambient factors such as temperature and humidity variations on the measured results. Analysis of the measured results and the ambient temperature data revealed that the measured results were influenced by external factors such as temperature and external vibrations. Considering this influence of the external factors on the sensor's response, the sensing apparatus was modified. Permanent fixtures and foams were incorporated into the sensing apparatus to reduce external vibrations. The

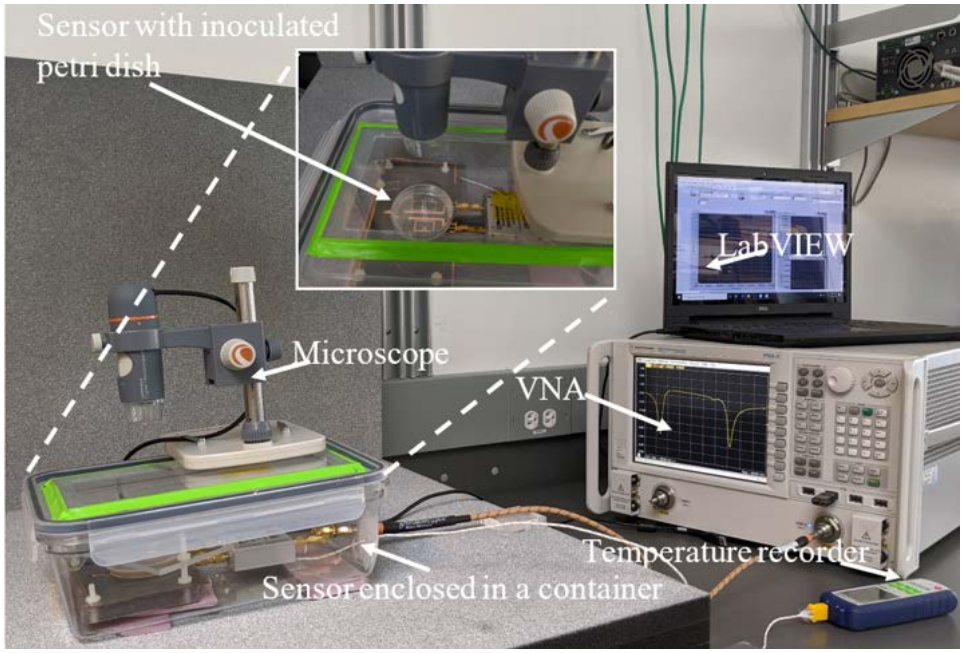

Figure 4.4: Experimental setup to monitor bacterial growth under various nutrient conditions. The setup consists of a container with sensor enclosed within it, a temperature probe, a microscope, VNA and LabVIEW to control the VNA.

first 60 minutes of recorded data were excluded from the experimental measurements accounting stabilization of the sensing apparatus and the VNA after calibration. The residual impact of temperature on the differential response due to non-uniformity of the agar plate was identified and eliminated by normalizing (Δ Resonant Amplitude (dB)) with the recorded temperature. The measured resonant amplitude variation and resonant frequency variation versus time representing growth phases of *E. coli* on LB agar with varying glucose concentrations (0%, 2%, 5% and 10%) is shown in Figure 4.5. From the measured results, variation in the resonant amplitude(Δ resonant amplitude) resembles with the growth profile of *E. coli* as opposed to variation in the resonant frequency (Δ Resonant frequency) and was thus selected for further analysis.

Studies have reported that high concentrations of solutes such as sugar or glucose in the environment surrounding the bacteria alters the water levels surrounding the bacteria resulting in a high osmotic pressure in the vicinity

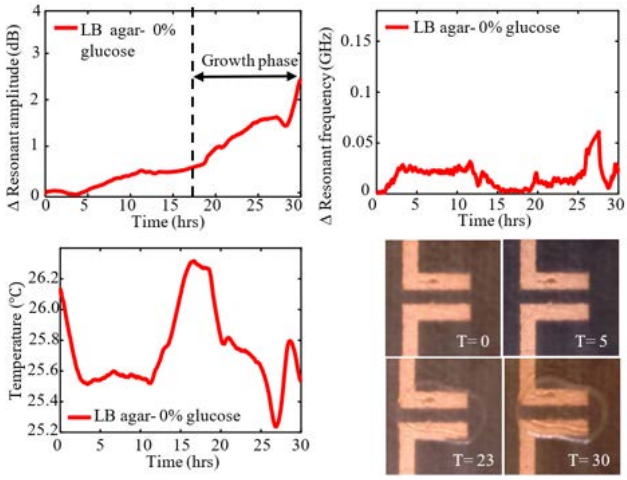

(a) LB agar with 0% glucose

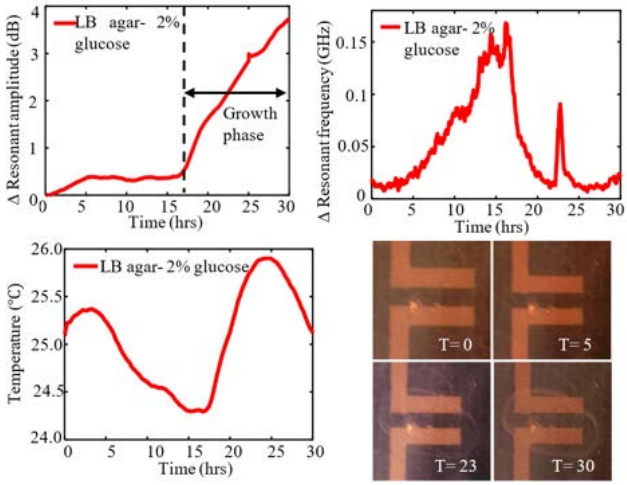

(b) LB agar with 2% glucose

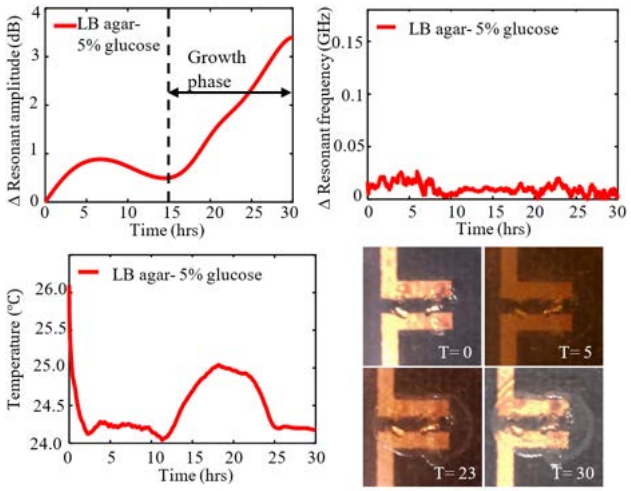

(c) LB agar with 5% glucose

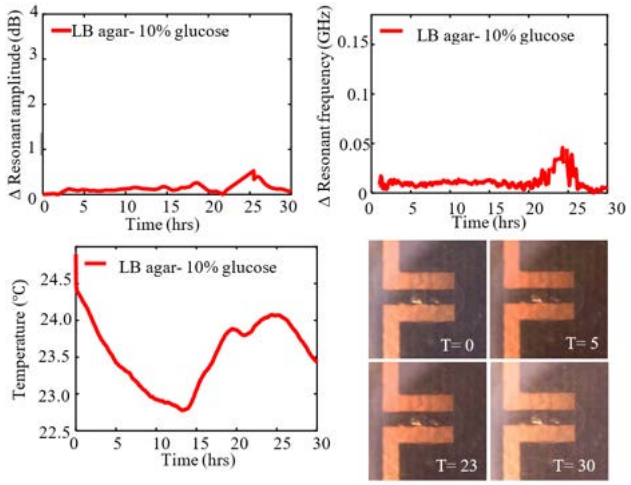

(d) LB agar with 10% glucose

Figure 4.5: Measured Δ Resonant amplitude (dB), Δ Resonant frequency (GHz), recorded temperature (∘C), and microscopic images of *E. coli* captured at constant time intervals for 0% (a), 2% (b), 5% (c), and 10% (d) of glucose in LB agar.

of the bacteria [115]. High osmotic pressures exerts stress on the bacteria which suppresses bacterial growth [115]. Therefore, a complete inhibition of bacterial growth was witnessed at 10 % glucose. The signal equivalent to no growth was derived from this (0.52 dB) and was selected as a threshold to differentiate between no growth phase and growth phase essential for growth measurements. The region of the measured response below the threshold i.e 0.52 dB was classified as no growth region. As *E. coli* is introduced into the growth medium through inoculation, the bacteria gradually adapts to the new environment, consumes nutrients and prepares for cell division. Various factors such as availability of nutrients, environment temperature, culture medium, pH, inoculum size, the physiological history of the cells, and the precise physiochemical environment of both the original and the new growth medium can impact the generation time of *E. coli* during no growth or lag phase [116–118]. Therefore, due to various ambiguities in the no- growth phase, this study focused on detection and monitoring of changes in the growth phase of bacteria under various nutrient conditions. The growth phase is the region where rapid multiplication of *E. coli* occurs. Based on the threshold value i.e. 0.52 dB, the onset of the growth phase for 0%, 2%, and, 5 % glucose was noted at 17, 17.03, 15.6 hr. respectively.

The slope of the linear growth phase representing the rate of change of the resonant amplitude due to change in the growth rate was calculated and found to be 0.10913 dB/hr, 0.23646 dB/hr and 0.21410 dB/hr with a coefficient of determination 0.9004, 0.98545 and 0.99752, respectively as presented in Table 4.1.

Table 4.1: Measured growth phase and rate of change of resonant amplitude for *E. coli* at various concentrations of glucose in LB agar

Glucose Percentage %	Onset of growth phase hr	Rate of change of amplitude variation (dB/hr)	Coefficient of determination R^2
0	17	0.10913	0.90042
2	17.03	0.23646	0.98545
5	15.6	0.21410	0.99752

The data shows that the rate of change in resonant amplitude was highest at 2 % glucose (0.23646 dB/hr) compared to 0 % (0.10913 dB/hr.). However, a slight decrease of the rate was observed as the glucose concentration reached 5 % (0.2141 dB/hr.) and a complete inhibition of bacterial growth

was observed at a glucose concentration of 10%. The accuracy and performance of the designed sensor to monitor bacterial growth on various LB agar- glucose media was further backed by microscope images as shown in Figure 4.5. This further confirms the effectiveness of the designed microwave resonator to study factors influencing bacterial growth in solid agar thereby overcoming the shortcomings of conventional bacterial growth monitoring methods.

4.2 Microwave resonators to detect and monitor subsurface growth of *E. coli* on solid agar.

4.2.1 Background

Infectious diseases caused by biofilm forming bacteria such as periodontitis and cystic fibrosis pneumonia pose serious challenges to public health and global economy [119–123]. Most biofilm related infections are difficult to treat as they tend to resist various antibiotics and biocides [124–126]. Moreover, contamination of medical devices and implants by biofilm forming bacteria can limit the usability of the device and could also lead to life threatening infections[121, 127–130]. The U.S Department of Health and Human Services have reported that roughly one among 24 infection cases in USA are related to contaminated medical devices such as catheters, heart valves, and prosthesis [127, 131]. Therefore, it is of paramount importance to detect and monitor subsurface bacteria biofilm growth on tissues due to contaminated implants to prevent life threatening infections.

Prior to detecting and monitoring subsurface bacterial growth, it is necessary to understand the growth mechanism of bacteria biofilms. A bacterial colony in a biofilm initially grows on the surface of the medium in 2D and later progresses into 3D [132, 133]. In the absence of any obstruction, the transition from 2D to 3D occurs by bacteria expanding in the space above the surface of the growth medium. However, in the presence of an obstruction, the bacteria tend to proliferate and expand into the medium [132]. Studies on the behavior of such transitions suggested that various mechanical forces on the bacteria played a vital role in the transition of microcolonies from 2-D to 3-D [129, 134]. Various forces act on the bacterium such as i) repulsive forces between the bacterium ii) frictional force between the bacterium and iii) elastic forces of the surrounding media [129, 132]. Such forces can strain the bacteria to a transition point known as “buckling transition” at which bacteria begin to invade its surrounding media.

The current technologies to detect these pathogens rely on either conventional culture–based assays or molecular methods such as polymerase chain reaction (PCR), enzyme-linked immunosorbent assays (ELISA) and mass spectroscopy. However, these are often limited by longer detection time as in the case of culture based assays or requires extensive sample preparation and expensive instrumentation in the case of molecular tools [12–14]. To overcome these limitations, researchers developed biosensors for rapid detection and monitoring of microbial growth that can be used in pathogenic detection [15–20]. Of these techniques, optical and electrochemical biosensors were widely used owing to their real-time, automated and label-free detection. However optical biosensors suffer from high cost and quick degradation of reagents whereas electrochemical biosensors suffer from a low selectivity and limit of detection (LoD) [20]. Bio-FET are another class of biosensors which are gaining popularity due to their label-free, ultra-high sensitivity, scalability, low cost of fabrication and minimum power consumption [20, 135–137]. Although, the benefits of bio-FET make it a promising candidate for detection and monitoring of bacteria, these sensors cannot be used in contactless applications. Recently, microwave sensors have emerged as a potential detection method for various applications including dielectric spectroscopy, monitoring cancer, detection of glucose and electrolyte level in aqueous solution, and classification and monitoring of bacteria in liquid medium owing to their numerous advantages such as low cost, real time, label-free and non-contact monitoring [31, 50, 68, 138]. Interestingly, bacterial monitoring using microwave sensors is gaining more attention in recent years.

Through this current research, the capability of the microwave sensor to monitor subsurface bacterial growth was explored. To the best of our knowledge, this is a maiden attempt in this direction. The experiment was carried out at two different initial volumes of *E. coli* i.e. 3 μL and 9 μL sandwiched between two layers of solid LB-agar using microwave resonator owing to their robustness, low fabrication cost, contactless and label-free properties. The changes in the characteristics of the medium due to the lateral and subsurface growth of the bacteria are studied by measuring the variation in the resonant amplitude of the microstrip resonator at two different volumes of bacteria.

4.2.2 Material and method

Sample preparation

To measure subsurface bacteria growth on solid agar media, a 1 mm thick sterilized soft agar media sample(1 gm of LB broth and 0.5 gm of LB agar) was prepared.

Three μL of *E. coli* was then spotted at the designated position on the agar plate. The inoculated bacteria were then covered by a sterilized 18 x 18 mm glass cover slip coated with 8 ml of soft agar as shown in Figure 4.6. The agar was cooled to room temperature to avoid precipitation and sealed using a parafilm. The process of encapsulating the *E. coli* was crucial and required a month of practice prior to performing the study.

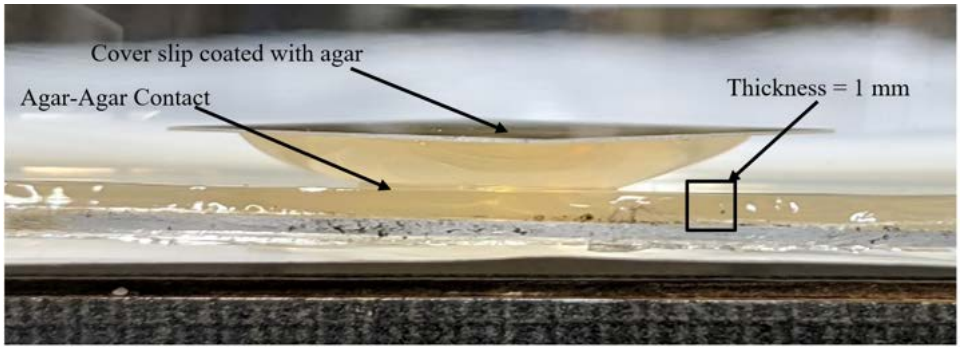

Figure 4.6: Cross section of a solid agar with a coverslip covered with agar.

Experimental setup and procedure

In this study, a thermally insulated Styrofoam enclosure was used to stabilize the variation in the external ambient factors such as temperature and humidity. Therefore, as the ambient temperature fluctuations were minimized, the differential-mode resonator was replaced with a simple yet efficient frequency variation resonator to detect subsurface bacteria growth. The frequency variation resonator was compact, required no additional components such as power splitter and was cost efficient. The sensor was secured to the base of the Styrofoam container and the sample *E. coli* plate was firmly placed on the sensor. The *E. coli* spot was aligned with the sensing region as shown in the Figure 4.7.

Figure 4.7: Solid media plate on a microstrip resonator with the inoculated *E. coli* aligned with the sensitive region of the resonator.

The Styrofoam enclosure was equipped with an LED light source, a temperature probe to monitor temperature in the vicinity of the sensor and a microscope to capture images of test sample at constant time intervals. To measure the response of the fabricated resonator, the sensor was connected to a vector network analyzer, ZNB20 from Rhode and Schwarz. The VNA was calibrated from 1 GHz to 2 GHz with an Intermediate frequency bandwidths of 300 Hz and an input power of 0 dBm. The resolution or number of points was set to 6401 prior to measurements. An automated program was coded in LabVIEW to extract the resonant profile details such as resonant amplitude and resonant frequency at a rate of every 2 minutes. The experimental setup is shown in the Figure 4.8.

The measured resonant amplitude for various volumes of *E. coli* was normalized by subtracting it from the initial measured amplitude. The measured data pertained to the initial 90 minutes of the experiment was excluded accounting time for stabilization of the apparatus.

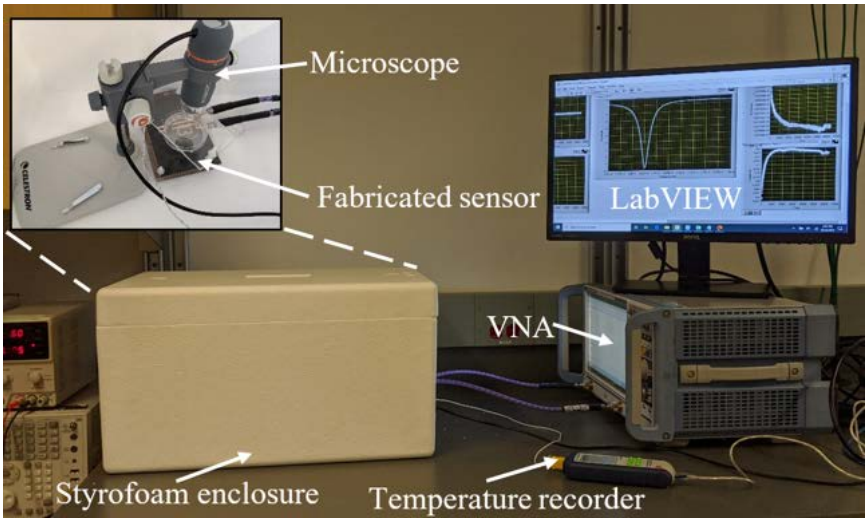

Figure 4.8: Experimental setup to functionally verify the operation of the sensor and monitor bacteria growth. The setup consists of a thermally insulated Styrofoam container with sensor enclosed within it, a temperature probe, a microscope, VNA and LabVIEW to control the VNA.

4.2.3 Measurement result and discussion

Prior to subsurface bacteria detection using microwave sensor, a preliminary test was conducted with two solid agar plates with and without the presence of a cover-slip to study the bacterial penetration in the medium. Both plates were incubated for 48 hours and later visually observed to determine the nature of bacteria growth on solid agar with and without the presence of a cover slip. The *E. coli* grown on control plate exhibited three-dimensional growth on the surface of agar. However, in the presence of a cover slip, a lateral surface growth was observed followed by a penetrated growth into the subsurface agar medium as shown in Figure 4.9.

Previous studies on the growth of microorganisms have shown that a crucial stage in the subsurface bacterial growth involves the transition of lateral or 2-Dimensional growth into 3-Dimensional growth into the medium due to mechanical forces acting on the bacteria [132]. Various studies have investigated the effects of mechanical forces on the planar to bulk transition of bacteria sandwiched between two mediums [129, 134]. Bacterial growth and its correlation with dielectric variations in the surrounding environment has been successfully demonstrated [139–142]. A similar observation was

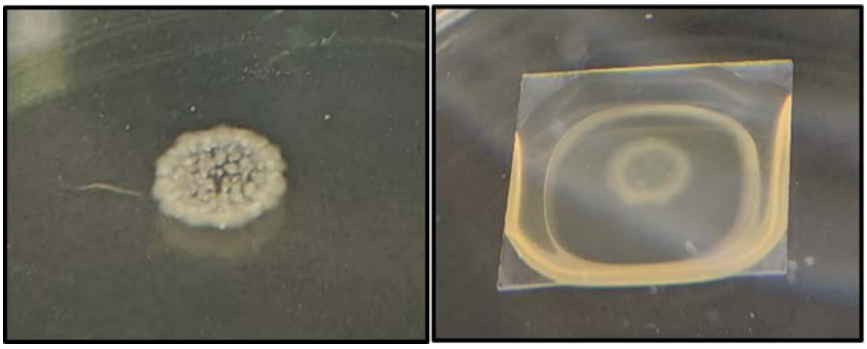

Figure 4.9: Three-dimensional growth of *E. coli* on solid media with and without the presence of cover slip.

found in this study where dielectric properties of the medium changed as bacterial subsurface growth proceeded. A significant variation in resonant amplitude was noticed compared to resonant frequency which is reasonable as bacterial metabolism alters the conductivity of the growth medium and resonant frequency is dependent on permittivity and conductivity [143].

In another study, a planar microstrip resonator was used to measure resonant amplitude variation representing growth phases of *E. coli* confined between two layers of agar. The measured results are presented in Figure 4.10.

From the measured Δ Resonant amplitude (dB), a clear distinction between the measured *E. coli* growths can be drawn between 0 μL (control), 3 μL and 9 μL volume of the bacteria. A maximum amplitude of 0.037 dB was measured for control i.e. with no bacteria. Considering this as a threshold value to distinguish between growth and no growth, the rate of change of the measured amplitude correlating to bacterial growth was found by fitting the measured results with Type I Gompertz growth model. This was obtained by plotting change in resonant amplitude (Y axis) and bacterial growth time (X axis). Type I Gompertz growth model is a sigmoid model often used to describe growth of animals, plants and various bacteria and cancer cells [144].

Although Gompertz model requires an upper asymptote or adult value to determine the growth rate of bacteria, due to the constant availability of nutrients in the vicinity of *E. coli*, it would take weeks or months of continuous monitoring of bacterial growth until stationary phase is achieved and adult value is extracted. Stationary phase is defined as the period during

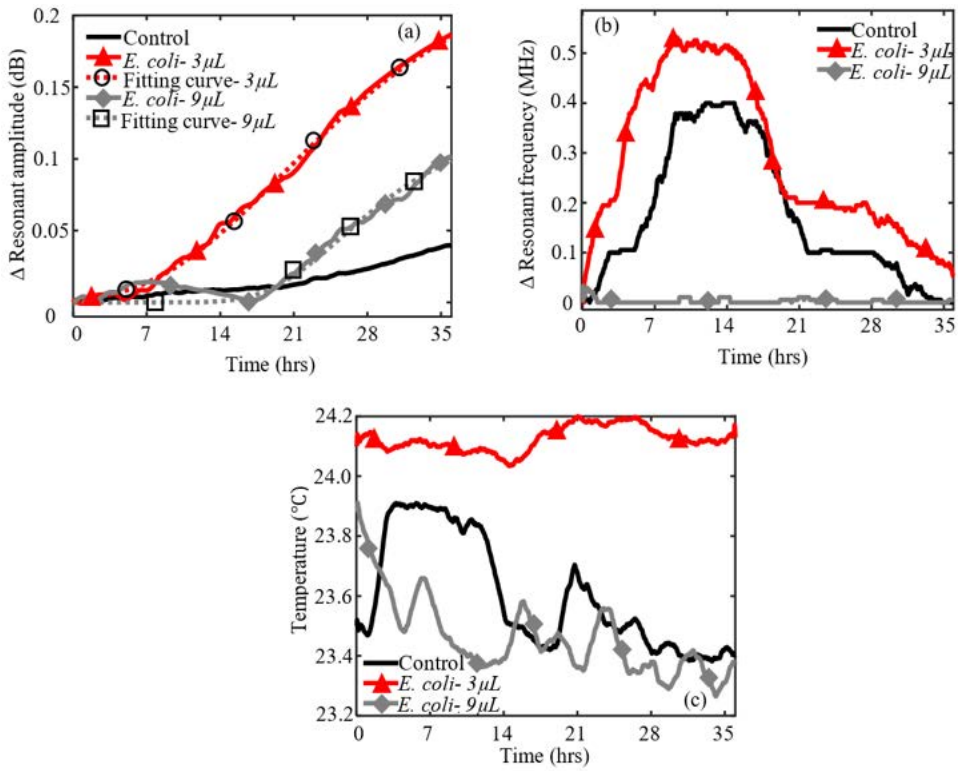

Figure 4.10: Measured amplitude variation (Δ resonant amplitude (dB)) with the fitted Gompertz model curve (a), measured frequency variation (Δ resonant frequency (MHz)) (b), and the recorded temperature (Temperature $\circ C$) (c) for 3 μL and 9 μL of *E. coli* on soft LB agar.

the life cycle of a microorganisms when the growth rate of bacteria equals the death rate of bacteria. Therefore,in this work, the Gompertz model was utilized to fit the initial linear growth phases of the selected volumes of *E. coli* and determine the rate of change of resonant amplitude variation which is related to the growth rate of bacteria.

The equation governing the Type I Gompertz model is given by equation 4.1.

$$y(t) = A * exp(-exp(-k_G * (t - T_i))) \tag{4.1}$$

Where $y(t)$ is the expected variation in the resonant amplitude as a function of time (t) due to bacteria growth, A represents the upper asymptote (adult value) (dB), k_G is the growth rate coefficient (dB/hr.) (which af-

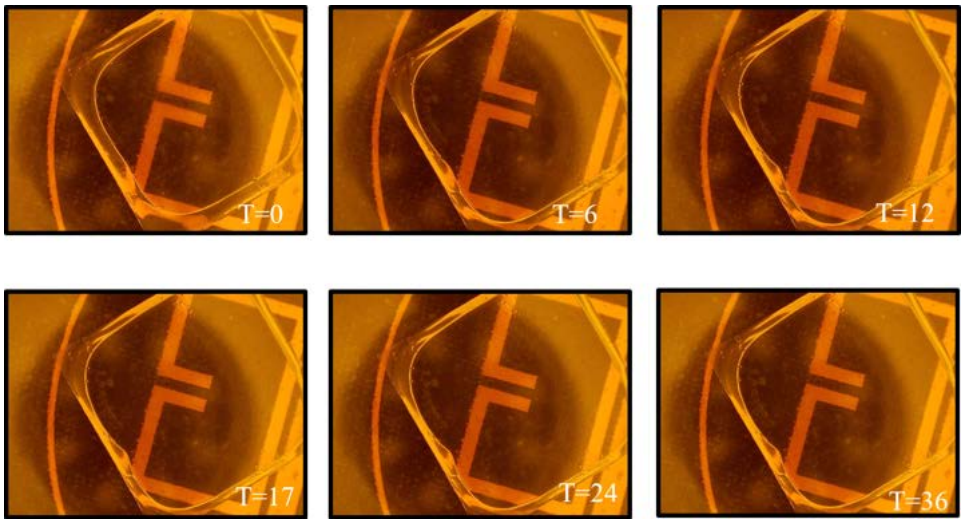

(a) Control- no bacteria

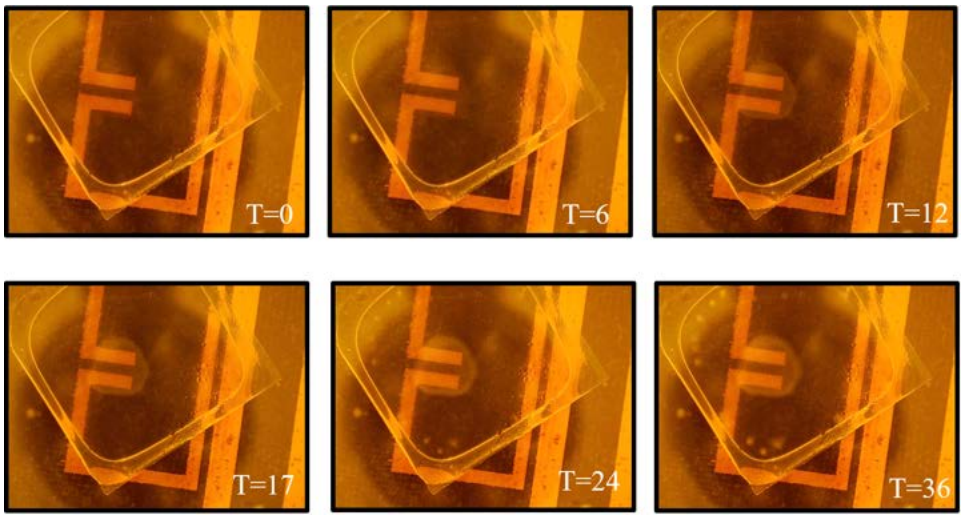

(b) *E. coli*- 3 μ L

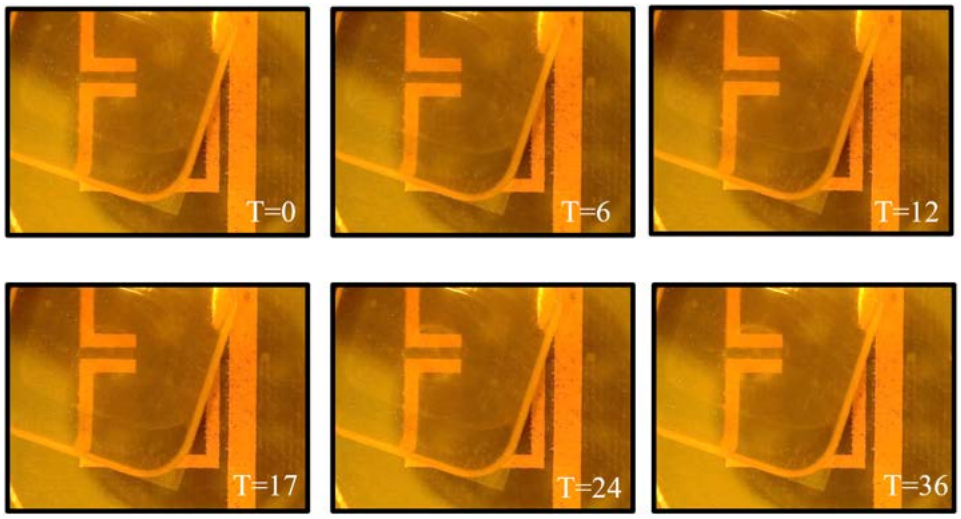

(c) *E. coli*- 9 μ L

Figure 4.11: Microscopic images depicting the growth of 3 μL and 9 μL captured at constant time intervals.

fects the slope), and T_i represents time at inflection (hr.). The T_i parameter shifts the growth curve horizontally without changing it shape and is therefore what is often termed a location parameter (whereas A and k_G are shape parameters). Table 4.2 presents the calculated Gompertz model parameters for 3 μL, and 9 μL of *E. coli*.

The fitted Gompertz growth curve demonstrated a good agreement with the measured microwave response. The performance and accuracy of the sensor was further validated by microscope images captured at constant time intervals as shown in Figure 4.11. The microscope images are in good agreement with the measured results.

Table 4.2: Measured growth phase and rate of change of resonant amplitude for *E. coli* at various concentrations of glucose in LB agar

E. coli volume (μL)	A	K_G	T_i	R^2
3	0.24182	0.08173	19.88572	0.99753
9	0.12456	0.139543	25.59338	0.96736

This work exhibits a unique approach of a real-time, contactless and, label-free microwave resonator to detect subsurface growth of *E. coli* confined between two layers of solid LB-agar. The fitting of bacterial growth measurement to the Gompertz growth model with a coefficient of determination above 96 % shows the potential of the currently used sensing tool for bacterial monitoring. A positive correlation between the measured results and microscopic images further strengthened the application of microwave sensors to measure subsurface bacteria growth.

4.3 Microwave resonator to monitor the impact of erythromycin on *E. coli* growth.

4.3.1 Background

Antibiotics have played a pivotal role in treating and killing pathogenic strains of bacteria thereby improving the health of patients suffering from infections caused by bacteria [145–147]. However, due to industrialization and overuse of antibiotics, microorganisms, as a mechanism of defense, have evolved strategies capable of resisting the antibiotics [148]. These microorganisms are known as multidrug-resistant (MDR) bacteria or "super-bugs" and pose a serious threat to humans, animals, and the health of the environment. It is predicted that causalities related to antibiotic resistance could be 10 million lives per year by 2050 [145]. Thus, it is essential to manufacture new antibiotics and determine the appropriate dose required to treat life-threatening infections [146–149].

To determine the antibiotic appropriate to treat a certain kind of infection, an antibiotic susceptibility test (AST) is performed. AST is a laboratory procedure performed by medical technologists (clinical laboratory scientists) to determine the minimum inhibitory concentration (MIC) and identify which antimicrobial regimen is specifically effective for individual patients against deadly infections [9, 150]. Various AST techniques such as Disk diffusion, dilution, Epsilometer test, PCR, DNA microarrays/chips have been studied and developed to determine the minimum inhibitory concentration [9, 151]. These techniques are simple and effective in determining the minimum inhibitory concentration for a certain type of infection but are time-consuming and require expensive equipment. With the recent developments in the field of Lab-on-a-chip devices, a network of micro-channels, sensors, and electrical circuits can be incorporated and fabricated on small chips. This offers numerous advantages such as non-contact interface, porta-

bility, quick reaction, and analysis time. Biosensors based on lab on a chip technology have revolutionized the field of a clinical study and pharmaceutical sciences [17, 136]. They are also a promising tool for rapid and accurate ASTs. Recently, microwave sensors are being widely used in pharmaceutical, biological and industrial applications owing to low cost, non-contact, label-free detection, high sensitivity, and ease of integration with other Lab-on-Chip (LoC) devices [48, 50, 53]. Thus, in this study, a microwave sensor capable of monitoring bacteria growth in the presence of 7.5 μg, 30 μg, and 45 μg of Erythromycin is presented. Based on the variation of growth rate, the concentrations of erythromycin achieving total inhibition of *E. coli* will be determined.

4.3.2 Material and method

Sample preparation

To measure the impact on the growth-inhibiting substance, such as antibiotics, on the growth profile of bacteria, a Mueller Hinton (MH) agar media was prepared. Due to low levels of thymidine and thymine (excess amounts can have adverse effects on the performance of various antibiotics), MH agar is widely used for antibiotic susceptibility tests by the disk diffusion method.

To prepare MH agar media 1.91 gm of MH agar was mixed with 50 ml of RO water in a flask. The mixture was sterilized in an autoclave at 121 $^{\circ}C$ for 15 minutes. The mixture was cooled to 50 $^{\circ}C$ prior to plating. Three ml of the MH agar was poured into a Petri dish to achieve a uniform agar thickness of 1 mm across the petri dish. The process was performed in a fume hood or under a Bunsen burner flame to avoid contamination of agar samples by fungi and other microorganisms. Three ml of *E. coli* was then spotted at the designated position on the agar plate.

Prior to preparing antibiotic paper disks, sample solutions containing various concentrations of erythromycin was prepared. Erythromycin, in powdered form, is freely soluble in alcohol, acetone, and other organic solvents. However, in water, the solubility of erythromycin is limited to 2 mg/ml. Thus, a concentration of 7.5 μg and 30 μg per 30 μL was achieved by series dilution of the parent erythromycin solution containing 2 mg/ml.

To prepare antibiotic paper disks, sterile blank paper disks and E- 15 μg paper disks procured by Fisher Scientific were used. Each paper disk was hydrated with 30 μL of the prepared stock solution to maintain consistency among the antibiotic paper disks. A control disk containing 0 μg

of erythromycin was prepared by hydrating a blank paper disk with 30 μL of RO water. E- 45 μg paper disk was prepared by pouring 30 μL of E-30 μg solution to an E-15 μg paper disk. The hydrated antibiotic paper disks with 0 μg, 7.5 μg, 30 μg, and 45 μg erythromycin was tapped on the solid agar 5 mm from the inoculated *E. coli*. The plate was sealed using parafilm at room temperature to avoid precipitation and fungal contamination.

Experimental setup and procedure

The fabricated frequency variation sensor was mechanically stabilized and enclosed in a thermally insulated Styrofoam enclosure to avoid the impact of ambient factors such as external vibrations, temperature, and humidity on the response of the resonator. The Styrofoam enclosure was equipped with an LED light source, a temperature probe to monitor the temperature in the vicinity of the sensor, and a microscope to capture images of test samples at constant time intervals. The sensor was connected to the VNA using SMA cables. The experimental setup and the VNA calibration details are discussed in section 4.2.2 (experimental setup and procedure).

The measured resonant amplitude for various concentrations of antibiotics was normalized by subtracting it from the initially measured amplitude. The measured data pertained to the initial 90 minutes of the experiment were excluded accounting for mechanical stabilization of the apparatus.

4.3.3 Measurement result and discussion

To study the impact of a dry paper disk (with no antibiotics) on an agar plate with no bacteria, a series of measurements were performed using a microwave resonator. Analysis of the measured results revealed that dry paper disks tend to dehydrate the growth media in their vicinity. The dehydration of the agar media alters the electrical characteristics of the growth media and result in false measurements. Therefore, to avoid dehydration of the growth media in the vicinity of the sensor's sensitive region, the blank disks were hydrated with an equal volume of RO water similar to antibiotic volume and used in all the further experiments. The steps followed to hydrate the paper disks are presented in section 4.3.2 (sample preparation).

Another study on antibiotic disk diffusion assay showed a differential response against tested concentrations with an increase in an inhibition zone corresponding to antibiotic concentration. The zone of inhibition was measured as 1.7 cm and 2.8 cm for 30 and 45 μg respectively (Figure 4.12).

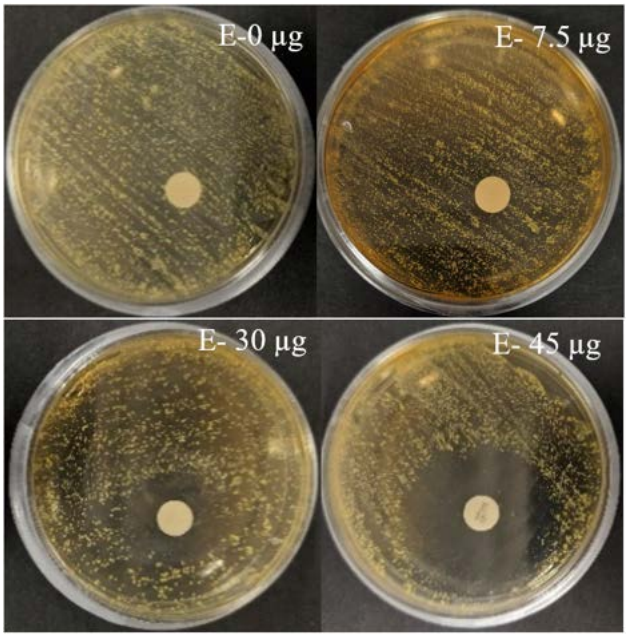

Figure 4.12: Zone of inhibition formed by 0 μg, 7.5 μg, 30 μg and 45 μg of erythromycin.

This was compared with a control (plain disk) and 7.5 μg where no inhibition of *E. coli* was observed. The preliminary zone of inhibition study was performed at room temperature which was measured to be 22 $°C$. The zone of inhibition is the diameter of the region where no bacteria growth was measured and shown in Figure 4.12. Therefore, based on the results presented in Figure 4.12, it can be concluded that 45 μg and 30 μg of erythromycin was able to effectively inhibit *E. coli* growth on solid MH agar in contrast to 7.5 μg and 0 μg.

Table 4.3: Measured zone of inhibition formed by 0 μg, 7.5 μg, 30 μg and 45 μg of erythromycin.

Erythromycin concentration (μg)	0.0	7.5	30	45
Diameter of zone of inhibition (cm)	0	0	1.7	2.8

As bacteria grows, the interaction between the nutrients present in the medium and the bacteria such as transfer of protein to amino acids, lipids to acetate, or carbohydrates to lactate results in the creation of new charged end products that are expelled into the surrounding media. However, the presence of an antibiotic can severely affect the growth of bacteria. At low lethal concentrations of antibiotics, bacteria growth is observed as shown in Figure 4.13. Low non-lethal concentration of erythromycin triggers a different cellular response against the antibiotic. The low concentration of antibiotics can stress the bacteria, but the bacteria continues to multiply and alter the conductivity of the surrounding growth media [152, 153].

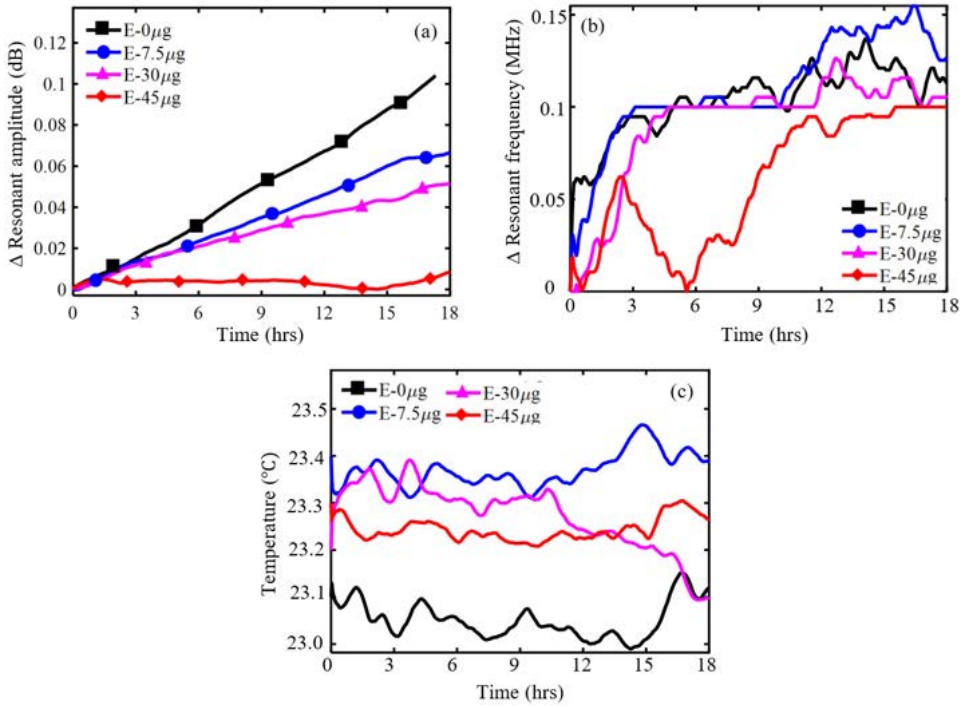

Figure 4.13: Measured resonant amplitude variation (Δ Resonant amplitude (dB)) (a), resonant frequency variation(Δ Resonant frequency (MHz)) (b), and recorded temperature (Temperature $\circ C$) (c) for bacterial growth in the presence of 0 μg, 7.5 μg, 30 μg, and 45 μg of erythromycin.

However, at high concentrations, bacterial growth is inhibited as observed in the measured results (Figure 4.13). At lethal or high concentrations of erythromycin, inhibition of protein slows down or suppresses bacterial

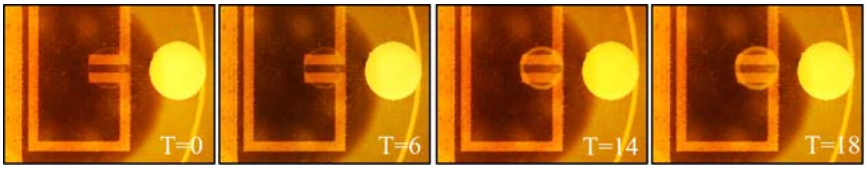

(a) E-0 μg

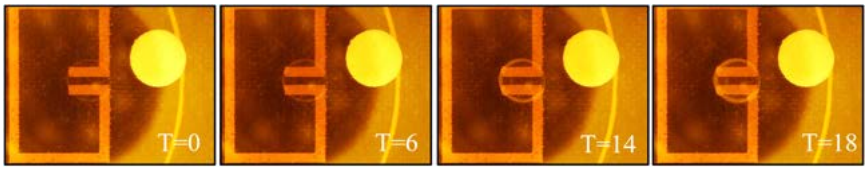

(b) E-7.5 μg

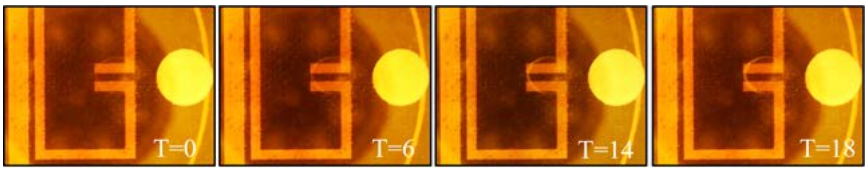

(c) E-30 μg

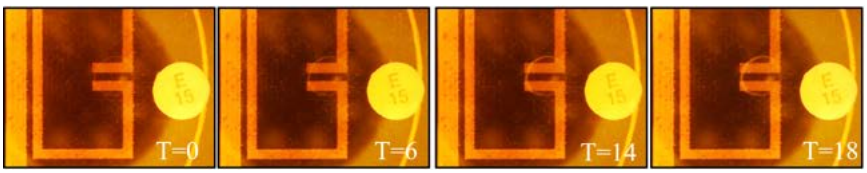

(d) E-45 μg

Figure 4.14: Microscope images captured at constant time intervals depicting bacteria growth in the presence of 0 μg (a), 7.5 μg (b), 30 μg (c), and 45 μg (d) of erythromycin.

growth [152, 153] This change in the growth rate of bacteria is reflected by a change in the conductivity of the medium. The microwave sensor measures

the change in the conductivity of the medium surrounding the bacteria which is interpreted by analyzing the change in the resonant amplitude which is shown in Figure 4.13.

It is known from the previous literature that the zone of inhibition is proportional to the strength of the antibiotics [154]. Thus, an increase in the zone of inhibition prevents bacterial growth in the sensitive region of the resonator. As evident from the bacterial growth images of E- 30 μg, a small portion of bacteria grow within the sensitive region of the resonator. This small growth was monitored by the microwave sensor and was visible distinctively in the response of the sensor (Figure 4.13).

However, the zone of inhibition for E- 45 μg covered the entire sensitive region. Thus, the growth of *E. coli* was inhibited by the antibiotic concentration and the resonant amplitude variations recorded was minimal (0.01 dB). Based on the microwave resonator response, E- 30 μg and E- 45 μg were able to resist the growth of *E. coli* with $OD_{600} = 1.5$ which matches with the preliminary test conducted. Therefore, at optimum growth conditions, the microwave resonator successfully distinguished the impact of different concentrations of erythromycin on the growth of *E. coli* within 18 hours as opposed to the conventional disk diffusion technique that takes around 24 to 36 hours to produce visual results. Therefore, the microwave resonator's ability to rapidly detect microbial growth as compared to conventional AST techniques was successfully demonstrated through this study. Moreover, a positive correlation between the measured results with the preliminary zone-of-inhibition study and the microscope images captured at constant time intervals further strengthen the potency of the sensor to monitor the influence of bacterial growth due to antibiotics.

4.4 Chapter conclusion

In this chapter, we have demonstrated the application of microwave resonator for real-time and contactless monitoring of bacterial growth. Furthermore, the microwave sensor's ability to detect microbial growth before any visual indications was demonstrated. The designed sensors were able to successfully sense the growth of bacteria in both temperature-controlled and temperature-uncontrolled environments.

From these studies and the simulation results presented in chapter 2, it is evident that resonant amplitude was sensitive to changes in the conductivity or loss tangent of the growth medium. As bacterial metabolism alters the conductivity of the growth medium, the resonant amplitude was selected

over resonant frequency to monitor bacterial growth.

The first study established the efficacy of the microwave resonator to detect and differentiate the impact of glucose concentration on the growth profile of *E. coli*. The rate of change of amplitude that can be associated with the growth rate of bacteria was calculated for *E. coli* at various glucose concentrations. The presence of carbon sources (0- 2 % w/v) in LB agar enhances the growth of *E. coli*. Therefore, based on the measured results, the highest rate of change in resonant amplitude was observed at 2% glucose (0.23646 dB/hr) compared to 0% (0.10913 dB/hr). However, at higher concentrations (10 % w/v), carbon sources inhibited bacterial growth as observed from the measured results. The measured results were supported by previous microbiology studies. In addition to this, a positive correlation of the measured results with the microscope images captured at constant intervals further established the sensor's ability to monitor bacterial growth. The results of this study are explained thoroughly in a paper entitled "Differential Microwave Resonator Sensor Reveals Glucose Dependent Growth Profile of *E. coli* on Solid Agar" [53]

In the second study, we demonstrated the ability of microwave sensors to detect and monitor subsurface *E. coli* growth. The changes in the dielectric properties of growth media during 2D and 3D growth in the solid growth media were measured using microwave resonators. The successful fitting of bacterial growth measurement to the Gompertz growth model with a coefficient of determination above 96% shows the potential of the currently used sensing tool for bacterial monitoring. A positive correlation between the measured results and microscopic images further strengthened the application of microwave sensors to measure subsurface bacterial growth. The findings of this study are submitted as a research paper and is under review.

The third study successfully demonstrated the potential of the designed microwave resonator to differentiate the impact of antibiotics, erythromycin (0, 7.5, 30, 45 μg) on the growth profile of *E. coli*. From the measured response of the sensor, it was observed that the growth of microorganisms was inversely proportional to the concentration of antibiotics. Among the tested concentrations of erythromycin (0, 7.5, 30 and, 45 μg), E-30 μg and E-45 μg were able to successfully inhibit bacterial growth. The microwave resonator successfully distinguished the impact of different concentrations of erythromycin on the growth of *E. coli* within 18 hours as opposed to the conventional disk diffusion technique that takes around 24 to 36 hours to produce visual results. The positive correlation between the measured results with the preliminary zone-of-inhibition study and the microscope images captured at constant time intervals further strengthen the potency

of the sensor to monitor bacterial growth. The findings of this study are submitted as a research paper and is under review.

Chapter 5

Conclusion

In this chapter, the main findings and contributions of the thesis are summarized and the areas of possible improvements and research are presented.

5.1 Thesis conclusions

The thesis begins with an introduction to microwave technology and its applications in industrial, food, biomedical, and pharmaceutical industries. Among the available microwave sensing technologies, planar microstrip resonators were chosen for the current research due to its advantages such as portability, ease of fabrication, label-free, and contactless sensing capabilities. The unique ability of microwave sensors to detect variations in the conductivity in the surrounding medium related to microbial growth makes it a promising candidate for microbial growth monitoring and related applications. In this work, microstrip resonators were employed to monitor bacteria growth due to numerous advantages which include contactless, label-free monitoring, portable, cost effective, and ease of development and fabrication. The proposed planar microwave resonators were designed in two arrangements: frequency variation resonator and differential-mode resonator. They were designed to operate as a one-port device with their operating frequency confined to the L-band. The sensor's response to dielectric material was studied through HFSS simulations. The simulation results are presented in chapter 2. The sensors were fabricated using in-house fabrication techniques, and the details of sensor operation are explained in chapter 3.

The fabricated sensors were later employed to detect and monitor microbial growth on solid growth matrices. The sensors were used to monitor the impact on the growth of microorganisms subjected to various factors such as nutrient availability, bacterial position, and presence of inhibiting compounds such as antibiotics were conducted as three independent studies. The conclusions and contributions from these studies are summarized as follows:

1. The first study demonstrated the ability of the designed sensor to successfully monitor and distinguish the impact of nutrient availability on microbial growth. The impact of temperature on the response of the sensor was observed and corrected by redesigning the microstrip resonator. The measured results obtained after eliminating the influence of ambient temperature and mechanical stabilization was presented in Chapter 4. The measured data was supported by microscopic images revealing changes in microbial growth at different nutrient concentrations. The results of this study are explained thoroughly in a paper entitled "Differential Microwave Resonator Sensor Reveals Glucose Dependent Growth Profile of *E. coli* on Solid Agar" [53].

2. The second study investigated the potential of the sensors to monitor subsurface bacterial growth between two layers of solid growth matrices. Through the measured results and microscope images of various experiments, the impact of the relaxation of the solid-solid interface of the medium and stabilization of electronic components and VNA after calibration was identified and eliminated from the measured results. Additional experimental results further demonstrated a positive correlation between microbial growth and microwave sensor's response and further demonstrated the extended capacity of the sensor to monitor subsurface bacterial growth unlike previous studies confined to surface growth. The findings of this study are submitted and under review.

3. The third study investigated the effect of various concentrations of antibiotics on microbial growth. The effect of the dry antibiotic paper disks on the solid agar matrices was identified through numerous futile attempts. By using an equal volume of antibiotic solution to hydrate the paper disks, the impact of dry paper disks was eliminated. Additional experiments confirmed a positive relationship between the zone of inhibition, measured result, and the microscopic images. This further strengthened the use of the sensor as a tool to determine the minimum inhibitory concentration of antibiotics and can be applied for antibiotic sensitivity assays. The results of this study are submitted and under review.

5.2 Contributions

– Resonators with various configurations were designed and simulated to achieve a highly sensitive device exclusively for monitoring microbial

growth. Numerous futile attempts, design modifications, and optimization led to the final working model of a microwave resonator.

- Contributed to the current state of the art sensor technology aimed for contactless and label-free bacterial growth monitoring on solid growth medium.
- Designed a one-port sensing system by utilizing a wide band power splitter.
- Analyzed the impact of nutrient availability, subsurface growth and presence of antibiotics on growth of bacteria using contactless microwave resonator sensor.
- Observed the impact of ambient factors such as temperature, stabilization of sensing apparatus and implemented corrective measures to minimize or diminish the impact of the above mentioned factors on the response of the sensor.
- Optimized solid agar plating techniques to achieve successful bacterial growth monitoring using microwave resonator sensor technology.
- Designed series of experiments to understand various aspects of bacterial growth on solid agar.

5.3 Future works

This research successfully demonstrated the potential of a prototype microwave sensor for contactless real-time monitoring of microbial growth on solid growth matrices. However, based on the current research outcomes, we identified the following research ideas could scale up the designed sensor to industrial scale:

- Sensor design: Modification of sensor design by incorporating active resonators can improve the sensitivity of the resonator. Using an array of active resonators multiple bacteria can be tested in a single assay. Similarly, array of resonators can be used to monitor the effect of multiple antibiotics on a microbial specimen and determine the appropriate antibiotics for treatment. There is a prospective to implement wireless resonators which can eliminate microwave cables and soldered SMA connectors for ease in installation.

- Sample preparation: Using microfluidic devices to inject varying concentrations of antibiotics can expand the application range of the current sensor. It also facilitates the reusability of the device by following simple cleaning procedures.
- Sensor readout circuit: Including a customizable readout circuit/device to measure the reflected power from the sensor can eliminate the system's dependence on the vector network analyzers. By developing such a self-reliant system, the cost of the sensor can also be reduced significantly.
- Sensing apparatus: Appending an incubator for bacterial growth can enhance the growth rate and will facilitate early detection of bacterial growth which can be monitored with precision using a wireless sensor.

Bibliography

[1] N. Zhu, D. Zhang, W. Wang, X. Li, B. Yang, J. Song, X. Zhao, B. Huang, W. Shi, R. Lu, P. Niu, F. Zhan, X. Ma, D. Wang, W. Xu, G. Wu, G. F. Gao, and W. Tan, "A Novel Coronavirus from Patients with Pneumonia in China, 2019," *New England Journal of Medicine*, vol. 382, pp. 727–733, feb 2020. → pages 1

[2] E. K. Stevenson, A. R. Rubenstein, G. T. Radin, R. S. Wiener, and A. J. Walkey, "Two decades of mortality trends among patients with severe sepsis: a comparative meta-analysis*.," *Critical care medicine*, vol. 42, pp. 625–31, mar 2014. → pages

[3] H.-U. Meier-Kriesche, A. O. Ojo, J. A. Hanson, and B. Kaplan, "Exponentially increased risk of infectious death in older renal transplant recipients," *Kidney International*, vol. 59, pp. 1539–1543, apr 2001. → pages

[4] L. van der Hoek, K. Pyrc, M. F. Jebbink, W. Vermeulen-Oost, R. J. M. Berkhout, K. C. Wolthers, P. M. E. Wertheim-van Dillen, J. Kaandorp, J. Spaargaren, and B. Berkhout, "Identification of a new human coronavirus," *Nature Medicine*, vol. 10, pp. 368–373, apr 2004. → pages

[5] J. M. O'Brien, N. A. Ali, S. K. Aberegg, and E. Abraham, "Sepsis," *The American Journal of Medicine*, vol. 120, pp. 1012–1022, dec 2007. → pages

[6] B. K. Romanov, "Coronavirus disease COVID-2019," *Safety and Risk of Pharmacotherapy*, vol. 8, pp. 3–8, mar 2020. → pages 1

[7] S. Wong and B. Tan, "Megatrends in Infectious Diseases: The Next 10 to 15 Years," *Ann Acad Med Singapore*, vol. 48, no. 6, pp. 188–194, 2019. → pages 1

[8] A. L. Schaefer, N. Cook, S. V. Tessaro, D. Deregt, G. Desroches, P. L. Dubeski, A. K. Tong, and D. L. Godson, "Early detection and predic-

tion of infection using infrared thermography," *Canadian Journal of Animal Science*, vol. 84, pp. 73–80, mar 2004. → pages 1

[9] Z. A. Khan, M. F. Siddiqui, and S. Park, "Current and Emerging Methods of Antibiotic Susceptibility Testing.," *Diagnostics (Basel, Switzerland)*, vol. 9, may 2019. → pages 1, 2, 66

[10] E. Engvall, "[28] Enzyme immunoassay ELISA and EMIT," in *Methods in Enzymology*, ch. 28, pp. 419–439, Elsevier Inc., 1980. → pages

[11] S. Henry, E. Baudoin, J. C. López-Gutiérrez, F. Martin-Laurent, A. Brauman, and L. Philippot, "Quantification of denitrifying bacteria in soils by nirK gene targeted real-time PCR," *Journal of Microbiological Methods*, vol. 59, pp. 327–335, dec 2004. → pages 1

[12] S. A. Barghouthi, "A Universal Method for the Identification of Bacteria Based on General PCR Primers," *Indian Journal of Microbiology*, vol. 51, pp. 430–444, oct 2011. → pages 1, 58

[13] J.-C. Lagier, S. Edouard, I. Pagnier, O. Mediannikov, M. Drancourt, and D. Raoult, "Current and Past Strategies for Bacterial Culture in Clinical Microbiology," *Clinical Microbiology Reviews*, vol. 28, pp. 208–236, jan 2015. → pages

[14] R. Franco-Duarte, L. Černáková, S. Kadam, K. S. Kaushik, B. Salehi, A. Bevilacqua, M. R. Corbo, H. Antolak, K. Dybka-Stępień, M. Leszczewicz, S. Relison Tintino, V. C. Alexandrino de Souza, J. Sharifi-Rad, H. D. Melo Coutinho, N. Martins, and C. F. Rodrigues, "Advances in Chemical and Biological Methods to Identify Microorganisms—From Past to Present," *Microorganisms*, vol. 7, p. 130, may 2019. → pages 1, 58

[15] P. Cheng, Z.-G. Huang, Y. Zhuang, L.-C. Fang, H. Huang, J. Deng, L.-L. Jiang, K.-K. Yu, Y. Li, and J.-S. Zheng, "A novel regeneration-free E. coli O157:H7 amperometric immunosensor based on functionalised four-layer magnetic nanoparticles," *Sensors and Actuators B: Chemical*, vol. 204, pp. 561–567, dec 2014. → pages 1, 58

[16] Y. Wang, Z. Ye, C. Si, and Y. Ying, "Monitoring of Escherichia coli O157:H7 in food samples using lectin based surface plasmon resonance biosensor," *Food Chemistry*, vol. 136, pp. 1303–1308, feb 2013. → pages 3, 5

[17] A.-R. H. A.-A. Hassan, A. de la Escosura-Muñiz, and A. Merkoçi, "Highly sensitive and rapid determination of Escherichia coli O157:H7 in minced beef and water using electrocatalytic gold nanoparticle tags," *Biosensors and Bioelectronics*, vol. 67, pp. 511–515, may 2015. → pages 67

[18] M. Pohanka, "The Piezoelectric Biosensors: Principles and Applications, a Review," *International Journal of Electrochemical Science*, pp. 496–506, jan 2017. → pages

[19] L. Yao, P. Lamarche, N. Tawil, R. Khan, A. M. Aliakbar, M. H. Hassan, V. P. Chodavarapu, and R. Mandeville, "CMOS Conductometric System for Growth Monitoring and Sensing of Bacteria," *IEEE Transactions on Biomedical Circuits and Systems*, vol. 5, pp. 223–230, jun 2011. → pages

[20] M. Salami, A. Mhs, M. Sawan, and A. Nsk, "Biosensors & Bioelectronics BioFET-based Integrated Platform for Accurate and Rapid Detection of E . coli Bacteria : A Review," *Journal of Biosensors & Bioelectronics*, vol. 10, no. 1, pp. 1–11, 2019. → pages 1, 2, 58

[21] P. Damborský, J. Švitel, and J. Katrlík, "Optical biosensors," *Essays in Biochemistry*, vol. 60, pp. 91–100, jun 2016. → pages 1

[22] F. S. Ligler, "Perspective on Optical Biosensors and Integrated Sensor Systems," *Analytical Chemistry*, vol. 81, pp. 519–526, jan 2009. → pages

[23] S. Zhang, "Materials and techniques for electrochemical biosensor design and construction," *Biosensors and Bioelectronics*, vol. 15, pp. 273–282, aug 2000. → pages

[24] D. Ivnitski, "Electrochemical biosensor based on supported planar lipid bilayers for fast detection of pathogenic bacteria," *Electrochemistry Communications*, vol. 2, pp. 457–460, jul 2000. → pages 1

[25] M. H. Zarifi and M. Daneshmand, "High-Resolution RFID Liquid Sensing Using a Chipless Tag," *IEEE Microwave and Wireless Components Letters*, vol. 27, pp. 311–313, mar 2017. → pages 2

[26] M. Fayaz, M. H. Zarifi, M. Abdolrazzaghi, P. Shariaty, Z. Hashisho, and M. Daneshmand, "A Novel Technique for Determining the Adsorption Capacity and Breakthrough Time of Adsorbents Using a Non-

contact High-Resolution Microwave Resonator Sensor," *Environmental Science & Technology*, vol. 51, pp. 427–435, jan 2017. → pages

[27] M. H. Zarifi, S. Deif, M. Abdolrazzaghi, B. Chen, D. Ramsawak, M. Amyotte, N. Vahabisani, Z. Hashisho, W. Chen, and M. Daneshmand, "A Microwave Ring Resonator Sensor for Early Detection of Breaches in Pipeline Coatings," *IEEE Transactions on Industrial Electronics*, vol. 65, pp. 1626–1635, feb 2018. → pages 2, 11

[28] M. H. Zarifi, A. Gholidoust, M. Abdolrazzaghi, P. Shariaty, Z. Hashisho, and M. Daneshmand, "Sensitivity enhancement in planar microwave active-resonator using metal organic framework for CO2 detection," *Sensors and Actuators B: Chemical*, vol. 255, pp. 1561–1568, feb 2018. → pages

[29] M. A. Rafi, B. D. Wiltshire, and M. H. Zarifi, "Wideband Tunable Modified Split Ring Resonator Structure Using Liquid Metal and 3-D Printing," *IEEE Microwave and Wireless Components Letters*, pp. 1–4, 2020. → pages 2

[30] S. Mohammadi, A. V. Nadaraja, K. Luckasavitch, M. C. Jain, D. June Roberts, and M. H. Zarifi, "A Label-Free, Non-Intrusive, and Rapid Monitoring of Bacterial Growth on Solid Medium Using Microwave Biosensor," *IEEE Transactions on Biomedical Circuits and Systems*, vol. 14, pp. 2–11, feb 2020. → pages 2, 5, 19, 31, 49

[31] S. Mohammadi, A. V. Nadaraja, D. J. Roberts, and M. H. Zarifi, "Real-time and hazard-free water quality monitoring based on microwave planar resonator sensor," *Sensors and Actuators A: Physical*, vol. 303, p. 111663, mar 2020. → pages 16, 58

[32] B. D. Wiltshire, T. Zarifi, and M. H. Zarifi, "Passive Split Ring Resonator Tag Configuration for RFID-Based Wireless Permittivity Sensing," *IEEE Sensors Journal*, vol. 20, pp. 1904–1911, feb 2020. → pages

[33] M. Amirian, G. Karimi, B. D. Wiltshire, and M. H. Zarifi, "Differential Narrow Bandpass Microstrip Filter Design for Material and Liquid Purity Interrogation," *IEEE Sensors Journal*, vol. 19, pp. 10545–10553, nov 2019. → pages 19

[34] B. D. Wiltshire and M. H. Zarifi, "3-D Printing Microfluidic Channels With Embedded Planar Microwave Resonators for RFID and Liq-

uid Detection," *IEEE Microwave and Wireless Components Letters*, vol. 29, no. 1, pp. 65–67, 2019. → pages

[35] B. D. Wiltshire, S. Mohammadi, and M. H. Zarifi, "Integrating 3D Printed Microfluidic Channels With Planar Resonator Sensors for Low Cost and Sensitive Liquid Detection," in *2018 18th International Symposium on Antenna Technology and Applied Electromagnetics (ANTEM)*, pp. 1–2, 2018. → pages

[36] M. Abdolrazzaghi, M. H. Zarifi, C. F. A. Floquet, and M. Daneshmand, "Contactless Asphaltene Detection Using an Active Planar Microwave Resonator Sensor," *Energy & Fuels*, vol. 31, pp. 8784–8791, aug 2017. → pages

[37] M. Abdolrazzaghi, M. H. Zarifi, and M. Daneshmand, "Sensitivity enhancement of split ring resonator based liquid sensors," in *2016 IEEE SENSORS*, pp. 1–3, IEEE, oct 2016. → pages 11

[38] M. H. Zarifi, P. Shariaty, M. Abdolrazzaghi, Z. Hashisho, and M. Daneshmand, "Particle size characterization using a high resolution planar resonator sensor in a lossy medium," *Sensors and Actuators B: Chemical*, vol. 234, pp. 332–337, oct 2016. → pages

[39] M. H. Zarifi, M. Rahimi, M. Daneshmand, and T. Thundat, "Microwave ring resonator-based non-contact interface sensor for oil sands applications," *Sensors and Actuators, B: Chemical*, vol. 224, pp. 632–639, 2015. → pages 2, 11

[40] N. R. Tanguy, B. Wiltshire, M. Arjmand, M. H. Zarifi, and N. Yan, "Highly Sensitive and Contactless Ammonia Detection Based on Nanocomposites of Phosphate-Functionalized Reduced Graphene Oxide/Polyaniline Immobilized on Microstrip Resonators," *ACS Applied Materials & Interfaces*, vol. 12, pp. 9746–9754, feb 2020. → pages 2

[41] M. Fayaz, M. Jahandar Lashaki, M. Abdolrazzaghi, M. H. Zarifi, Z. Hashisho, M. Daneshmand, J. E. Anderson, and M. Nichols, "Monitoring the residual capacity of activated carbon in an emission abatement system using a non-contact, high resolution microwave resonator sensor," *Sensors and Actuators B: Chemical*, vol. 282, pp. 218–224, mar 2019. → pages

[42] Z. Abbasi, M. H. Zarifi, P. Shariati, Z. Hashisho, and M. Daneshmand, "Flexible coupled microwave ring resonators for contactless microbead

assisted volatile organic compound detection," in *2017 IEEE MTT-S International Microwave Symposium (IMS)*, vol. 2, pp. 1228–1231, IEEE, jun 2017. → pages

[43] M. H. Zarifi, P. Shariaty, Z. Hashisho, and M. Daneshmand, "A non-contact microwave sensor for monitoring the interaction of zeolite 13X with CO2 and CH4 in gaseous streams," *Sensors and Actuators B: Chemical*, vol. 238, pp. 1240–1247, jan 2017. → pages 2

[44] B. Wiltshire, K. Mirshahidi, K. Golovin, and M. H. Zarifi, "Robust and sensitive frost and ice detection via planar microwave resonator sensor," *Sensors and Actuators B: Chemical*, vol. 301, p. 126881, dec 2019. → pages 2, 16

[45] M. Benlamri, S. Deif, N. Mahdi, M. Baghelani, M. H. Zarifi, D. W. Barlage, K. Shankar, and M. Daneshmand, "Planar microwave resonator with electrodeposited ZnO thin film for ultraviolet detection," *Semiconductor Science and Technology*, vol. 35, p. 025003, feb 2020. → pages 2

[46] M. H. Zarifi, H. Sadabadi, S. H. Hejazi, M. Daneshmand, and A. Sanati-Nezhad, "Noncontact and Nonintrusive Microwave-Microfluidic Flow Sensor for Energy and Biomedical Engineering," *Scientific Reports*, vol. 8, p. 139, dec 2018. → pages 2

[47] M. H. Zarifi, B. Wiltshire, N. Mahdi, P. Kar, K. Shankar, and M. Daneshmand, "Ultraviolet sensing using a TiO 2 nanotube integrated high resolution planar microwave resonator device," *Nanoscale*, vol. 10, no. 10, pp. 4882–4889, 2018. → pages 2

[48] N. M. Ceron Hurtado, M. H. Zarifi, M. Daneshmand, and J. Aguilo Llobet, "Flexible Microdisplacement Sensor for Wearable/ Implantable Biomedical Applications," *IEEE Sensors Journal*, vol. 17, pp. 3873–3883, jun 2017. → pages 2, 3, 67

[49] M. H. Zarifi and M. Daneshmand, "Monitoring Solid Particle Deposition in Lossy Medium Using Planar Resonator Sensor," *IEEE Sensors Journal*, vol. 17, pp. 7981–7989, dec 2017. → pages 2

[50] R. Narang, S. Mohammadi, M. M. Ashani, H. Sadabadi, H. Hejazi, M. H. Zarifi, and A. Sanati-Nezhad, "Sensitive, Real-time and Non-Intrusive Detection of Concentration and Growth of Pathogenic Bac-

teria using Microfluidic-Microwave Ring Resonator Biosensor," *Scientific Reports*, vol. 8, p. 15807, dec 2018. → pages 2, 49, 58, 67

[51] S. Mohammadi, R. Narang, M. Mohammadi Ashani, H. Sadabadi, A. Sanati-Nezhad, and M. H. Zarifi, "Real-time monitoring of Escherichia coli concentration with planar microwave resonator sensor," *Microwave and Optical Technology Letters*, vol. 61, pp. 2534–2539, nov 2019. → pages

[52] C.-F. Liu, M.-H. Wang, and L.-S. Jang, "Microfluidics-based hairpin resonator biosensor for biological cell detection," *Sensors and Actuators B: Chemical*, vol. 263, pp. 129–136, jun 2018. → pages

[53] M. C. Jain, A. V. Nadaraja, B. M. Vizcaino, D. J. Roberts, and M. H. Zarifi, "Differential Microwave Resonator Sensor Reveals Glucose-Dependent Growth Profile of E. coli on Solid Agar," *IEEE Microwave and Wireless Components Letters*, pp. 1–4, 2020. → pages 2, 67, 73, 76

[54] F. BAKER and R. SILVERTON, "The Use of Culture Media," in *Introduction to Medical Laboratory Technology*, pp. 476–480, Elsevier, 1976. → pages 2

[55] I. De Leersnyder, L. De Gelder, I. Van Driessche, and P. Vermeir, "Influence of growth media components on the antibacterial effect of silver ions on Bacillus subtilis in a liquid growth medium," *Scientific Reports*, vol. 8, p. 9325, dec 2018. → pages 2

[56] K. Grenier, D. Dubuc, P.-E. Poleni, M. Kumemura, H. Toshiyoshi, T. Fujii, and H. Fujita, "Integrated Broadband Microwave and Microfluidic Sensor Dedicated to Bioengineering," *IEEE Transactions on Microwave Theory and Techniques*, vol. 57, pp. 3246–3253, dec 2009. → pages 2, 11

[57] D. M. Pozar, *Microwave engineering; 3rd ed.* Hoboken, NJ: Wiley, third ed., 2005. → pages 3, 5, 14, 15, 28

[58] S. Ullah, C. Ruan, M. S. Sadiq, T. U. Haq, and W. He, "High Efficient and Ultra Wide Band Monopole Antenna for Microwave Imaging and Communication Applications," *Sensors*, vol. 20, p. 115, dec 2019. → pages 3, 5

[59] Y. Sun, F. Dang, C. Yuan, J. He, Q. Zhang, and X. Zhao, "A Beam-steerable Lens Antenna for Ku-band High-Power Microwave Applications," *IEEE Transactions on Antennas and Propagation*, pp. 1–1, 2020. → pages 3

[60] L. Gil-Flores, M. Salvador, F. Penaranda-Foix, A. Dalmau, A. Fernández, and A. Borrell, "Tribological and wear behaviour of alumina toughened zirconia nanocomposites obtained by pressureless rapid microwave sintering," *Journal of the Mechanical Behavior of Biomedical Materials*, vol. 101, p. 103415, jan 2020. → pages 3

[61] D. Belamri, A. Harabi, N. Karbouaa, and N. Benyahia, "The effect of KF on the structural evolution of natural hydroxyapatite during conventional and microwave sintering," *Ceramics International*, vol. 46, pp. 1189–1194, jan 2020. → pages

[62] E. A. Anli, "Possibilities for using microwave-vacuum drying in Lor cheese production," *International Dairy Journal*, vol. 102, p. 104618, mar 2020. → pages

[63] M. Nadeem, E. Ul Haq, F. Ahmed, M. Asif Rafiq, G. Hameed Awan, and M. Zain-ul Abdein, "Effect of microwave curing on the construction properties of natural soil based geopolymer foam," *Construction and Building Materials*, vol. 230, p. 117074, jan 2020. → pages

[64] D. Agrawal, "Microwave sintering of metal powders," in *Advances in Powder Metallurgy*, pp. 361–379, Elsevier, 2013. → pages 3, 5

[65] X. Lin, Y. Chen, Z. Gong, B.-C. Seet, L. Huang, and Y. Lu, "Ultra-Wideband Textile Antenna for Wearable Microwave Medical Imaging Applications," *IEEE Transactions on Antennas and Propagation*, pp. 1–1, 2020. → pages 3

[66] F. Fiore, V. Stoia, and F. Somma, "Surgical recurrence of solitary fibrous tumor of the pleura treated with microwave (MW) thermoablation: A case report," *Thoracic Cancer*, vol. 11, pp. 443–446, feb 2020. → pages

[67] K. Imajo, Y. Ogawa, M. Yoneda, S. Saito, and A. Nakajima, "A review of conventional and newer generation microwave ablation systems for hepatocellular carcinoma," *Journal of Medical Ultrasonics*, vol. 47, pp. 265–277, apr 2020. → pages 3

[68] L. Wang, "Microwave Sensors for Breast Cancer Detection," *Sensors*, vol. 18, p. 655, feb 2018. → pages 3, 58

[69] S. J. Ling, J. Sanny, and W. Moebs, *University Physics Volume 2*. Houston, Texas: OpenStax University Physics, 2016. → pages 3, 4

[70] I. Zivkovic and A. Murk, "Free-Space Transmission Method for the Characterization of Dielectric and Magnetic Materials at Microwave Frequencies," in *Microwave Materials Characterization*, InTech, nov 2012. → pages 4, 5

[71] S. Y. Huang, "Loss tangent," feb 2012. → pages 4

[72] D. Markl, M. Warman, M. Dumarey, E.-L. Bergman, S. Folestad, Z. Shi, L. F. Manley, D. J. Goodwin, and J. A. Zeitler, "Review of real-time release testing of pharmaceutical tablets: State-of-the art, challenges and future perspective," *International Journal of Pharmaceutics*, vol. 582, p. 119353, may 2020. → pages 5

[73] K. Chee Yaw, "Measurement of Dielectric Material Properties," 2012. → pages 5, 6, 7, 8, 9

[74] E. Håkansson, A. Amiet, and A. Kaynak, "Dielectric characterization of conducting textiles using free space transmission measurements: Accuracy and methods for improvement," *Synthetic Metals*, vol. 157, pp. 1054–1063, dec 2007. → pages 5

[75] N. Vohra, L. R. Rodriguez-Aguilar, J. S. Batista, and M. El-Shenawee, "Free-Space Characterization of Radar Absorbing Non-Magnetic Materials in the W-Band," in *2020 94th ARFTG Microwave Measurement Symposium (ARFTG)*, pp. 1–4, IEEE, jan 2020. → pages 6

[76] D. Ghodgaonkar, V. Varadan, and V. Varadan, "A free-space method for measurement of dielectric constants and loss tangents at microwave frequencies," *IEEE Transactions on Instrumentation and Measurement*, vol. 38, pp. 789–793, jun 1989. → pages

[77] D. Ghodgaonkar, V. Varadan, and V. Varadan, "Free-space measurement of complex permittivity and complex permeability of magnetic materials at microwave frequencies," *IEEE Transactions on Instrumentation and Measurement*, vol. 39, pp. 387–394, apr 1990. → pages

[78] S. Trabelsi and S. O. Nelson, "Free-space measurement of dielectric properties of cereal grain and oilseed at microwave frequencies," *Measurement Science and Technology*, vol. 14, pp. 589–600, may 2003. → pages

[79] F. Wee, P. Soh, A. Suhaizal, H. Nornikman, and A. Ezanuddin, "Free space measurement technique on dielectric properties of agricultural residues at microwave frequencies," in *2009 SBMO/IEEE MTT-S International Microwave and Optoelectronics Conference (IMOC)*, pp. 183–187, IEEE, nov 2009. → pages 6

[80] D. Popovic, L. McCartney, C. Beasley, M. Lazebnik, M. Okoniewski, S. Hagness, and J. Booske, "Precision open-ended coaxial probes for in vivo and ex vivo dielectric spectroscopy of biological tissues at microwave frequencies," *IEEE Transactions on Microwave Theory and Techniques*, vol. 53, pp. 1713–1722, may 2005. → pages 7

[81] J.-Y. Shim and J.-Y. Chung, "Complex Permittivity Measurement of Artificial Tissue Emulating Material Using Open-Ended Coaxial Probe," *IEEE Sensors Journal*, vol. 20, pp. 4688–4693, may 2020. → pages 7

[82] T. Marsland and S. Evans, "Dielectric measurements with an open-ended coaxial probe," *IEE Proceedings H Microwaves, Antennas and Propagation*, vol. 134, no. 4, p. 341, 1987. → pages 7

[83] A. Mavrovic, J.-B. Madore, A. Langlois, A. Royer, and A. Roy, "Snow liquid water content measurement using an open-ended coaxial probe (OECP)," *Cold Regions Science and Technology*, vol. 171, p. 102958, mar 2020. → pages

[84] S. K. Lau, D. Dag, S. Ozturk, F. Kong, and J. Subbiah, "A comparison between the open-ended coaxial probe method and the parallel plate method for measuring the dielectric properties of low-moisture foods," *LWT*, p. 109719, jun 2020. → pages

[85] V. Guihard, F. Taillade, J.-P. Balayssac, B. Steck, J. Sanahuja, and F. Deby, "Permittivity measurement of cementitious materials with an open-ended coaxial probe," *Construction and Building Materials*, vol. 230, p. 116946, jan 2020. → pages

[86] G. Maenhout, T. Markovic, I. Ocket, and B. Nauwelaers, "Effect of Open-Ended Coaxial Probe-to-Tissue Contact Pressure on Dielectric Measurements," *Sensors*, vol. 20, p. 2060, apr 2020. → pages 7

[87] A. Bogle, M. Havrilla, D. Nyquis, L. Kempel, and E. Rothwell, "Electromagnetic Material Characterization using a Partially-Filled Rectangular Waveguide," *Journal of Electromagnetic Waves and Applications*, vol. 19, pp. 1291–1306, jan 2005. → pages 8

[88] A. Tamer, F. Karadağ, E. Ünal, Y. I. Abdulkarim, L. Deng, O. Altintas, M. Bakır, and M. Karaaslan, "Metamaterial based sensor integrating transmission line for detection of branded and unbranded diesel fuel," *Chemical Physics Letters*, vol. 742, p. 137169, mar 2020. → pages 8

[89] C.-K. Lee, S. Zhang, S. S. Bukhari, D. Cadman, J. C. Vardaxoglou, and W. G. Whittow, "Complex Permittivity Measurement System for Solid Materials Using Complementary Frequency Selective Surfaces," *IEEE Access*, vol. 8, pp. 7628–7640, 2020. → pages 8

[90] T. R. Jones, M. H. Zarifi, and M. Daneshmand, "Miniaturized Quarter-Mode Substrate Integrated Cavity Resonators for Humidity Sensing," *IEEE Microwave and Wireless Components Letters*, vol. 27, pp. 612–614, jul 2017. → pages 9

[91] K. Saeed, R. D. Pollard, and I. C. Hunter, "Substrate integrated waveguide cavity resonators for complex permittivity characterization of materials," *IEEE Transactions on Microwave Theory and Techniques*, vol. 56, no. 10, pp. 2340–2347, 2008. → pages 10, 11

[92] J. Baker-Jarvis, R. Geyer, J. Grosvenor, M. Janezic, C. Jones, B. Riddle, C. Weil, and J. Krupka, "Dielectric characterization of low-loss materials a comparison of techniques," *IEEE Transactions on Dielectrics and Electrical Insulation*, vol. 5, no. 4, pp. 571–577, 1998. → pages 10

[93] M. H. Zarifi, T. Thundat, and M. Daneshmand, "High resolution microwave microstrip resonator for sensing applications," *Sensors and Actuators, A: Physical*, vol. 233, pp. 224–230, 2015. → pages 11

[94] M. H. Zarifi, M. Rahimi, M. Daneshmand, and T. Thundat, "Microwave ring resonator-based non-contact interface sensor for oil sands

applications," *Sensors and Actuators B: Chemical*, vol. 224, pp. 632–639, mar 2016. → pages 11

[95] J. Muñoz-Enano, P. Vélez, M. Gil, and F. Martín, "Planar Microwave Resonant Sensors: A Review and Recent Developments," *Applied Sciences*, vol. 10, p. 2615, apr 2020. → pages 17, 18, 19, 20

[96] J. Naqui, J. Coromina, A. Karami-Horestani, C. Fumeaux, and F. Martín, "Angular Displacement and Velocity Sensors Based on Coplanar Waveguides (CPWs) Loaded with S-Shaped Split Ring Resonators (S-SRR)," *Sensors*, vol. 15, pp. 9628–9650, apr 2015. → pages 17

[97] J. Naqui, A. Horestani, F. Martín, C. Fumeaux, and D. Abbott, "Two-dimensional displacement and alignment sensor based on reflection coefficients of open microstrip lines loaded with split ring resonators," *Electronics Letters*, vol. 50, pp. 620–622, apr 2014. → pages

[98] J. Naqui, M. Durán-Sindreu, and F. Martín, "Novel Sensors Based on the Symmetry Properties of Split Ring Resonators (SRRs)," *Sensors*, vol. 11, pp. 7545–7553, jul 2011. → pages

[99] J. Naqui, M. Durán-Sindreu, and F. Martín, "Alignment and Position Sensors Based on Split Ring Resonators," *Sensors*, vol. 12, pp. 11790–11797, aug 2012. → pages 17

[100] A. K. Horestani, J. Naqui, Z. Shaterian, D. Abbott, C. Fumeaux, and F. Martín, "Two-dimensional alignment and displacement sensor based on movable broadside-coupled split ring resonators," *Sensors and Actuators A: Physical*, vol. 210, pp. 18–24, apr 2014. → pages 18

[101] A. Ebrahimi, J. Scott, and K. Ghorbani, "Differential Sensors Using Microstrip Lines Loaded With Two Split-Ring Resonators," *IEEE Sensors Journal*, vol. 18, pp. 5786–5793, jul 2018. → pages 19

[102] P. Velez, L. Su, K. Grenier, J. Mata-Contreras, D. Dubuc, and F. Martin, "Microwave Microfluidic Sensor Based on a Microstrip Splitter/Combiner Configuration and Split Ring Resonators (SRRs) for Dielectric Characterization of Liquids," *IEEE Sensors Journal*, vol. 17, pp. 6589–6598, oct 2017. → pages

[103] L. Su, J. Mata-Contreras, P. Velez, and F. Martin, "Splitter/Combiner Microstrip Sections Loaded With Pairs of Complementary Split Ring

Resonators (CSRRs): Modeling and Optimization for Differential Sensing Applications," *IEEE Transactions on Microwave Theory and Techniques*, vol. 64, pp. 4362–4370, dec 2016. → pages 18, 19

[104] A. Ebrahimi, J. Scott, and K. Ghorbani, "Transmission Lines Terminated With LC Resonators for Differential Permittivity Sensing," *IEEE Microwave and Wireless Components Letters*, vol. 28, pp. 1149–1151, dec 2018. → pages 19

[105] R. Corporation, "Product Selector Guide," 2013. → pages 22, 23

[106] A. Shrivastava, "Plastic Properties and Testing," in *Introduction to Plastics Engineering*, pp. 49–110, Elsevier, 2018. → pages 22

[107] F. Gustrau, *RF and microwave engineering: fundamentals of wireless communications*. John Wiley & Sons, 2012. → pages 24

[108] K. Chang and L.-H. Hsieh, *Microwave Ring Circuits and Related Structures*. Hoboken, NJ, USA: John Wiley & Sons, Inc., apr 2004. → pages 28

[109] W. J Highton, "Capacitance of a rectangular capacitor, with edge effect, calculator," 2009. → pages 30

[110] C. S. Westfall and P. A. Levin, "Comprehensive analysis of central carbon metabolism illuminates connections between nutrient availability, growth rate, and cell morphology in Escherichia coli," *PLOS Genetics*, vol. 14, p. e1007205, feb 2018. → pages 49

[111] A. Bren, Y. Hart, E. Dekel, D. Koster, and U. Alon, "The last generation of bacterial growth in limiting nutrient," *BMC Systems Biology*, vol. 7, no. 1, p. 27, 2013. → pages 49

[112] E. R. Sanders, "Aseptic Laboratory Techniques: Plating Methods," *Journal of Visualized Experiments*, may 2012. → pages 49

[113] S. Oberoi, K. S. Daya, and P. S. Tirumalai, "Microwave sensor for detection of E. coli in water," in *2012 Sixth International Conference on Sensing Technology (ICST)*, pp. 614–617, IEEE, dec 2012. → pages 49

[114] I. Piekarz, S. Górska, S. Odrobina, M. Drab, K. Wincza, A. Gamian, and S. Gruszczynski, "A microwave matrix sensor for multipoint label-free Escherichia coli detection," *Biosensors and Bioelectronics*, vol. 147, p. 111784, jan 2020. → pages 49

[115] A. Tholakalabavi, J. J. Zwiazek, and T. A. Thorpe, "Effect of mannitol and glucose-induced osmotic stress on growth, water relations, and solute composition of cell suspension cultures of poplar (Populus deltoides var.Occidentalis) in relation to anthocyanin accumulation," *In Vitro Cellular & Developmental Biology - Plant*, vol. 30, pp. 164–170, jul 1994. → pages 56

[116] B. Mackey and C. M. Derrick, "Conductance measurements of the lag phase of injured Salmonella typhimurium," *Journal of Applied Bacteriology*, vol. 57, pp. 299–308, oct 1984. → pages 56

[117] L. Machlis, "FACTORS AFFECTING THE LAG PHASE OF GROWTH OF THE FILAMENTOUS FUNGUS, ALLOMYCES MACROGYNUS," *American Journal of Botany*, vol. 44, pp. 113–119, feb 1957. → pages

[118] M. D. Rolfe, C. J. Rice, S. Lucchini, C. Pin, A. Thompson, A. D. S. Cameron, M. Alston, M. F. Stringer, R. P. Betts, J. Baranyi, M. W. Peck, and J. C. D. Hinton, "Lag Phase Is a Distinct Growth Phase That Prepares Bacteria for Exponential Growth and Involves Transient Metal Accumulation," *Journal of Bacteriology*, vol. 194, pp. 686–701, feb 2012. → pages 56

[119] P.-Y. Litzler, L. Benard, N. Barbier-Frebourg, S. Vilain, T. Jouenne, E. Beucher, C. Bunel, J.-F. Lemeland, and J.-P. Bessou, "Biofilm formation on pyrolytic carbon heart valves: Influence of surface free energy, roughness, and bacterial species," *The Journal of Thoracic and Cardiovascular Surgery*, vol. 134, pp. 1025–1032, oct 2007. → pages 57

[120] R. Donlan, "Biofilms and Device-Associated Infections," *Emerging Infectious Diseases*, vol. 7, pp. 277–281, apr 2001. → pages

[121] Z. Khatoon, C. D. McTiernan, E. J. Suuronen, T.-F. Mah, and E. I. Alarcon, "Bacterial biofilm formation on implantable devices and approaches to its treatment and prevention," *Heliyon*, vol. 4, p. e01067, dec 2018. → pages 57

[122] M. A. Nazir, "Prevalence of periodontal disease, its association with systemic diseases and prevention.," *International journal of health sciences*, vol. 11, no. 2, pp. 72–80, 2017. → pages

[123] A. Arigbede, B. Babatope, and M. Bamidele, "Periodontitis and systemic diseases: A literature review," *Journal of Indian Society of Periodontology*, vol. 16, no. 4, p. 487, 2012. → pages 57

[124] C. de la Fuente-Núñez, F. Reffuveille, L. Fernández, and R. E. Hancock, "Bacterial biofilm development as a multicellular adaptation: antibiotic resistance and new therapeutic strategies," *Current Opinion in Microbiology*, vol. 16, pp. 580–589, oct 2013. → pages 57

[125] A. K. Epstein, B. Pokroy, A. Seminara, and J. Aizenberg, "Bacterial biofilm shows persistent resistance to liquid wetting and gas penetration," *Proceedings of the National Academy of Sciences*, vol. 108, pp. 995–1000, jan 2011. → pages

[126] P. S. Stewart, "Mechanisms of antibiotic resistance in bacterial biofilms," *International Journal of Medical Microbiology*, vol. 292, pp. 107–113, jan 2002. → pages 57

[127] M. Hassan, E. Gonzalez, V. Hitchins, and I. Ilev, "Detecting bacteria contamination on medical device surfaces using an integrated fiber-optic mid-infrared spectroscopy sensing method," *Sensors and Actuators B: Chemical*, vol. 231, pp. 646–654, aug 2016. → pages 57

[128] T. Javanbakht, B. Ghane-Motlagh, and M. Sawan, "Comparative study of antibiofilm activity and physicochemical properties of microelectrode arrays," *Microelectronic Engineering*, p. 111305, mar 2020. → pages

[129] M. A. A. Grant, B. Wacław, R. J. Allen, and P. Cicuta, "The role of mechanical forces in the planar-to-bulk transition in growing Escherichia coli microcolonies," *Journal of The Royal Society Interface*, vol. 11, p. 20140400, aug 2014. → pages 57, 61

[130] D. Lebeaux, J.-M. Ghigo, and C. Beloin, "Biofilm-Related Infections: Bridging the Gap between Clinical Management and Fundamental Aspects of Recalcitrance toward Antibiotics," *Microbiology and Molecular Biology Reviews*, vol. 78, pp. 510–543, sep 2014. → pages 57

[131] S. S. Magill, J. R. Edwards, W. Bamberg, Z. G. Beldavs, G. Dumyati, M. A. Kainer, R. Lynfield, M. Maloney, L. McAllister-Hollod, J. Nadle, S. M. Ray, D. L. Thompson, L. E. Wilson, and S. K. Fridkin,

"Multistate Point-Prevalence Survey of Health Care–Associated Infections," *New England Journal of Medicine*, vol. 370, pp. 1198–1208, mar 2014. → pages 57

[132] R. J. Allen and B. Waclaw, "Bacterial growth: a statistical physicist's guide," *Reports on Progress in Physics*, vol. 82, p. 016601, jan 2019. → pages 57, 61

[133] P.-T. Su, C.-T. Liao, J.-R. Roan, S.-H. Wang, A. Chiou, and W.-J. Syu, "Bacterial Colony from Two-Dimensional Division to Three-Dimensional Development," *PLoS ONE*, vol. 7, p. e48098, nov 2012. → pages 57

[134] F. Si, B. Li, W. Margolin, and S. X. Sun, "Bacterial growth and form under mechanical compression," *Scientific Reports*, vol. 5, p. 11367, sep 2015. → pages 57, 61

[135] G. Nabovati, E. Ghafar-Zadeh, A. Letourneau, and M. Sawan, "Towards High Throughput Cell Growth Screening: A New CMOS 8 × 8 Biosensor Array for Life Science Applications," *IEEE Transactions on Biomedical Circuits and Systems*, vol. 11, pp. 380–391, apr 2017. → pages 58

[136] G. Nabovati, E. Ghafar-Zadeh, and M. Sawan, "A 64 pixel ISFET-based biosensor for extracellular pH gradient monitoring," in *2015 IEEE International Symposium on Circuits and Systems (ISCAS)*, pp. 1762–1765, IEEE, may 2015. → pages 67

[137] E. Ghafar-Zadeh, M. Sawan, V. P. Chodavarapu, and T. Hosseini-Nia, "Bacteria Growth Monitoring Through a Differential CMOS Capacitive Sensor," *IEEE Transactions on Biomedical Circuits and Systems*, vol. 4, pp. 232–238, aug 2010. → pages 58

[138] L. Y. Zhang, C. Bounaix Morand du Puch, C. Dalmay, A. Lacroix, A. Landoulsi, J. Leroy, C. Mélin, F. Lalloué, S. Battu, C. Lautrette, S. Giraud, A. Bessaudou, P. Blondy, M. O. Jauberteau, and A. Pothier, "Discrimination of colorectal cancer cell lines using microwave biosensors," *Sensors and Actuators A: Physical*, vol. 216, pp. 405–416, sep 2014. → pages 58

[139] A. Sanchis, A. P. Brown, M. Sancho, G. Martínez, J. L. Sebastián, S. Muñoz, and J. M. Miranda, "Dielectric characterization of bacterial

cells using dielectrophoresis," *Bioelectromagnetics*, vol. 28, pp. 393–401, jul 2007. → pages 61

[140] W. Bai, K. Zhao, and K. Asami, "Dielectric properties of E. coli cell as simulated by the three-shell spheroidal model," *Biophysical Chemistry*, vol. 122, pp. 136–142, jul 2006. → pages

[141] B. Zavizion, Z. Zhao, A. Nittayajarn, and R. J. Rieder, "Rapid microbiological testing: monitoring the development of bacterial stress.," *PloS one*, vol. 5, p. e13374, oct 2010. → pages

[142] M. Schaechter, "A brief history of bacterial growth physiology," *Frontiers in Microbiology*, vol. 6, apr 2015. → pages 61

[143] P. Jurtshuk, *Bacterial Metabolism*. University of Texas Medical Branch at Galveston, 1996. → pages 62

[144] K. M. C. Tjørve and E. Tjørve, "The use of Gompertz models in growth analyses, and new Gompertz-model approach: An addition to the Unified-Richards family," *PLOS ONE*, vol. 12, p. e0178691, jun 2017. → pages 62

[145] D. M. Brogan and E. Mossialos, "A critical analysis of the review on antimicrobial resistance report and the infectious disease financing facility.," *Globalization and health*, vol. 12, p. 8, mar 2016. → pages 66

[146] K. I. Mohr, *History of Antibiotics Research*, vol. 398. Springer, Cham, 2016. → pages 66

[147] S. Simoens, "Health Economics of Antibiotics.," *Pharmaceuticals (Basel, Switzerland)*, vol. 3, pp. 1348–1359, apr 2010. → pages 66

[148] B. Aslam, W. Wang, M. I. Arshad, M. Khurshid, S. Muzammil, M. H. Rasool, M. A. Nisar, R. F. Alvi, M. A. Aslam, M. U. Qamar, M. K. F. Salamat, and Z. Baloch, "Antibiotic resistance: a rundown of a global crisis," *Infection and Drug Resistance*, vol. Volume 11, pp. 1645–1658, oct 2018. → pages 66

[149] G. D. Wright, "The antibiotic resistome: the nexus of chemical and genetic diversity," *Nature Reviews Microbiology*, vol. 5, pp. 175–186, mar 2007. → pages 66

[150] M. L. Bayot and B. N. Bragg, *Antimicrobial Susceptibility Testing*. StatPearls Publishing, 2019. → pages 66

[151] I. Galani, F. Kontopidou, M. Souli, P.-D. Rekatsina, E. Koratzanis, J. Deliolanis, and H. Giamarellou, "Colistin susceptibility testing by Etest and disk diffusion methods," *International Journal of Antimicrobial Agents*, vol. 31, pp. 434–439, may 2008. → pages 66

[152] S. P. Bernier and M. G. Surette, "Concentration-dependent activity of antibiotics in natural environments.," *Frontiers in microbiology*, vol. 4, p. 20, 2013. → pages 70, 71

[153] G. Kapoor, S. Saigal, and A. Elongavan, "Action and resistance mechanisms of antibiotics: A guide for clinicians.," *Journal of anaesthesiology, clinical pharmacology*, vol. 33, no. 3, pp. 300–305. → pages 70, 71

[154] H. Bhargav, S. D. Shastri, S. Poornav, K. Darshan, and M. M. Nayak, "Measurement of the Zone of Inhibition of an Antibiotic," in *2016 IEEE 6th International Conference on Advanced Computing (IACC)*, pp. 409–414, IEEE, feb 2016. → pages 72

Appendix A

A.1 Measurement of effective dielectric properties of solid agar

To measure the dielectric properties or complex permittivity of materials, the N1501 dielectric probe kit by Keysight Technologies, Inc. was used. The probe setup is shown in Figure A.1.

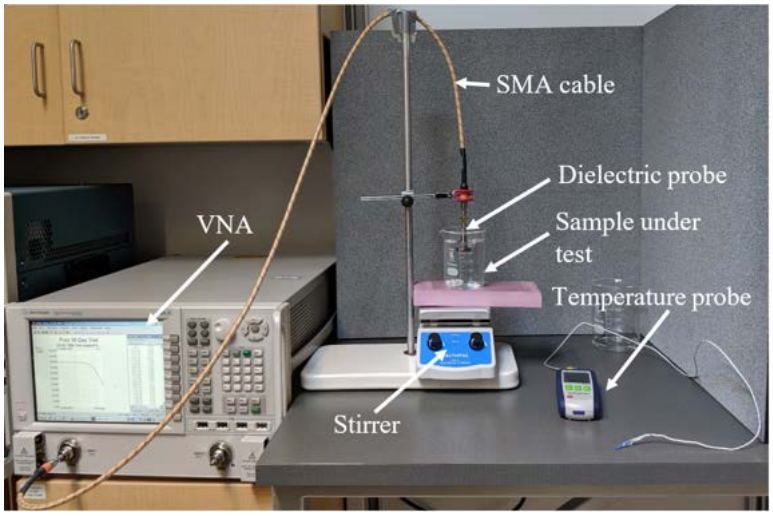

Figure A.1: Experimental setup to measure the dielectric properties of sample under test.

It consists of an N1501A dielectric probe connected to a VNA through an SMA cable. The probe is immersed into a test liquid or placed in close contact with the solid material under test to perform the dielectric measurement.

To measuring the effective dielectric properties of solid agar, the solid agar sample was enclosed in a plastic petri dish. The combination was then placed in proximity of the dielectric probe such that the face of the dielectric probe is completely covered by the sample as shown in Figure A.2.

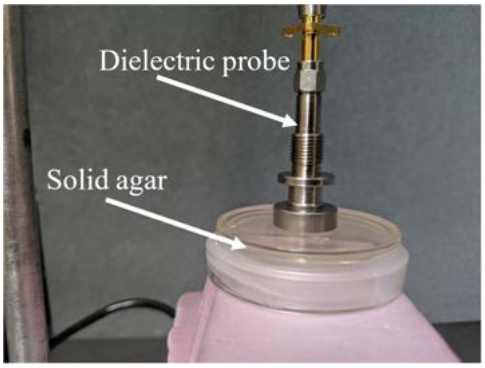

Figure A.2: Solid agar plate in conjunction with the N1501A dielectric probe.

The probe was calibrated from 200 MHZ to 20 GHz with a resolution of 1001 and intermediate frequency bandwidth of 300 Hz prior to measurements. Sixteen measurements were taken and an average of the measured results were calculated and recorded using N1500A Materials Management Suite provided by Keysight Technologies, Inc. The measured results for MH agar and LB agar is shown in Figure A.3 (a) and (b) respectively.

According to the measured result, the effective permittivity of LB agar and MH agar at frequency 1.76 GHz is 2.156 and 2.258 respectively. The loss tangent however is measured to be 0.077 and 0.08 for LB and MH agar respectively.

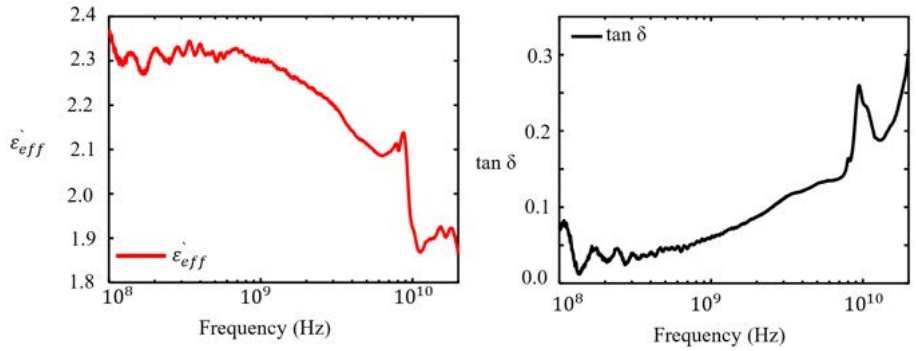

(a) MH agar

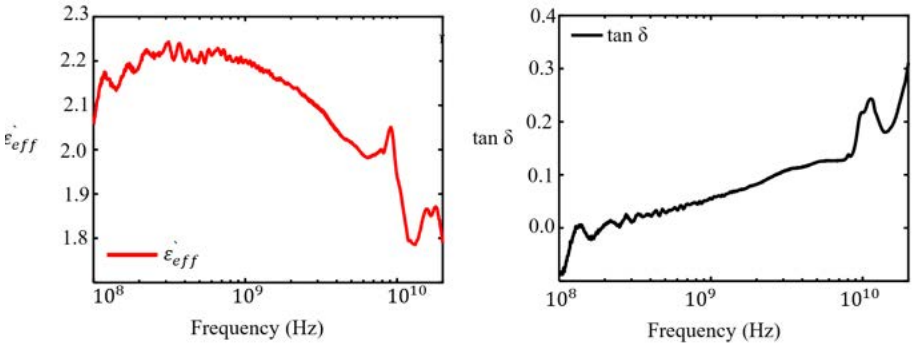

(b) LB agar

Figure A.3: Measured effective permittivity and loss tangent of MH agar (a) and LB agar (b).